Uppsala 1977

UPTEC 77 23 R
APRIL 1977

ENOCH - AN INTEGRATED SYSTEM FOR MEASUREMENT AND ANALYSIS OF HUMAN GAIT

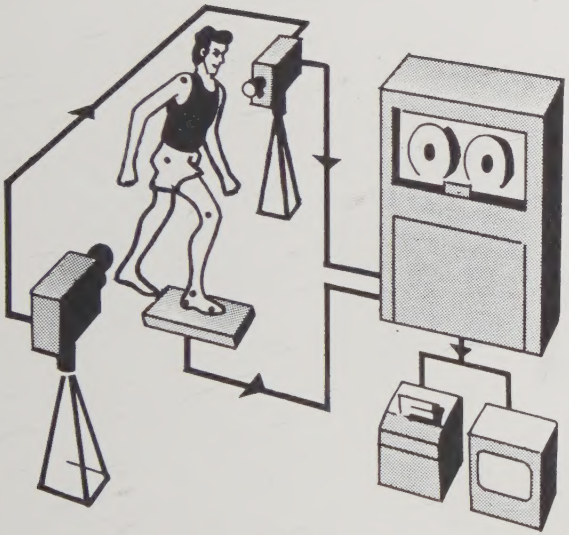

LEIF GUSTAFSSON
HÅKAN LANSHAMMAR

TEKNIKUM
INSTITUTE OF TECHNOLOGY
UPPSALA UNIVERSITY

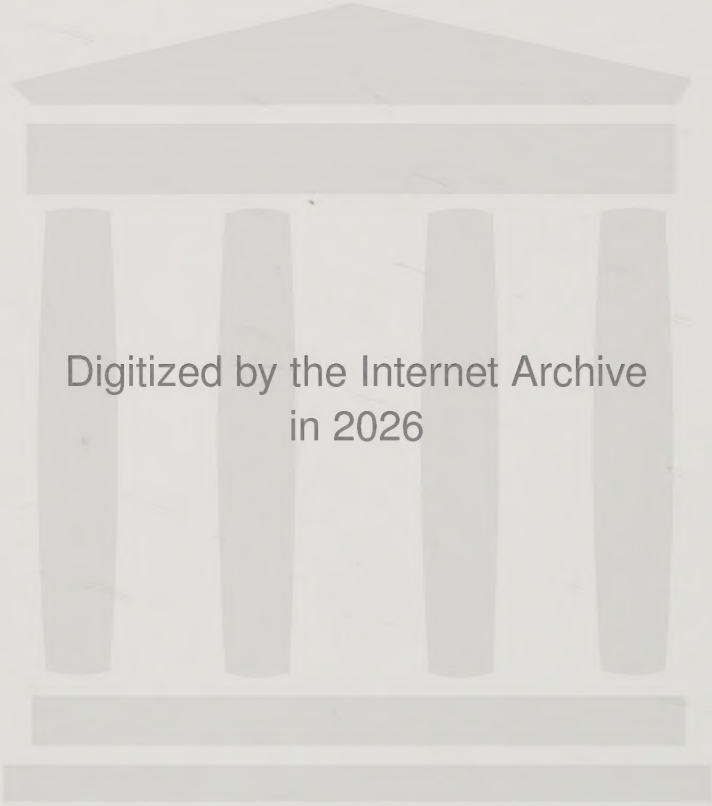
Digitized by the Internet Archive
in 2026

https://archive.org/details/IA41548926_0010

UPTEC 77 23 R

Leif Gustafsson

Håkan Lanshammar

ENOCH - AN INTEGRATED SYSTEM FOR MEASUREMENT AND ANALYSIS OF HUMAN GAIT

UPPSALA 1977

ISBN 91-506-0120-2

UNIV.
LEIDEN
BIBL.

© Leif Gustafsson & Håkan Lanshammar 1977

Institute of Technology
Uppsala University
S-751 21 Uppsala, Sweden

Uppsala 1977

Leif Gustafsson

Håkan Lanshammar

ENOCH - AN INTEGRATED SYSTEM FOR MEASUREMENT AND ANALYSIS OF HUMAN GAIT

ABSTRACT

Quantitative measurement and analysis of human gait are important for the evaluation of the functioning of prostheses and orthoses on patients, and also for the evaluation of surgical operations, gait training, and other clinical treatments.

A software based system has been developed, where measurement devices are interfaced to a computer. The displacements of the subject are measured with an opto-electronic device (Selspot), and the ground reaction force with a force plate. In the computer these data are analysed by an interactive program package.

The analysis of basic gait characteristics includes stride length and stride frequency. The kinematic analysis gives the flexions at the hip, knee, and ankle joints of both legs, as well as the cartesian coordinates of the joints. A new method has been developed for numerical differentiation of displacement data, which allows the calculation of velocities and accelerations for different parts of the body. Forces and moments at the joints are also estimated. A high accuracy in these estimate has been demonstrated. Flexible graphical result presentation routines allow conventional diagrams, gait pattern diagrams, phase plane diagrams, and symmetry diagrams.

PREFACE

This publication gives a description of a system for measurement and analysis of human gait. It also constitutes the doctoral theses of the authors.

Gait analysis

The scientific study of human gait has traditions from the works by Fischer in Germany in the end of the 19th century. Different methods for kinematic registration of the gait and the construction of force plates for the determination of the ground reaction forces have formed the basis for the following development. The combination of simultaneous kinematic and ground reaction measurements with antrophometrical studies has made it possible to calculate resultant forces and moments at the joints. Another line of development has been the study of muscle activity with EMG, sometimes combined with kinematic measurements.

Important application areas where there is a need for quantified gait descriptions are:

- Research about human gait.
- Diagnosis on pathological gait.
- Evaluation of surgical incisions, gait training and other treatment.
- Evaluation of and comparison between different prosthetic and ortothic devices.

However, until recently gait analysis has not been used clinically in a larger scale. The main reason for this is that the complex structure of the human body requires a model for the analysis of the gait, which have to be rather extensive, even when many simplifying assumptions are being made. Further, for an accurate analysis the displacement of the different parts of the body must be measured with high accuracy. With

the introduction of high speed and low cost computers the use of model based gait analysis has become clinically feasible.

Project history

Our purpose has been to develop a system which is sufficiently fast, regarding the time required for a measurement and subsequent analysis, and flexible enough to be used for clinical purposes and for research of the human gait.

This project has been developed on assignment of the Een och Holmgren Ortopediska AB (EoH) and it has been financed by the Swedish Board for Technical Development (STU). The plans for a system for measurement and analysis began to take form in 1973, after a thorough investigation, by Pål Krüger, Teknikum and Kurt Öberg, EoH. Among other instruments the investigation included an optoelectronic system, called Selspot, that was not commerically available at that time.

In the years 1973 - 1977 the system was planned and realized by the authors. The work has been carried out at the Institute of Technology, Uppsala University. The computer facilities of the Institute have been utilized for all the software work.

In the work a systems approach have been used. The main objective with the work has been to obtain an integrated solution, where gait philosophy, methodological aspects of gait, hardware and software are compatible parts of a unity. To achieve this we have used a modular software centered approach.

The work has been of an interdisciplinairy nature and the goals of the project have been governed by the biomechanical objectives. Disciplines such as Mechanics, Computer Science, Digital Filtering Theory, Biomechanics, a certain amount of Anathomy, Electronics etc., have been important ingredients of the work. To fulfil the project goals, a hierarchical approach have been used, where the different parts have been systematically broken down into operational tasks.

In a project of this extensiveness we have found it a necessity to give a higher priority to the demand that all parts of the system must work satisfactorily, than to the desire of thorough penetration into certain details.

Project results

The result of the work is the ENOCH system which is the subject of this publication. This system has several characteristics not found in other systems for gait analysis.

- The system design is based on a modular, software realization of the entire process including calibration, measurement, analysis, and result presentation. It is unique as a strongly integrated system rather than containing unique parts.

  The qualities of this system have been carefully examined. It is verified in this publication that the system produces accurate estimates of the different basic gait parameters and of the kinematic and kinetic variables.
  The time between measurement and result presentation is 1-10 minutes depending on the complexity of the analysis involved. This makes the system well suited for clinical applications.

- It is the first system that utilizes the opto-electronic device, Selspot, for the measurement of kinematic data. In this context, investigations have been made on the characteristics of this device, and routines have been developed for the compensation of systematic errors in its output.

- A model for determination of body segment parameters has been constructed. However, many of the ideas, and all of the statistical data have been taken from other researchers.

- A new method for numerical differentiation of noisy data has been developed and successfully applied to gait data. The method is based on a least squares minimization of the total estimation error.

- The result presentation part of the system has been strongly emphasized. The graphical output routines are characterized by flexibility and simplicy in their use.

It should be noted that the existing system in April 1977 differs from a desired complete system in three respects: 1) It includes one force plate instead of two which is a necessity for obtaining the same accuracy in the kinetic variables for both legs. 2) Therefore we use algorithmical criterions to determine gait phase changes instead of using the force plates. 3) Of the same reason, and also for the evaluation of the system, the force plate data are used in the calculation of joint forces and moments only when both legs are in contact with the ground. Better estimates of the joint forces and moments can of course be obtained for the stance leg during single limb support if force plate data are used.

Description of contents

The material of this publication is divided into three parts:

Part I gives an introduction to the subsequent system description. In chapter 1 an introduction to the field of gait analysis is given. A brief survey of the technological and methodological development within this field is then given in chapter 2 and in chapter 3 a problem specification is presented.

In part II a detailed description of the ENOCH system is given. In chapter 4 the system ENOCH is briefly described from functional, technical realization, and software structure point of view. Chapter 5 gives a description of the measurement part of the system, chapter 6 of the analysis part, and chapter 7 of the result presentation part. Chapter 8 finally gives an account of the administrative part of the system.

Part III contains an evaluation of the sytem. In chapter 9 the ENOCH system is evaluated with respect to its properties and to the accuracy that is obtained for the different variables.

The program documentation for the ENOCH system is published in [Gustafsson, Lanshammar, 1977].

All figures and tables are numbered within each chapter.

All units are given in SI-units. The only ambiquity is that degrees sometimes are used instead of radians.

Acknowledgements

We want to thank all them who helped us to carry out this project. Especially we want to thank Gunnar Holmgren and Kurt Öberg at Een och Holmgren Ortopediska AB for an excellent and stimulating cooperation. The many discussions with Kurt Öberg have been very valuable, especially on questions concerning the applications.

An experimental evaluation of the precision in calculated angles has been performed in cooperation with Larry Lamoreux, University of California, Berkeley, for which he is greatfully acknowledged. We are also indebted to Dave Winter, University of Waterloo, Waterloo, Canada, who has provided us with data for the evaluation of the numerical differentiation.

At Uppsala Institute of Technology, Hans Olofsson has been of great help both in discussions and in the practical work. Pål Krüger, Svante Burström and Göran Lundström as well as other members of the Department of Computer Technology are acknowledged for their assistance in questions concerning computer technology. Bjarne Norman and Rolf Carlsson in the Department of Electronics are acknowledged for their cooperation on the modification of electronical hardware. Torsten Söderström has been deeply involved in the mathematical formalization of the numerical differentiation for which is is greatfully acknowledged. We are also indepted to Torgny Schütt, who gave us the oppurtunity to enter this project.

Concerning this publication, we are indepted to Birger Qvarnström, Department of Automatic Control, Chalmers Institute of Technology, Larry Lamoreux, University of California, Berkely, Torsten Söderström, Department of Automatic Control and Systems Analysis, and Hans Olofsson, Department of Solid Mechanics, both at Uppsala Institute of Technology. They all read the manuscript and their comments have influenced the writing of this thesis.

We are also extremely greatful to Margareta Hallenberg, who patiently and excellently typed the manuscript, even during her Easter holidays, and to Ingrid Strandh, who drew the figures, somtimes late at night.

The cover figure is used by the courtesy of the Journal Forskning och Framsteg.

Uppsala in April 1977

Leif Gustafsson Håkan Lanshammar

LIST OF CONTENTS

Page

ABSTRACT

PREFACE

LIST OF SYMBOLS 1

PART I INTRODUCTION 3

Chapter 1 AN APPROACH TO HUMAN GAIT ANALYSIS 5

Chapter 2 TECHNOLOGICAL AND METHODOLOGICAL REVIEW 10

Chapter 3 OBJECTIVE AND PROBLEM SPECIFICATION 16

PART II DESCRIPTION OF THE SYSTEM 19

Chapter 4 SURVEY OF THE SYSTEM 21

4.1 Functional survey 22
4.2 Technical realization 24
4.3 Software philosophy, structure and implementation 27

Chapter 5 MEASUREMENT SUBSYSTEM 33

5.1 Body data 34
5.2 Kinematic data 36
5.2.1 Measurement technique 37
5.2.2 Measurement arrangement 43
5.2.3 Calibration of the measurement system 44
5.2.4 Calibration of the camera positioning 54
5.3 Force plate data 61
5.4 Measurement control 64

Chapter 6 ANALYSIS SUBSYSTEM 66

6.1 Computation of body segment parameters 67
6.2 Numerical differentiation 73
6.2.1 Some fundamental properties of numerical differentiation of noisy data 75
6.2.2 Review of some methods for digital filtering 82
6.2.3 Description of a method for numerical differentiation 88

Page

6.2.3.1 Notations and basic assumption 90
6.2.3.2 Derivation of the method 92
6.2.3.3 Practical considerations 97
6.2.3.4 Determination of filter parameters and estimation of the errors 102
6.2.4 Evaluation of the differentiation method 117
6.2.5 Comparison with two related methods 122
6.3 Determination of times for gait phase changes 124
6.4 The mechanical model 129
6.4.1 Calculation of the displacements of the segments' centers of mass 133
6.4.2 Calculation of angles 135
6.4.3 Calculation of forces and moments 136
6.5 Estimation of gait stationarity 141

Chapter 7 RESULT PRESENTATION SUBSYSTEM 143

7.1 Raw data display 145
7.2 Display of the motion of the body in space 147
7.3 Diagram output 148
7.4 Tabular output 151

Chapter 8 ADMINISTRATION SUBSYSTEM 154

8.1 User-system communication 155
8.2 Data management 157
8.3 Measurement data error tests 159

PART III EVALUATION OF THE SYSTEM 161

Chapter 9 EVALUATION 163

9.1 Description of the system from the evaluation point of view 164
9.2 Types of errors in the system 166
9.3 Error evaluation from two different aspects 168
9.3.1 The BSP branch 169
9.3.2 The time variable 179
9.3.3 The kinematic branch 181
9.3.4 The geometrical model 195
9.3.5 The force plate branch 206

Page

9.3.6 The gait parameter branch 208
9.3.7 The kinetic gait model 211
9.3.8 The experimental condition branch 224
9.4 The time consumption for investigation of a subject 226

REFERENCES 227

LIST OF SYMBOLS

The listed notations will be used in several of the chapters. Units are given in parenthesis.

t	time (s)
tr	relative time (fraction of a gait cycle)

Body segment parameters

l	length of a body segment (m)
h	distance from proximal joint to the segments center of mass (m)
m	segment mass (kg)
j	moment of inertia for a segment (kg m^2)

Gait parameters

stride length	the displacement of the body during one gait cycle (m)
stride frequency	number of gait cycles per second (1/s)
P	horizontal impulse transferred between the floor and the subject during one step (kg m/s)
Pr	relative impulse as defined in section 6.5.
pc	variable giving type of gait phase change

Time depending variables

x	horizontal coordinate, positive in the walking direction (m)
y	vertical coordinate, positive upward (m)
$\dot{x}$, $\dot{y}$	first order derivatives of x and y (m/s)
$\ddot{x}$, $\ddot{y}$	second order derivatives of x and y (m/s^2)

φ	angle of rotation (rad, but presented in degrees on the graphical outputs)
$\dot{\varphi}$	angular velocity (rad/s, presented in degree/s)
$\ddot{\varphi}$	angular acceleration (rad/s^2, presented in degree/s^2)
FX	horizontal force component (N)
FY	vertical force component (N)
T	moment in z-direction (perpendicular to the x-y-plane) (Nm)
FXFR	horizontal floor reaction force (N)
FYFR	vertical floor reaction force (N)
TFR	ankle moment as derived from the floor reaction (Nm)
XF	horizontal coordinate for the point of application of floor reaction force (m)
FXFP	horizontal force exerted on the force plate (N)
FYFP	vertical force exerted on the force plate (N)
TFP	ankle moment as derived from the force plate (Nm)
XFFP	horizontal coordinate for the point of application of the force exerted on the force plate (m)

Some other symbols

$\hat{z}$	denotes an estimate of a variable z
$\bar{z}$	denotes a mean value
$\underline{z}$	denotes a vector
$\underline{\underline{z}}$	denotes a matrix
E	expected value

For many of the variables subscripts are used when the variables are referring to a specific part of the body. The meaning of these subscripts are defined in section 6.4.

PART I INTRODUCTION

Chapter 1 serves as a short introduction to the field of human gait analysis. In chapter 2 a review is given of the technological and methodological development and in chapter 3 a specification is given of the problems to be treated in the succeeding chapters.

1. AN APPROACH TO HUMAN GAIT ANALYSIS

In the field of human gait analysis, we have felt the lack of a generally accepted approach. When new measurements and investigations on different gait variables are presented, they often are not related, or even cannot be related, to a general picture.

For our personal use it is necessary to have a general philosophy for two main reasons. First, because the underlying philosophy, conscious or not, will deeply influence the manner of working as well as the resulting gait analysis system. Therefore, it is crucial to rely on an explicit, logical and practical philosophy as a background for objective formulations, thinking, discussions, and control of the work. Second, a common base is needed when working together in a team.

As an introduction, an account is given of our philosophy of gait analysis. This is constructed through systematic classification of fundamental questions of gait in hierarchical levels which we have found fruitful for comparison and classification of results in a scientific way.

Concepts

The natural starting point when studying human gait is to define the purpose of gait. Here we are satisfied with describing this purpose as to move the body from one point to another utilizing the legs. The person also wants to accomplish this displacement with a certain velocity and in a comfortable manner. Even restrictions of a cosmetic nature can be involed. His desired movements also have to be accomplished with the resources available for the person in question, i.e. usually with the legs, prostheses or orthoses.

The locomotion can be divided into repetitive parts, gait cycles, which containe two steps or one stride. After a transient start the gait reaches a stationary state.

If the gait is "normal" we also find a good symmetry between right and left.

Pathological gait usually exhibits an asymmetric pattern (though symmetry is not a sufficient condition for normal gait).

To discuss the nature of gait we also need some more concepts. Thus we subdivide the gait cycle into phases determined from the positions of the feet in relation to the ground. We also define events which separate the phases.

A study of gait also has to deal with the variations due to the subject's objectives with the gait and with the gait conditions. There are also statistical variations between different persons and between the motions of one person on different occasions. Therefore, it is important also to record the above mentioned conditions for an experiment and not only the results.

The above outlines can be a base for a verbal qualitative description of human gait. To reach a deeper understanding a quantitative description is required. Such a description can be performed at different hierarchical levels.

Level 1 - parametric description

The subject's purpose of gait is to move. The basic level to characterize the resulting gait is to give some scalar measurements on the overall motion, mostly connected to the gait cycle. Such measures, which we call gait parameters, are e.g. step length, step frequency, velocity, and time or relative time for the gait phases. From these measurements one can also compare symmetry between right and left, stationarity etc, but the studies are limited to the overall aggregated performance of the gait. The main tools are a measuring tape, a clock, and eventually, footswitches.

Level 2 - Kinematic description

When the conditions for an experiment are determined and when we also have measured the fundamental gait parameters that describe the resultant performance for the subject, then, but not before, it is meaningful to refine the studies. This brings us to a second level which means a kinematic study of the motion as a function of time for some selected points or segments.

In kinematics the studies concern the nature of the motions such as the positions, velocities and accelerations of the segments as well as the related angles, angular velocities and angular accelerations between the segments as functions of time. These studies also require much more equipment to follow the trajectories in time, or at least to give time samples with a sufficient frequency. Alternatively one can use equipment for velocity or acceleration measurement.

Level 3 - Kinetic description

Kinematics concern the study of the motion in time but not its causes. The motions are generated by the resultant forces and moments acting on the segments. This leads us to the kinetic or dynamic level of study. The study of kinetic variables is meaningful when the experimental condition, the fundamental gait parameters and the kinematic variables are specified.

The kinetic relations are based on the Newtonian equations which relate the resultant force on a segment to its acceleration with its mass as a proportionality constant, and the resultant moment to angular acceleration and moment of inertia. This is illustrated in figure 1.

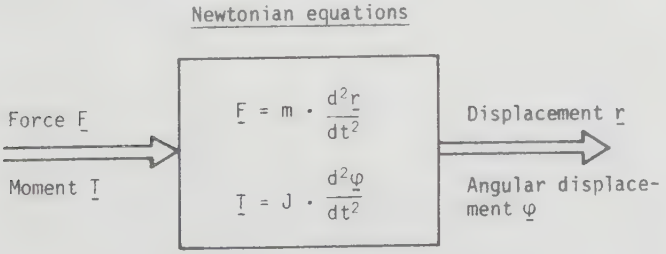

Figure 1. Relations between resultant force and moment acting on one segment and its displacements.

To obtain the resultant force and moment for a free segment in motion one must solve two new problems. 1) One has to estimate the constants in the Newtonian equations i.e. mass and moment of inertia and one also have to locate the center of mass. (In fact, center of mass and moment of interita are not true constants but vary a little during gait.) These quantities for a human segment are called body segment parameters, or BSP.
2) The displacement as a function of time must be differentiated twice. This is theoretically well defined but constitutes a very delicate task in practice since noise always is present to some degree in the data.

What has been said concerns one separate segment but gait is performed by a person consisting of several segments mutually interacting with each other and with the ground. The dealing with this complex problem requires a mathematical description, a model, describing how the segments are linked together. In kinematics we do not need a model of the subject but regard him as a black-box. In kinetics though we have to change the black-box for an adequate structural model and by this we also gain in understanding.

We also want to point out that for physical reasons it is possible to completely compute the force and moment functions only for single limb support. For double limb support you also need to complement the measurements with the reaction forces from the floor which can be obtained from a force plate. This also implies that you need one force plate per stride. For practical reasons it is very difficult to use a force plate together with a treadmill so one often must rely on the repeatability of gait.

Information about mechanical energy also belongs to the kinetic level.

Further levels - Refined studies

The next hierachical level can be to separate the different muscle groups acting on the segments or studying their force contributions. Such studies require more detailed models and further measurements, e.g. EMG measurements. As always it is necessary to have the lower levels well determined so that the results can be understood in their context.

A natural conclusion from this philosophy is that it would be a very large advantage if an experiment simultaneously could record all the necessary parameters and variables up to the concerned level.

We close up this chapter with a summary.

Summary

It is important to know the subject's objectives with his gait and the experimental conditions in order to perform meaningful gait investigations. These investigations can be performed on different levels:

	Hierarchical level	Requirements	Results
1)	Measurement of static quantities in time	Measure stick and chronometer	Gait parameters e.g. step length, step frequency, timing of gait phases.
2)	Kinematics	Instruments for registration of displacement	Motion as a function of time
3)	Kinetics	Structural model Body segment parameters Force plate Kinematic equipment	Forces and moments (Mechanical energy)
4)	Higher levels e.g. muscle interactions	More complex models and equipment	More detailed information

We also have concluded that a high level has to be interpreted in the context of the lower levels. This also implies that it is an advantage if the investigation can record all the relevant information up to the concerned level in the same measurement.

2. TECHNOLOGICAL AND METHODOLOGICAL REVIEW

In this chapter a brief survey of the technological and methodological development within the field of human gait analysis is given. The presentation serves to illustrate the background for and alternatives to our work.

Some methods used for the measurement of basic gait parameters and kinematic variables will first be described, followed by a short account of the development in kinetic measurement and analysis.

Basic gait parameters

Gait parameters like steplength, step frequency and times for gait phase changes have been studied for quite a long time. Several investigations on these variables and their importance have been published. Traditionally these quantities have been measured with chronometers, measuring tapes, footswitches etc. They can also be derived for example from film techniques. An example of a technique can be found in [Lamoreux, 1971].

Kinematics

Kinematic measurements require instruments for the registration of motion in time. Several kinematical devices based on different techniques have been developed. We classify them as direct devices if they measure the desired motion and as indirect if velocities or accelerations are measured.

Direct devices:

- Cinephotography is the traditional kinematical device and it is still in wide use. It is very accurate and it can be run at a high speed. An example of the use of this technique is given in [Sutherland, Hagy, 1972]. The extremely laborious and time consuming work for the extraction of displacement data makes it impractical for clinical use.
- Stroboscopical devices have the same drawbacks as the cine camera. The flashing light can also disturb the experiments. This technique has been used for example in [Murray et al, 1964].
- Potentiometers actuated by retractable cords that are attached to the body have been developed. Such a system, which requires an overhead trolley, is described in [Wirta et al, 1970]. Five cords are used for the registration of the coordinates for the two hips.
- Goniometrical devices based on different principles have been presented. Electrical goniometers mounted on an exosceletal structure [Lamoreux, 1971] and polarization goniometers [Reed,

Reynolds, 1969] are both practical and accurate systems but confined to angular measurements.

- TV-devices are among the most interesting approaches. The electrical output enables interfacing with a computer which makes it possible to obtain the results shortly after a measurement. It is therefore suited for clinical use. However, it also has intrisic limitations. Firstly, a commersially available TV-system has a limited sampling frequency, usually 50 or 60 Hz, and the resolution is limited by the number of lines. (The resolution can be increased by the use of large landmarks which can be detected on several lines.) Secondly, it is based on scanning, not on a direct recording, which is an unnecessary complication. Such a system is described in [Winter et al, 1972].

- Optoelectronic devices based on the lateral photo effect of diodes have recently been developed. A commercially available device called Selspot is described in [Selspot System, (A)].

  The attractive points of Selspot are

  - High resolution. The signal to noise ratio is 1000:1
  - High sampling frequency. The maximal sampling frequency is over 300 Hz
  - Direct recording instead of scanning
  - The simplicity in construction, handling and interfacing
  - The promising development possibilites due to its construction.

  The measurement frequency can easily be increased and there are reasons to believe that the resolution can be further improved.

  A drawback is that the subject has to wear light emitting diodes as landmarks and also needs to carry a power supply or be connected via a cabel.

Indirect devices:

- Doppler devices measure the velocity. No succesful applications of this kind of devices have been reported.

- Accelerometer devices measures the accelerations. The interesting aspect is that it elimates the need for differentiation when accelerations are wanted. Of the drawbacks can be mentioned the severe problems with calibration, drift and the determination of the orientation of the accelerometer in space. We do not know of any succesful use of accelerometers for accurate determination of the whole gait.

A good description of some kinematic systems is given in [Cavanagh, 1975].

Kinetics

Fischer's investigations [Fischer, 1895-1904] are a starting point for kinetical studies. He used a form of stroboscopy for the recording of the motion. Together with Braune he had also performed a study on body segment parameters,[Braune, Fischer, 1889]. Since he had no equipment for measurement of the ground reaction force he was confined to single limb support where he calculated joint forces from the equations of motion.

In 1938 Elftman designed and developed a force plate, [Elftman, 1938], which registrated the three ground reaction force components and its point of attack. The force plate is now a standard component in many kinetic gait analysis systems.

In the paper [Bresler, Frankel, 1950], the authors describe a three dimensional investigation of resultant forces and moments in the leg during level walking. They used a force plate and cine cameras with 40 frames per second. Although they used a primitive differentiation technique and performed their calculations on desk calculators, the calculations only took 500 man hours for the first subject. For later measurements this figure was reduced to 250 man hours.

The next important step was the development of computers. In the 1950:s computers were very expensive, hard to handle, and as compared with today, very slow and inefficient. Compared with manual work on desk calculators the computer constituted an enormous capacity for the computations.

During the 1960:s relatively small and very fast and flexible minicomputers were developed and sold to a moderate price. This development made it possible to use the computer as a part of a system, not only as a computation device. Now it seems rational to fully utilize the capacity of the computer as the central part of an integrated gait analysis system and to let the software more and more replace the hardware.

Another important trend during the 1960:s and 70:s, compatible to the computer development, is the strive to replace cine cameras with their laborios and time consuming extraction of displacement data. Some alternative devices were mentioned above. Of these the TV-systems and especially the Selspot system are easily interfaced to a computer.

Modern kinetical systems have a similar structure. Their composition includes the following points.

- o Kinematic equipment for measuring displacement in time
- o Differentiation routine for the calculation of accelerations
- o One or several force plates for ground reaction measurements
- o Routine for estimation of necessary body segment parameters
- o A mathematical model of the subject
- o Computation equipment.

Although the systems are similar in structure they differ widely in their realizations. The main differing points are:

- o Type of kinematical equipment
- o Number of dimensions investigated
- o Camera positioning (in the case of cine film, TV, etc.)
- o The structure of the model
- o Method of solving the kinetical equations
- o Measurement frequency and resolution
- o Method for determination of body segment parameters
- o Differentiation method
- o Extensiveness of the investigations

- o Result presentation methods
- o Degree of system integration
- o Hardware or software approach.

An investigation of all these points is beyond the scope of this publication. We will only give very brief descriptions of two systems which contain a high degree of integration.

I) In [Winter et al, 1972], [Winter et al,1974b], a system using a television camera is described. In this system the television is interfaced to a large computer (CDC 1700). This interface was developed 1970 by Dinn. The cameras are positioned on one side and in front of the subject giving a three dimensional representation of the motion of one leg or one side of the body. The measurement frequency is 60 Hz and the picture is represented in a 96 × 96 binary matrix. The relatively coarse resolution is compensated for in two ways. First, a small measurement distance can be used since the operator tracks the subject by pushing the camera parallel to the walkway. Second, the use of large landmarks gives statistical reduction of the location errors. In [Winter et al, 1973] energy and power flow studies are presented.

II) In [Jarrett et al, 1974],[Jarrett et al, 1976] another TV based system is presented. This system uses a camera with a sampling rate of 50 Hz. Up to six cameras can be used simultaneously giving a combined frequency of 300 Hz. The resolution is 0.3% in the vertical direction. Measurements have included one leg in three dimensions over several strides.

The described technical development has made it possible to design integrated systems based on software. For future systems, the choice of suitable measurement devices and software structures are key questions. An extremely important part of the software concerns the result presentation. No matter how good the performance of a system are, if the output from the computer comes in a form that is difficult to understand, it is unlikely that the system will be much used. If, on the other hand, the output is easy to understand and flexible in its use there are great potentials for clinical applications, also for a system with a simple hardware and with a minimum of software analysis.

3. OBJECTIVE AND PROBLEM SPECIFICATION

The objective of the work described in this report has been the development of a system suitable for several different applications:

- o Research
  - Normal gait studies
  - Pathological gait studies
  - Experiments where several types of measurement devices are to be used simultaneously
- o Clinical use
  - Diagnosis of the patients disability
  - Evaluation of surgical operations, gait training and other treatments
  - Evaluation of the functioning of prosthesis, orthoses, stimulators etc on a patient
- o Construction
  - Test and experiments on, as well as comparisons between different types of, prosthetic and orthotic devices.

From the objective several demands that must be met by the system has been derived.

- o Measurement, analysis and result presentation should be integrated parts of the system.
- o The analysis must include the first three levels given in chapter 1, that is, basic gait parameters, kinematics and kinetics.
- o The system must be flexible enough in its use to allow for studies of a wide variety of problems concerning the human gait.
- o It must be easy to modify the system so that different kinds of measurement devices can be incorporated.

- It must be relatively easy to operate the system.

- The system must be secure. Possible failures caused by the measurement equipment or by the operator should be automatically tested for.

- The amount of time required for measurement and analysis should be kept down. A reasonable demand is that the results should be available within an hour from the patient's arrival.

- The accuracy demand differs widely between different applications. In any case it is important that the accuracy in the results are known, since otherwise it is hard to draw any useful conclusions from an experiment.

- The results should be presented in a way that is flexible and at the same time easy to understand.

Finally, the extension of the analysis will be further specified.

- The analysis is restricted to two dimensions.

The variables to be included in the analysis are

- stride length and stride frequency

- cartesian coordinates, velocities and accelerations for the ankle, knee and hip joints of both legs as well as of the segments centers of mass for the shanks, thighs and trunk.

- realtive ankle, knee and hip angles for both legs and the absolute angles of rotation for the feet, shanks, thighs and trunk. The angular velocities and accelerations should also be calculated.

- forces and moments transmitted at the ankle, knee and hip joints of both legs. However, the decomposition into muscle and joint forces is not attempted.

PART II DESCRIPTION OF THE SYSTEM

Chapter 4 gives a survey of the ENOCH system, and the following chapters contain a detailed description of the different parts of the system. The presentation is divided into four chapters following a decomposition into four subsystems:

Chapter 5. The measurement subsystem deals with the collection of measurement data and the calibration of the measurement equipment.

Chapter 6. The analysis subsystem performs the analysis of the measurement data.

Chapter 7. The result presentation subsystem produces the graphical and tabular presentation of the results of the analysis.

Chapter 8. The administration subsystem is composed of the parts that handle user-system communication, data file management, various error tests and other tasks that are not directly associated with any specific one of the other subsystems.

4. SURVEY OF THE SYSTEM

Before the system is described in detail in chapters 5-8, a brief outline of it from some aspects will be given. First a description of the functional composition is presented. Then a description of the technical realization follows. Last in this chapter the philosophy, structure, and implementation of the software are presented.

4.1 Functional survey

From a functional point of view the ENOCH system can be decomposed in several parts. See figure 1.

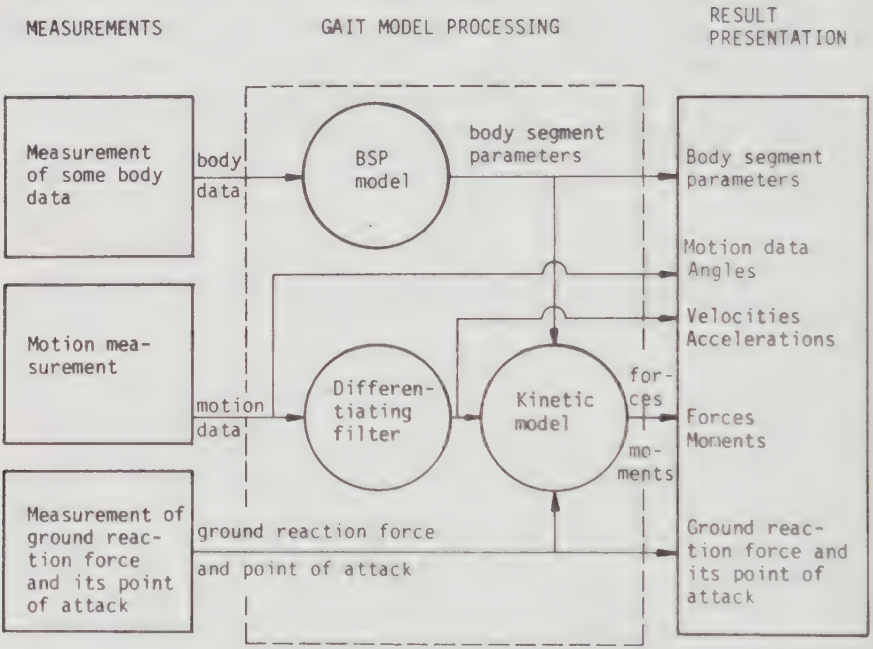

Figure 1. Functional view of the ENOCH system.

Gait model

The central part of the system is a mathematical-logical gait model of those relations that describe a human beeing during gait. In this model velocities and accelerations from measured motions are calculated. To obtain the corresponding forces and moments at the joints, the subject's mass distribution, in the form of body segment parameters, also has to be contained in the model. The accelerations, body segment parameters and also the ground reaction force and its points of attack enter a system of Newtonian equations. The solutions of these equations are the forces and moments at the joints as functions of time.

Measurements

A measurement system is needed to feed the central model with input data. This is composed of an opto-electronic system which samples the positions in two dimensions for a set of diodes attached to the subject. One or two force plates, to measure the ground reaction force and its point of attack are also parts of the measurement system. The input data must also include body measurements from which the mass distribution can be derived. Such measurements include the body weight and some characterstic distances and circumferences of the body.

Result presentation

The system contains flexible result presentation functions that handles the output in a suitable form. This is achieved by routines that can present any variable as a function of anyone else. Main forms of the result presentation are tables, displacement graphs, time diagrams and phase plane diagrams, especially symmetry diagrams. The system also includes means for automatic as well as manual scaling.

4.2 Technical realization

To get a hardware view of the ENOCH system we also present the technical realization. The system is composed of measuring equipment, a minicomputer with analog and digital input channels, output equipment and software. This is presented in figure 2.

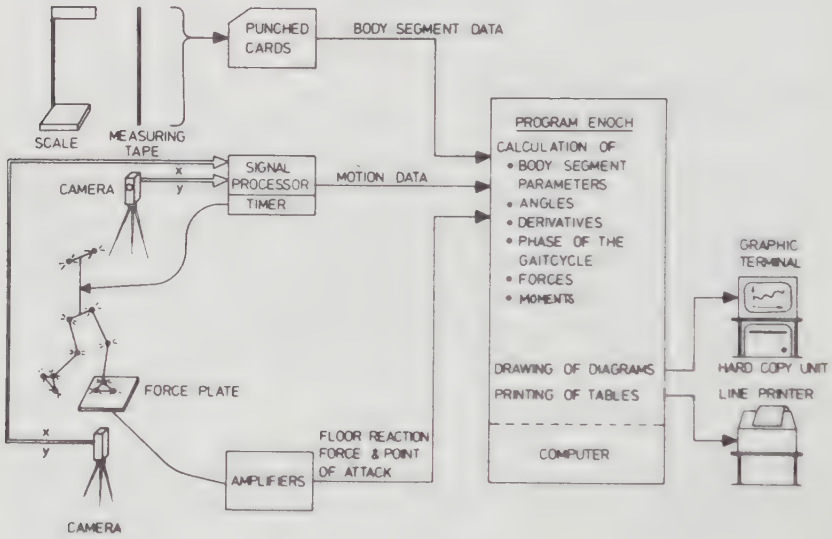

Figure 2. Technical realization of the ENOCH system.

Body measurement equipment

With a scale, or a force plate, and a measuring tape the subject's body weight and some characteristic distances and circumferences are obtained. These body data are fed into the computer before the gait measurement

Opto-electronic system

The kinematic registration is performed with an opto-electronic system (Selspot). Twelve light emitting diodes are attached to selected points of the subject such as axes, hips, knees and feet. The locations of

these diodes are measured with special cameras, where lateral photo-detectors are mounted in the focal plane of the lense for each camera. From this system, two-dimensional coordinates for the diodes are obtained in the form of electrical signals, that are transferred to the computer and stored in its memory.

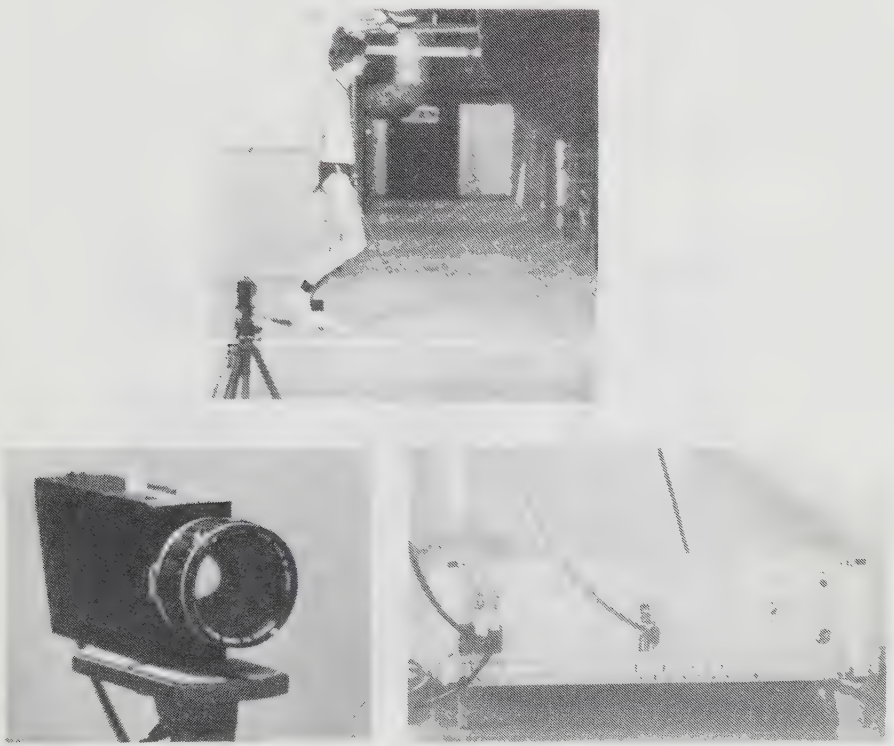

Figure 3. Selspot units: a) Diodes attached to a subject. b) Camera and c) Main unit.

Force plate equipment

In the walkway one force plate (Kistler) is positioned. (The complete system should have two force plates.) It gives the necessary ground reaction data to the computer during the experiment.

4.2

Computer

The specifications for rapid measurement and powerful analysis and result presentation require the use of a computer in the system. Therefore the opto-electronic device and the force plate are interfaced to a minicomputer (HP21 MX) with a disc memory unit. The communication with the computer is performed from a console or a graphic terminal.

Output equipment

A line printer and a graphic terminal are used to present the results. A hard copy unit is also connected with the graphic terminal.

Figure 4. Operator, console, graphic terminal with hard copy unit, and the computer.

4.3 Software philosophy, structure and implementation

Philosophy

A fundamental principle in our work with the ENOCH system has been that every function sould, if possible, be implemented in software. The advantages of such an approach are several. The system can be designed as an integrated unit with a clean and unified structure. The system will then become flexible in its use, and easy to modify and to expand. It is also relatively inexpensive to design or to modify software functions.

It is of great importance how the software is designed. The following principles are among the most important.

- To construct the system in a modular form.
- To associate modules and functions realized as subroutines.
- To work as unitarily as possibly, e.g. using common denotations, data handling, storing etc in the different modules.
- To give the programs a general form which facilitates modifications and extensions.

Another important question is whether all functions should be performed by one program package. Another alternative is to make a file centered system, for example a system where the input data are stored on a file on which one then operates with different programs. A program package solution will be easier and more secure to handle for the user, but it also makes it more difficult to use the system for more specialized purposes, not foreseen by the program writers.

Our solution is to use a program package, which we have called ENOCH, including measurement, analysis and result presentation routines. Some functional routines such as the BSP determination routine, calibration routines, test routines etc. have been separated. The effect of this is that the operator obtains command facilities by the operative system of the computer.

To obtain ease and security of operation we have chosen to use a dialogue communication form where the program asks and the operator answers questions concerning the program execution. A command controlled communication, though, could be more flexible and effective for a trained operator.

Several types of data files are being used. The data from each measurement are stored on one data file, which can be used to provide input for an analysis by the ENOCH program. The analysis can be done at any time after a measurement. Other programs can also use these files to inspect, edit or in some other way process the measurement data. This is very useful when there are errors to correct in the data, or when one wants to perform an experiment or analysis not foreseen during the system development. Beside this kind of files, which will be called "external", there are also three "internal" files, that are used by the program ENOCH to store intermediate values and final result values from an analysis. Besides decreasing the required computer time, these files also make it possible to restart the program from several points. This can be used for example if one wants to rerun the differentiation with other parameter values or if one wants to continue an analysis later.

Structure

From the operator's point of view the system looks like that one in figure 5.

Notice that to the three main functions, measurement, analysis and result presentation, the possibilities for calibration, tests and data preprocessing, are added. This software structure which governs the whole system is controlled by the operator from a console (although the operator can let a measurement be started by a separate button or by a photocell).

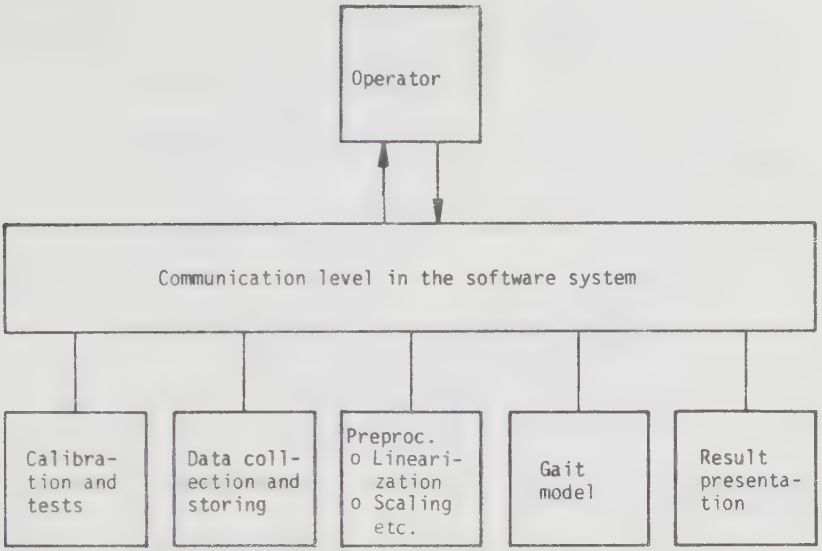

Figure 5. The system as seen by the operator.

Implementation

What has been said above about philosophy and structure of the software is implemented in the scheme in figure 6.

The program package, ENOCH, consists of the main program, 10 segments and 48 other subroutines, in Fortran and Assembler statements. Plenty of separate routines for special purposes such as a routine for computing the BSP from body data, calibration routines, routines for editing of data, test routines etc. are also written. Some of these are presented in figure 7.

The segments, denoted S1, ... , S7, in figure 6 have the only task to make it possible to place one segment at a time in the primary memory for processing, because of the limit of 24 kilowords available in the primary memory. The rest of the program is meanwhile located on the disc memory unit.

The subroutines are listed in [Gustafsson, Lanshammar, 1977]. The subroutine names and functions are also presented in figure 6. The same applies to the routines in figure 7, which also are listed in the same report.

Some sybols in figures 6 and 7 have to be explained.

Main program and segments
(A segment is a form of a subroutine)

Other subroutines

External files (Raw data file)

Internal files (Program file)

Specification of a jump to segment SX

The routine performs input

The routine performs output

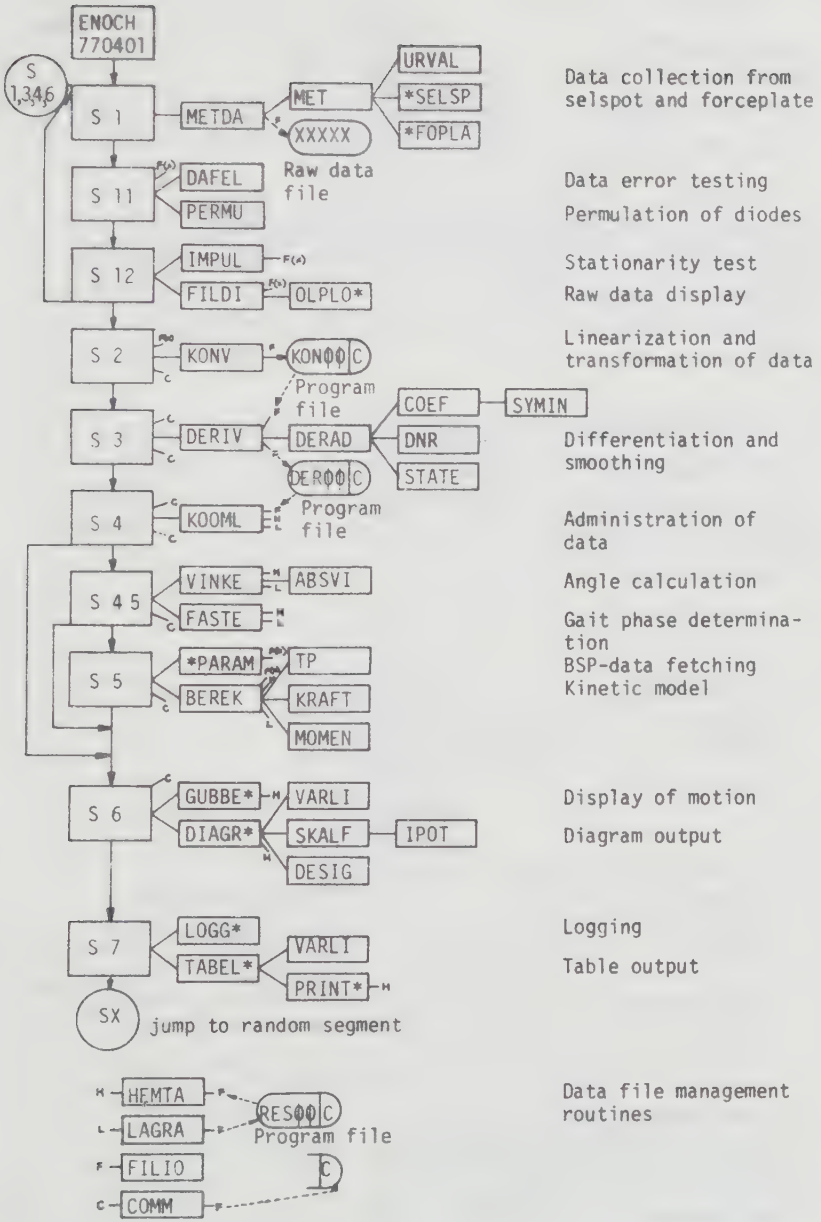

Figure 6. Structure of the program ENOCH.

Calibration of equipment

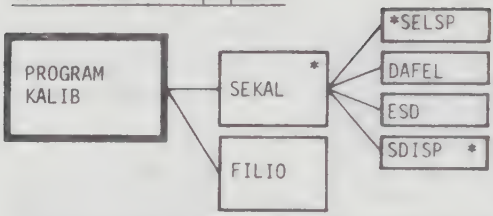

Determining body weight from forceplate measurement

Computation of body segment parameters

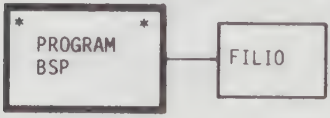

File inspection

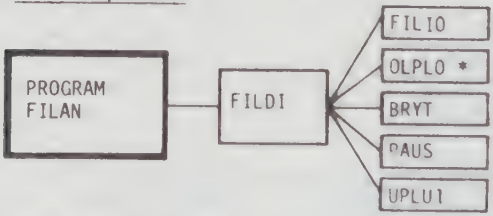

File editing of integer resp. real numbers

Automatic error detection and correction of kinematic data

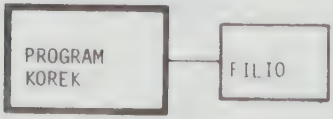

Figure 7. Some important programs.

5. MEASUREMENT SUBSYSTEM

The three types of necessary measurement data are the body segment data, the displacement data and the ground reaction forces. The techniques used for the registration of these data are described in section 5.1, 5.2 and 5.3, respectively. Section 5.4 deals with the operator control of this equipment.

Before we turn to the detailed description of the measurement equipment, the arrangement of the equipment will be given. Figure 1 describes the positioning of the cameras and the force plate. Two cameras are used to ensure that the coordinates of both legs can be recorded simultaneously.

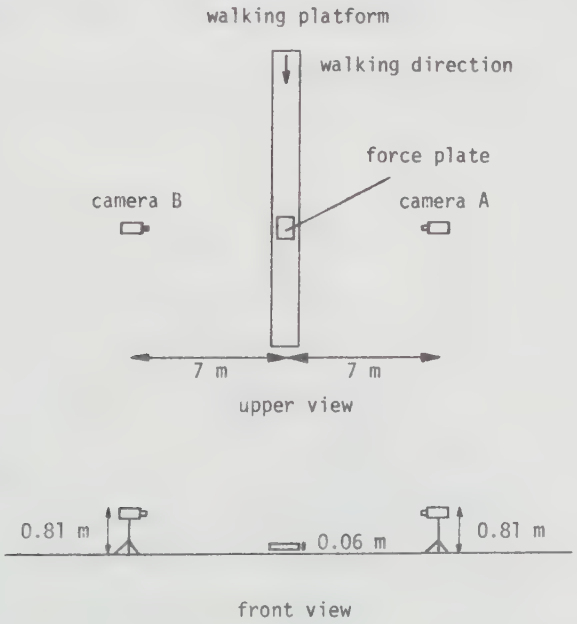

Figure 1 Measurement set up.

5.1 Body data

To obtain a description of the subject's mass distribution in the form of body segment parameters (BSP) different methods can be used. This paragraph describes the measurements needed to provide input data to our BSP calculation routine that is presented in section 6.1.

Measurements

The input data are:

- The sex
- The total body mass. This is measured with the force plate. The weight of the LCU-box (Logical Control Unit) and the shoes are also registrated.
- The distances S and s_1 - s_7, see figure 2, are measured with a measuring tape and a special measuring slide. If there are apparent differences between right and left, both distances are measured.
- The circumferential measurements p_1 - p_{10} are made with a measuring tape applied with sufficient pressure to make firm contact with the skin, but not to cause the skin to be indented. Differences between right and left are registrated.

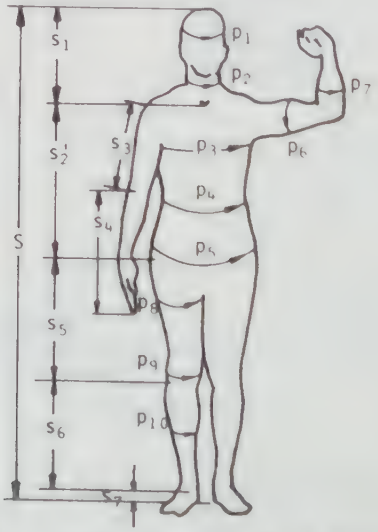

Figure 2. Distances and circumferences to be measured. (From [Contini, 1972].)

Specifications and landmarks (see figure 2)

Distances

S Total height i.e. floor - top of the head.

s_1 Top of the head - hollow of Sternum Manibrium.

s'_2 Hollow of Sternum Manibrium - Greater Trochanter of the Femur.

s_3 Acromion to Olecranon Process (Shoulder) - Elbow.

s_4 Elbow - Middle Finger Tip.

s_5 Greater Trochanter of the Femur - Medial Condyle (Knee inside).

s_6 Medial Condyle (Knee inside) - Lateral Malleolus (Anklebone outside).

s_7 Lateral Malleolus (Anklebone outside) - Floor.

The measurements of the arm s_3 and s_4, shall be made with the arm at the subject's side, with the fingers extended and palm towards the body.

The distance s'_2 is related to s_2 as $s_2 = s'_2 + 0.04 \cdot S$.

Circumferences

p_1 Head at greater circumferential extent.

p_2 Neck just below "Adam's Apple".

p_3 Chest at armpit level.

p_4 Waist at least circumferential extent.

p_5 Buttock at Greater Trochanter.

p_6 Biceps (flexed).

p_7 Forearm (flexed) at greatest circumferential extent.

p_8 Thigh at crotch level.

p_9 Knee at Medial Condyle.

p_{10} Calf at greatest circumferential extent.

The processing of these input data is described in section 6.1.

5.2 Kinematic data

The material is structured as follows: Section 5.2.1 contains the description of the equipment and program used for the kinematic data collection. 5.2.2 gives the measurement arrangement. In 5.2.3 the methods used for the calibration of the kinematic data system are described. The calibration of the camera orientation is a procedure that must be gone through each time the cameras have been moved. Therefore the technique for this calibration is described in detail in 5.2.4.

5.2.1 Measurement technique

The kinematic data are measured with an optoelectronic device, called Selspot. In this publication we will only give a short description of the main principles of this device. More detailed information can be found in [Selspot System (A)].

To obtain estimates of two-dimensional coordinates of a specified landmark on the human body, a small light emitting diode (led) is attached to that landmark. The image of the diode is focused by a lens on a semiconductor plate (see figure 3).

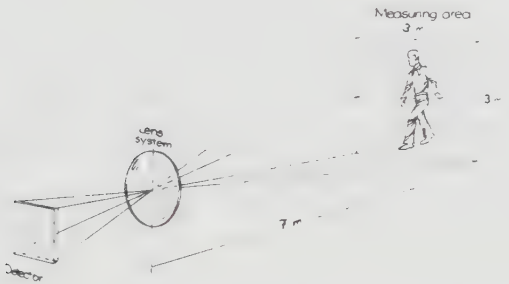

Figure 3. The subject and the camera. From [Selspot System (B)]

From four electrodes mounted on this semiconductor two currents are obtained, that are related to the two-dimensional coordinates of the light emitting diode. The equipment works with infrared light, so the result is not affected by visible light sources.

To be able to measure the coordinates of more than one point, several light emitting diodes are time multiplexed. First led no 1 gets a short pulse and its coordinates are registrated, and then no 2 gets a pulse and its coordinates are registrated, etc. When 30 diodes have been multiplexed in this fashion, a new measurement cycle starts and no 1 is pulsed again and its coordinates are registrated. Besides the 30 channels, occupied by led pulsing, two channels are used for synchronization between the led pulsing and coordinate registration parts of

the device. The time used by each channel is 99.2 μs, which gives a cycle time of 3.17 ms and thus a measurement frequency of 315 Hz for each one of the diodes. Even if the actual number of diodes is less than 30, all 30 channels are multiplexed, and the measurement frequency thus remains unchanged.

Figure 4 shows the different parts of the optoelectronic device, together with the computer.

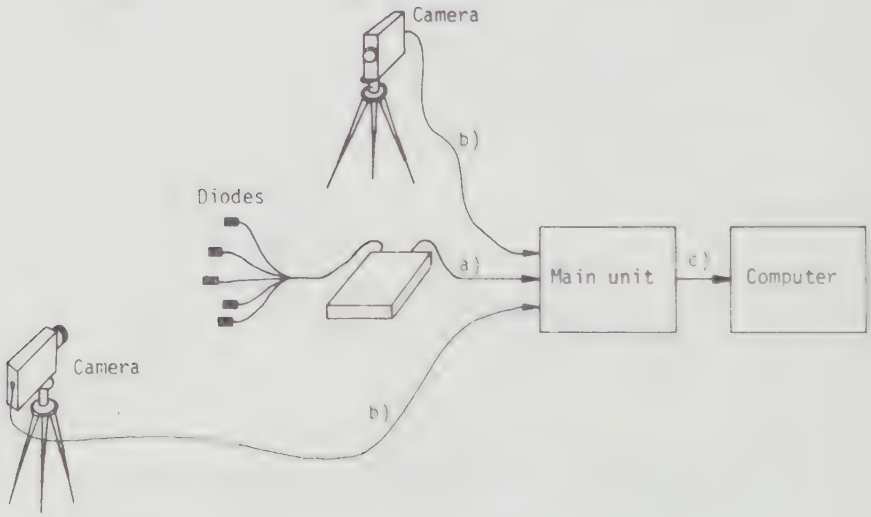

Figure 4. Selspot equipment.

The led control unit (LCU), which is carried by the measurement subject, contains the master clock of the system. The LCU performs the time multiplexing of the diodes. Cable a) carries power to the diodes and synchronization pulses for a slave clock contained in the main unit. Thereby the slave clock is kept in phase with the master clock.

The measurement device contains two cameras. Diode no 1, 3, 5, ..., are tracked by one camera, and diode no 2, 4, 6, ..., by the other one. Each camera contains lens, semiconductor plate and high gain amplifiers for the electrode currents from the semiconductor. Cables b) carry the measurement signals to the main unit.

The main unit contains a 10 bits A/D-converter. First x_m (voltage corresponding to the horizontal diode coordinate) is converted, and then y_m (voltage corresponding to the vertical diode coordinate). The digital signals are transferred to the computer by cable c) in the order: x_m diode 1, y_m diode 1, x_m diode 2, y_m diode 2, ...

Besides the 10 data bits, cable c) also transfers the following information to the computer

- Synchronization pulse indicating when the A/D-converter has performed a conversion.
- System on, informing the computer whether the main unit of the measurement device has power on or not.
- Channel sync, indicating when a new measuring cycle starts. This signal makes it possible to identify diode no 1.
- Synchronization fail, indicating a failure in the synchronization between the master clock of the device and the slave clock in the main unit.
- Overload, indicating that the semiconductor detector in a camera is saturated.
- Out of range, indicating that the semiconductor detector in a camera is not receiving enough light effect from the corresponding led.

Cable c) also carries one control bit from the computer to the measurement device. When the computer is ready to store measurement data, this bit contains a pulsed signal that will light an indicator lamp on the panel of the main unit, informing the operator that the computer is ready for a measurement. This feature is valuable when the computer is not located in the same room as the measurement equipment. Cable c) is connected to a 16 bits microcircuit interface card from which the data are read into the core memory of a HP-21MX computer (16 bits word length).

A program called SELSP, written in HP assembler, controls the storing of the data in core memory. The program has the following major parameters that can be optionally chosen by the user.

NCYK - number of measurement cycles to be stored.

KCYK - cycle no 1, KCYK + 1, 2·KCYK + 1 are stored.

NKAM1 - number of utilized diodes for camera 1.

NKAM2 - number of utilized diodes for camera 2.

The effective measurement frequency, f, is thus given by

$$f = \frac{315}{KCYK} \quad Hz$$

and the total measurement time, T, is

$$T = \frac{(NCYK-1)}{f} = \frac{(NCYK-1)\cdot KCYK}{315} \quad sec.$$

The number of cycles that can be stored is limited by the available number of cells in core memory, NCELL. Since the measurement is two-dimensional each sample from one diode occupies two cells in core memory and the maximum number of cycles that can be stored is

$$NCYK_{max} = \frac{NCELL}{2\cdot(NKAM1+NKAM2)}$$

and the total measurement time is thus limited by

$$T_{max} = \frac{\left(\frac{NCELL}{2\cdot(NKAM1+NKAM2)} - 1\right)\cdot KCYK}{315}$$

In the present configuration the number of cells in core memory, reserved for displacement data, is 10 000 and 6 diodes are tracked by each camera. Thus the maximum measurement time is

$$T_{max} = \frac{\left(\frac{10000}{24} - 1\right)\cdot KCYK}{315} = 1.32\cdot KCYK \text{ sec.} \quad \text{where KCYK = 1, 2, 3, ...}$$

For gait measurements, KCYK has often been given the value 2, which implies the measurement frequency 157.5 Hz and the maximum measurement time 2.64 s.

One very important feature with the program SELSP is that it has to operate with very high speed. The time interval between the incoming synchronization pulses from the measurement device is 24.8 μs, which means that program SELSP must be able to perform all its tasks within that time. Otherwise data will be lost and the sampling frequency of the stored data will be unknown.

To make SELSP sufficiently fast it is written in HP assembler language and all input operations are handled by the program. However, user-defined input operations are not allowed when working under Disc Operating System (DOS). It is thus necessary to inactivate DOS during the execution of SELSP. Since it is desirable to incorporate SELSP as an integrated part of the measurement and analysis program package and this package must be executed under DOS, the inactivating and subsequent activating of the DOS system have been implemented as an automatic feature of program SELSP.

The basic structure of the program SELSP is outlined in figure 5.

For a complete description of program SELSP the reader is referred to the program list in [Gustafsson, Lanshammar, 1977].

5.2.1

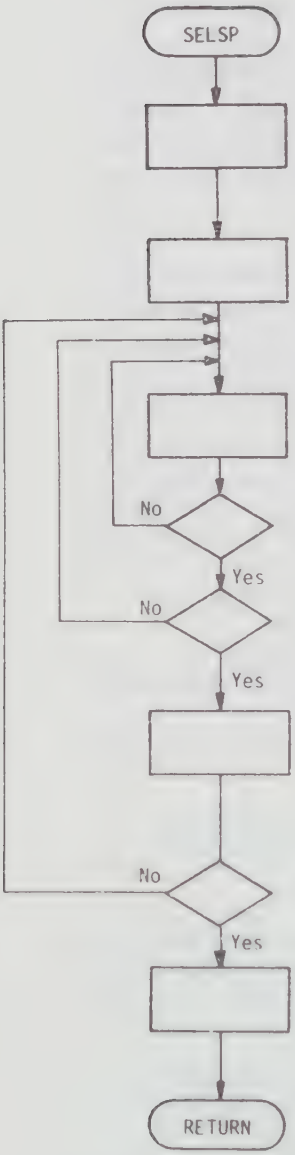

DOS is inactivated.

Control pulses are sent to the measurement main unit, informing that the computer is ready for measurement.

One data word is read from the micro circuit interface.

Did the data correspond to diode no. 1?

Have (KCYK-1) cycles been exluded from storing?

Control pulses are sent to the equipment. Data for diodes no. 1, 3, 5,.... NKAM1 and 2, 4,..., NKAM2 are read and stored

Have NCYK cycles been stored?

DOS is activated.

Figure 5. Basic structure of program SELSP.

5.2.2 Measurement arrangement

Figure 1 describes the measurement set up. Lenses with focal distance 50 mm are used and the detectors are squares with each side 20 mm which yields a measurementarea of 3 x 3 m (see figure 6).

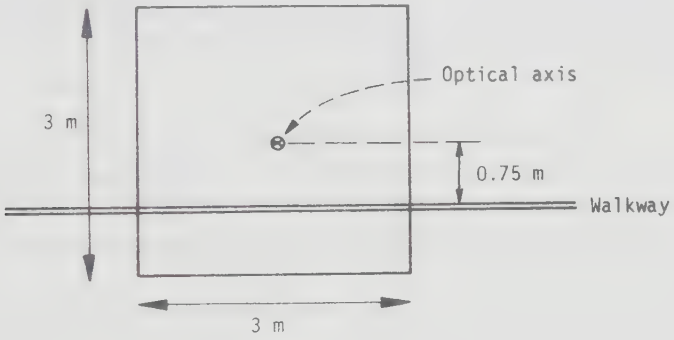

Figure 6. Measurement area.

Each camera is tracking six diodes mounted on one side of the subject according to figure 7.

Diode number	location
1, 2	hip joint
3, 4	knee joint
5, 6	ankle joint
7, 8	heel
9,10	toe base
11,12	shoulder

Figure 7. Location of landmarks

5.2.3 Calibration of the measurement system

Due to various effects, the output from the optoelectronic device will not be linearly related to the cartesian coordinates of the corresponding diode. The major causes are

- reflexion of the infrared light in the floor
- lens distortion
- the characteristics of the detector and the electronics. For simplicity they will be lumped together and referred to as the detector characteristics.

In this section these effects will be described together with the methods that we have developed for their compensation. The compensation and the coordinate transformation, described in section 5.2.4 are implemented in subroutine KONV, a list of which is found in [Gustafsson, Lanshammar, 1977].

It should be stressed that the purpose of the compensation was to reduce the resulting coordinate error, and not to obtain a model that is as good as possible of each one of the individual error sources. The obtained result was a reduction of the root mean squares error for any location within the measured area (3 x 3 m) from approximately 3 cm before compensation to less than 1 cm afterwards.

It is important to notice that the compensation must be applied in the reverse order as compared to the order of their original application. The compensation can be compared to the problem of undoing several knots on a string that has been tied one above the other. To untie these knots one must start with the knot that was last knitten, and finish with the one first knitten.

To each one of the effects we associate a coordinate transformation describing the effect (see figure 8).

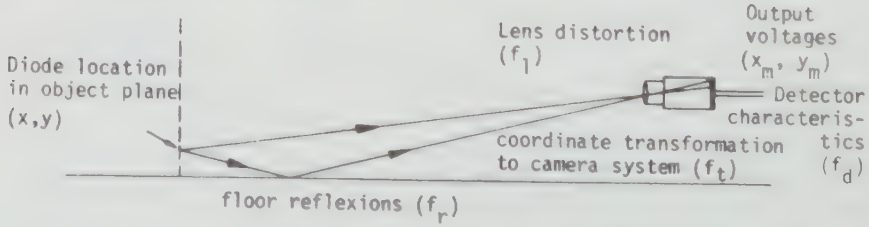
Diode location in object plane (x,y)
Lens distortion (f_l)
Output voltages (x_m, y_m)
Detector characteristics (f_d)
coordinate transformation to camera system (f_t)
floor reflexions (f_r)

Figure 8. Transformations characterizing the optoelectronic device.

f_r describes the reflexion

f_t describes the coordinate transformation from a coordinate system fixed in the measurement plane to a system in the camera. Although this transformation will be described in the next section, it is mentioned in this context because the reflexion is room dependent and therefore should be described in a coordinate system, fixed with respect to the measurement plane, while the lens distortion and detector characteristics should be described in a coordinate system fixed with respect to the camera

f_l describes the lens distortion

f_d describes the detector characteristics.

With each one of the transformations we also associate a coordinate system defined by

$$\begin{bmatrix} x_r \\ y_r \end{bmatrix} = f_r \left(\begin{bmatrix} x \\ y \end{bmatrix} \right)$$

$$\begin{bmatrix} x_t \\ y_t \end{bmatrix} = f_t \left(\begin{bmatrix} x_r \\ y_t \end{bmatrix} \right)$$

$$\begin{bmatrix} x_l \\ y_l \end{bmatrix} = f_l \left(\begin{bmatrix} x_t \\ y_t \end{bmatrix} \right)$$

$$\begin{bmatrix} x_d \\ y_d \end{bmatrix} = f_d \left(\begin{bmatrix} x_l \\ y_l \end{bmatrix} \right)$$

$$\begin{bmatrix} x_m \\ y_m \end{bmatrix} = \left(\begin{bmatrix} x_d \\ y_d \end{bmatrix} \right)$$

The somewhat loosely defined coordinate systems will be more precisely given below when the transformations are specified. These coordinate systems will be referred to as 0, 0_r, 0_t, 0_l, 0_d and 0_m.

The true diode location and the output voltages are related by

$$\begin{bmatrix} x_m \\ y_m \end{bmatrix} = f_d \left(f_l \left(f_t \left(f_r \left(\begin{bmatrix} x \\ y \end{bmatrix} \right) \right) \right) \right)$$

To compute the diode coordinates from $\begin{bmatrix} x_m \\ y_m \end{bmatrix}$, the above equation is solved with respect to $\begin{bmatrix} x \\ y \end{bmatrix}$

$$\begin{bmatrix} x \\ y \end{bmatrix} = f_r^{-1}\left(f_t^{-1}\left(f_l^{-1}\left(f_d^{-1}\left(\begin{bmatrix} x_m \\ y_m \end{bmatrix}\right)\right)\right)\right)$$

For this estimation it is thus necessary to find the inverses of the transformations describing the different effects, and to apply them in the reverse order. These transformations are only partially known and measurable, so it will be necessary to work with estimates of them.

The coordinates will be estimated by

$$\begin{bmatrix} \hat{x} \\ \hat{y} \end{bmatrix} = \hat{f}_r^{-1} \left(\hat{f}_t^{-1} \left(\hat{f}_l^{-1} \left(\hat{f}_d^{-1} \left(\begin{bmatrix} x_m \\ y_m \end{bmatrix} \right) \right) \right) \right)$$

where our estimated transformations $\hat{f}_r^{-1}$, $\hat{f}_t^{-1}$, $\hat{f}_l^{-1}$, $\hat{f}_d^{-1}$ will now be described.

Detector characteristics

Beside local nonlinearities in the detector surface, not to be modelled but instead regarded as a noise source, the detector has different amplification in the horizontal (x) and vertical (y) directions, as

illustrated by figure 9. It should be noted that the effect is exaggerated in figure 9, which also applies to figures 10, 11 and 13.

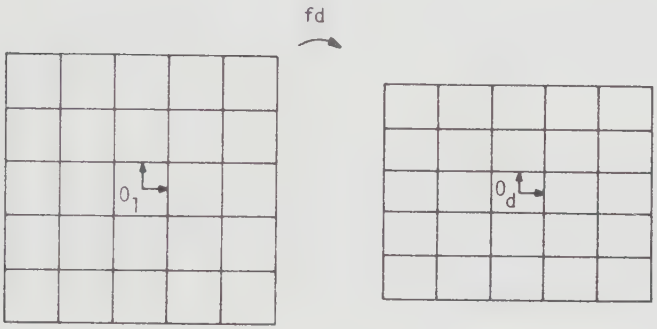

Figure 9. Detector characteristics.

This difference in amplification amounts to approximately 4%. It is modelled by the transformation f_d. The horizontal amplification is arbitrarily defined as unity, which gives the following model for f_d

$$\begin{bmatrix} x_d \\ y_d \end{bmatrix} = \hat{f}_d \left(\begin{bmatrix} \hat{x}_1 \\ \hat{y}_1 \end{bmatrix} \right) = \begin{bmatrix} 1 & 0 \\ 0 & k \end{bmatrix} \begin{bmatrix} \hat{x}_1 \\ \hat{y}_1 \end{bmatrix}$$

$$\Rightarrow$$

$$\begin{bmatrix} \hat{x}_1 \\ \hat{y}_1 \end{bmatrix} = \hat{f}_d^{-1} \left(\begin{bmatrix} x_d \\ y_d \end{bmatrix} \right) = \begin{bmatrix} 1 & 0 \\ 0 & \frac{1}{k} \end{bmatrix} \begin{bmatrix} x_d \\ y_d \end{bmatrix} = \begin{bmatrix} 1 & 0 \\ 0 & \frac{1}{k} \end{bmatrix} \begin{bmatrix} x_m \\ y_m \end{bmatrix}$$

To determine the factor 1/k two diodes were placed at the same distance (0.5 m) from the optical axis, one along the vertical and one along the horizontal detector axis, and 7 meters from the camera. The camera was placed high above the floor to avoid floor reflexions. By locating the diodes at the same distance from the optical axis, the lens distortion, which is circular symmetric, does not affect the result.

5.2.3

Results for the two detectors:

Camera A: k = 1.048
Camera B: k = 1.033

The number of significant digits is less than the number of presented digits. We are merely presenting the values that are implemented in the error compensation routine.

Lens nonlinearity

The dominant nonlinearity due to the lens, which can be assumed to be radially symmetric, is illustrated by figure 10. This type of error is often called lens distortion.

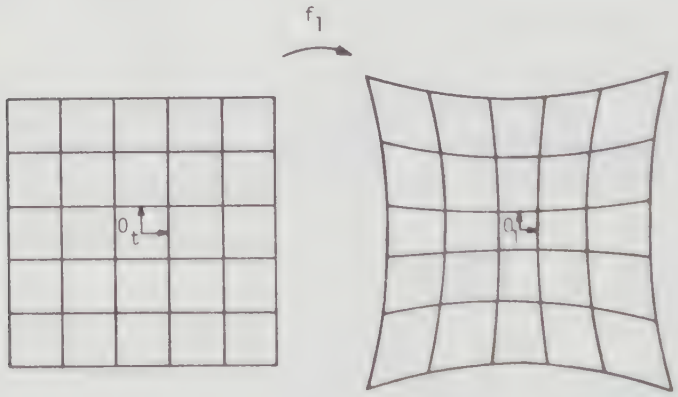

Figure 10. Lens distortion.

The distortion gives a maximal coordinate error of 5%. The transformation corresponding to the lens distortion is described with the function f_1.

f_1^{-1} was modelled by

$$\begin{bmatrix} \hat{x}_t \\ \hat{y}_t \end{bmatrix} = \hat{f}_1^{-1} \left(\begin{bmatrix} \hat{x}_1 \\ \hat{y}_1 \end{bmatrix} \right) = \begin{bmatrix} \sum_{i=0}^{n} a_i r_1^{\,i} & 0 \\ 0 & \sum_{i=0}^{n} a_i r_1^{\,i} \end{bmatrix} \begin{bmatrix} \hat{x}_1 \\ \hat{y}_1 \end{bmatrix}$$

where

$$r_1 = x_1^{\,2} + y_1^{\,2}$$

and $a_0, \ldots, a_n$ are model parameters. The parameters were determined by least square fitting to 20 different diode locations. The diodes were placed high above the floor to avoid floor reflexions from affecting the result. It was found suitable to use a second order model (n=2).

Result a_0=1.0866, a_1=-0.20743, a_2=0.076856

Our approach to the problem of lens distortion has some similarities with but is independent of the one described in [Woltring, 1975].

Coordinate transformation

The transformation $\hat{f}_t^{-1}$ from the camera system to the metric analysis system is described in the next section titled "Calibration of the camera positioning". The resulting transformation is

$$\begin{bmatrix} \hat{x}_r \\ \hat{y}_r \end{bmatrix} = \hat{f}_t^{-1} \left(\begin{bmatrix} \hat{x}_t \\ \hat{y}_t \end{bmatrix} \right)$$

This transformation is illustrated by figure 11.

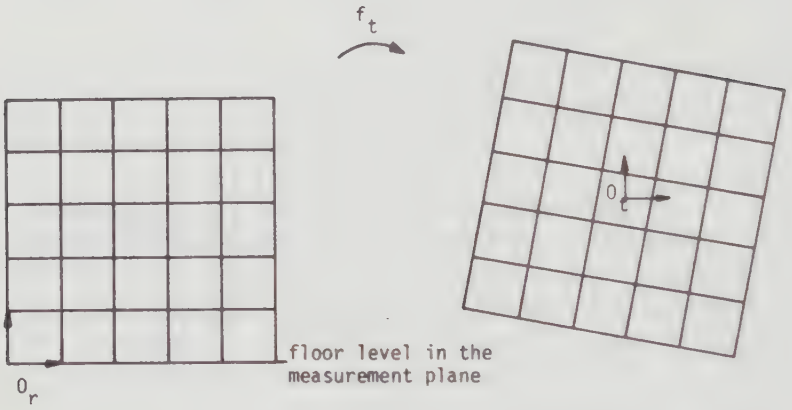

Figure 11. Coordinate transformation from a coordinate system in the measurement plane to a coordinate system in the camera.

Reflexions in the floor

The light from a diode is partly reflected in the floor according to figure 12.

Figure 12. Reflexions in the floor.

The effect of this reflexion is that the center of the light hitting the detector surface will be moved upward. Since the signal produced by the detector is corresponding to the light center, this will result in an apparent diode location that is nearer to the floor than the true position.

Assuming ideal lens and detector the image of a rectangular coordinate system will be according to figure 13.

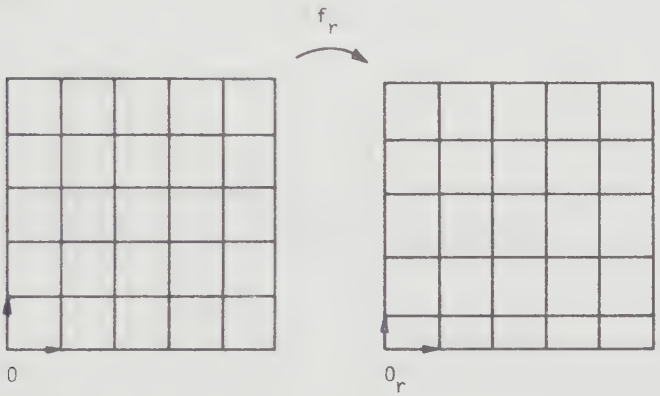

Figure 13. Floor reflexions.

The magnitude of the coordinate error due to reflexion is depending on the floor material. By covering the concrete floor with masonite we decreased the maximum error from approximately 10 cm to 4 cm.

The following assumptions are made about the reflexions:

- The horizontal (x) coordinate is not affected.
- The vertical coordinate (y) is affected by a factor only depending on the distance from the floor to the diode.
- No reflexions occur when the diode is placed in the floor level.
- The nonlinearities in the vertical coordinate can be modelled by a polynomial.

From these assumptions we get the following model for the inverse transformation f_r^{-1}:

$$\begin{bmatrix} \hat{x} \\ \hat{y} \end{bmatrix} = \hat{f}_r^{-1}\left(\begin{bmatrix} \hat{x}_r \\ \hat{y}_r \end{bmatrix}\right) = \begin{bmatrix} 1 & 0 \\ 0 & \sum_{i=0}^{n} b_i \cdot \hat{y}_r{}^i \end{bmatrix} \begin{bmatrix} \hat{x}_r \\ \hat{y}_r \end{bmatrix}$$

The parameters $b_0, \ldots, b_n$ were determined by least square fitting to 21 different diode locations. It was found suitable to use a third order model.

Result: $b_0 = 1.2475$, $b_1 = -0.43393$, $b_2 = 0.32306$, $b_3 = -0.08165$.

If y-coordinates on the floor are to be unchanged by this transformation it is important that the coordinates $(\hat{x}_r, \hat{y}_r)$ are defined in such a way that $\hat{y}_r = 0$ when the diode is in floor level. This is taken care of by the transformation $\hat{f}_t^{-1}$, from a system in the camera to a system fixed in the measurement plane.

Result of the compensation

To evaluate the compensation the following experiment was performed:

Diodes were placed at 35 different locations of the measurement plane with the true coordinate positions

x=0.30, 0.70, 1.10, 1.50, 1.90, 2.30, 2.70

and for each one of these x-coordinates

y=0, 0.40, 0.80, 1.20, 1.50.

The measured coordinate value for each diode location was calculated as the mean value over 100 samples.
When only a linear coordinate transformation was applied the following coordinate errors were noted:

Maximal errors	Root mean squares deviations over the 35 diode locations
$\Delta x_{max} = 0.087$ m	$\sigma_x = 0.025$ m
$\Delta y_{max} = 0.117$ m	$\sigma_y = 0.034$ m

When the compensation, described in this section, was applied the errors were reduced to:

Maximal errors	Root mean squares deviations over the 35 diode locations
$\Delta x_{max} = 0.031$ m	$\sigma_x = 0.010$ m
$\Delta y_{max} = 0.026$ m	$\sigma_y = 0.014$ m

Thus, by the compensation the expected coordinate error is reduced by approximately a factor 2.5, so after compensation the expected systematic coordinate error is approximately 0.01 m. Besides this error there is also a stochastic error, due to measurement noise, which is not appreciably altered by the compensation and which has a standard deviation of approximately 0.003 m. Since the values given above are mean values of 100 samples, the stochastic error does not appreciably affect these values.

5.2.4 Calibration of the camera positioning

Since two cameras are used for the coordinate measurement it is necessary to define one coordinate system, that is fixed with respect to the walkway, in which all coordinates are to be expressed.

Ideally the two cameras are to be positioned so that their optical axes are coinciding. These optical axes intersect the measurement plane according to figure 14. We will define the ideal optical axis as the straight line connecting the centers of the two camera lenses.

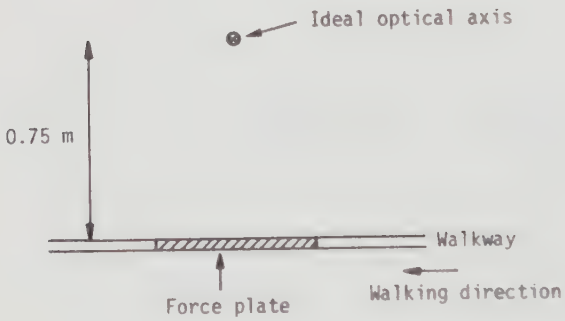

Figure 14. Intersection of the ideal optical axis with the measurement plane.

In practice, this can not be exactly achieved. Instead, the optical axis of each camera will intersect the measurement plane at another point, which is illustrated by figure 15. The effects have been strongly exaggerated. In practice the cameras are aligned within 0.1^{o}.

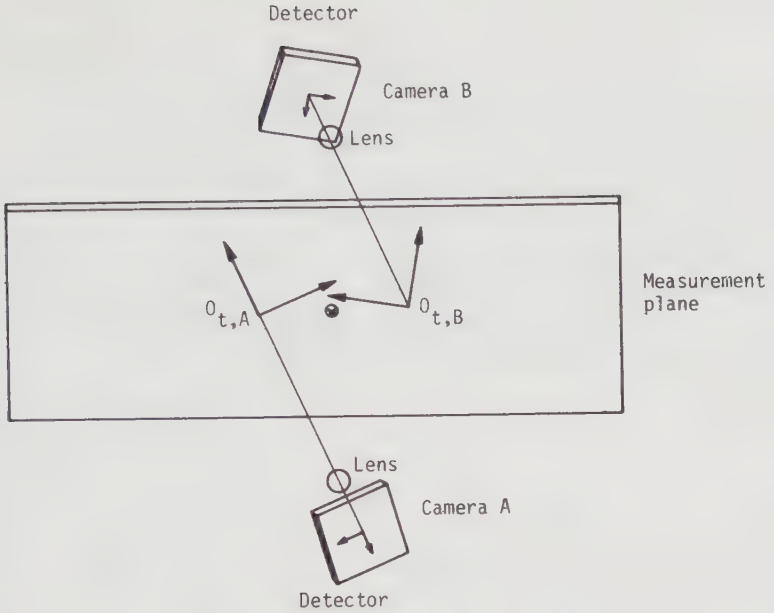

Figure 15. Illustration of the position and orientation of the camera systems when the cameras are not perfectly oriented.

In this section a method is described for automatic calibration of the camera orientation.

For this calibration a special calibration board has been constructed according to figure 16.

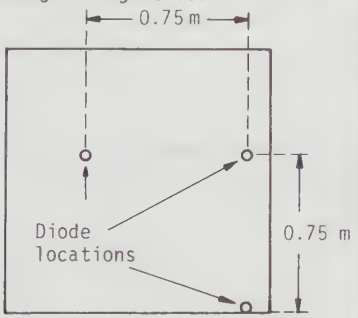

a)

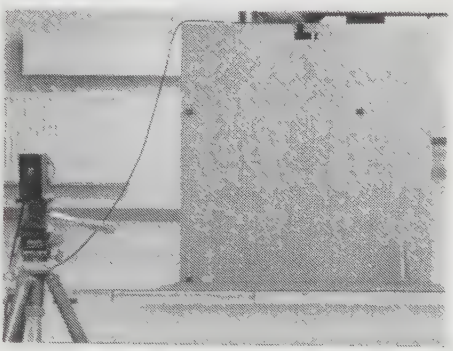

b)

Figure 16. Calibration platform. 3 diodes are mounted on each side of the platform. On the backside the diodes are mounted on the same locations. a) Schematic diagram of the platform seen from camera A. b) Photography of platform and camera B.

5.2.4

The calibration board is placed in the measurement plane so that diode 1 is coinciding with the ideal optical axis of the cameras. A measurement is then done under the control of a special calibration program, called SEKAL, that registrates the location of the diodes during 100 cycles. The coordinates, as measured in the coordinate system 0_t (compensated for detector and lens characteristics according to section 5.2.3), of the 3 diodes tracked by camera B will be called $(\hat{x}_1, \hat{y}_1)$, $(\hat{x}_2, \hat{y}_2)$, $(\hat{x}_3, \hat{y}_3)$. The estimates are mean values over the 100 samples. The rotation angle of the camera defined by figure 17 is called α.

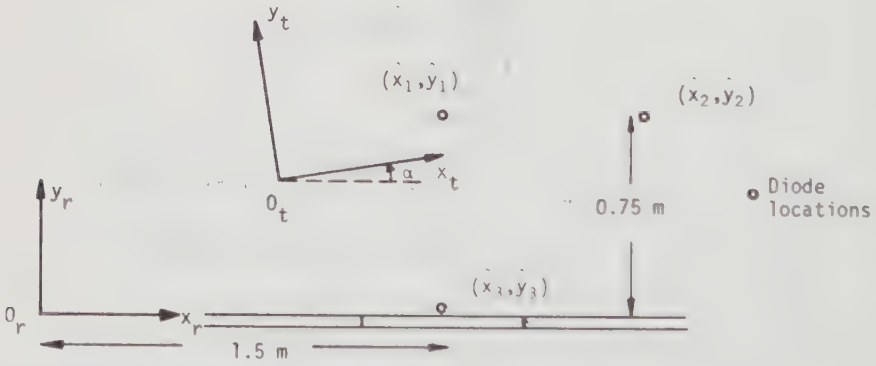

Figure 17. Coordinate system of camera B.

The coordinate transformation can be divided into four steps, as illustrated in figure 18.

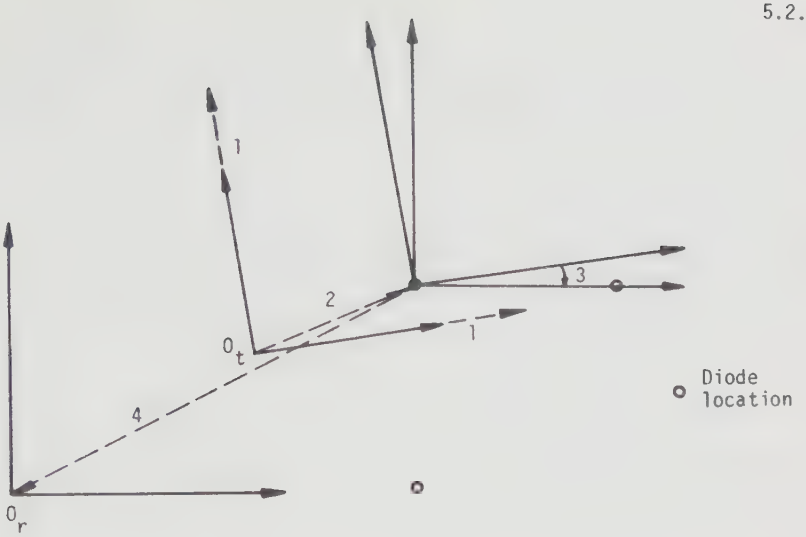

Figure 18. The different steps of the coordinate transformation.

1. Scaling of the coordinate axes. Different scaling factors SKX and SKY are used to decrease the remaining error.
2. Translation of the coordinate system to the ideal optical axis.
3. Rotation into horizontal and vertical directions.
4. Translation into a coordinate system with the origin on the floor and 1.5 meter from the projection of the optical axis on the floor.

Using the notations introduced in the preceding section, the transformation becomes

$$\begin{bmatrix}\hat{x}_r\\ \hat{y}_r\end{bmatrix} = \hat{f}_t^{-1}\left(\begin{bmatrix}\hat{x}_t\\ \hat{y}_t\end{bmatrix}\right) = \begin{bmatrix}\cos\alpha & -\sin\alpha\\ \sin\alpha & \cos\alpha\end{bmatrix}\left\{\begin{bmatrix}SKX & 0\\ 0 & SKY\end{bmatrix}\left(\begin{bmatrix}\hat{x}_t\\ \hat{y}_t\end{bmatrix} - \begin{bmatrix}x_{ko}\\ y_{ko}\end{bmatrix}\right)\right\} + \begin{bmatrix}x_o\\ y_o\end{bmatrix}$$

where the parameters

α	angle of rotation
SKX	scale factor in x-direction
SKY	scale factor in y-direction
$\begin{bmatrix}x_{ko}\\ y_{ko}\end{bmatrix}$	coordinates of the ideal optical axis expressed in the scaled O_t system

$\begin{bmatrix} x_o \\ y_o \end{bmatrix}$ coordinates of the ideal optical axis expressed in the system O_r

are yet to be determined.

To estimate these parameters we use the measured coordinates of the 3 calibration diodes. These coordinates must be expressed in the coordinate system O_t, i.e. they must be detector and lens distortion compensated by the transformations $\hat{f}_d^{-1}$ and $\hat{f}_l^{-1}$.

The parameters $\begin{bmatrix} x_o \\ y_o \end{bmatrix}$ are independent of the camera orientation. In the final system, compensated for reflexions, it equals $\begin{bmatrix} 1.5 \\ 0.75 \end{bmatrix}$ and hence

$$\begin{bmatrix} 1.5 \\ 0.75 \end{bmatrix} = \hat{f}_r^{-1}\left(\begin{bmatrix} x_o \\ y_o \end{bmatrix}\right)$$

According to the preceding section 5.2.3 we have

$$\hat{f}_r^{-1} = \begin{bmatrix} 1 & 0 \\ 0 & 1.2475-0.43393y_o+0.32306y_o^2-0.08165y_o^3 \end{bmatrix}$$

which gives

$$\begin{bmatrix} 1.5 \\ 0.75 \end{bmatrix} = \begin{bmatrix} 1 & 0 \\ 0 & 1.2475-0.43393y_o+0.32306y_o^2-0.08165y_o^3 \end{bmatrix}\begin{bmatrix} x_o \\ y_o \end{bmatrix}$$

This equation can be solved to give

$$\begin{bmatrix} x_o \\ y_o \end{bmatrix} = \begin{bmatrix} 1.5 \\ 0.69812 \end{bmatrix} = \hat{f}_r\left(\begin{bmatrix} 1.5 \\ 0.75 \end{bmatrix}\right)$$

Now from the known positions of the 3 calibration diodes we get the following equations

$$\begin{bmatrix}1.5\\0.75\end{bmatrix} = \hat{f}_r^{-1}\left(\hat{f}_t^{-1}\left(\begin{bmatrix}\hat{x}_1\\\hat{y}_1\end{bmatrix}\right)\right)$$

$$\begin{bmatrix}2.25\\0.75\end{bmatrix} = \hat{f}_r^{-1}\left(\hat{f}_t^{-1}\left(\begin{bmatrix}\hat{x}_2\\\hat{y}_2\end{bmatrix}\right)\right) \quad \Rightarrow$$

$$\begin{bmatrix}1.5\\0\end{bmatrix} = \hat{f}_r^{-1}\left(\hat{f}_t^{-1}\left(\begin{bmatrix}\hat{x}_3\\\hat{y}_3\end{bmatrix}\right)\right)$$

$$\begin{cases} \hat{f}_r\begin{bmatrix}1.5\\0.75\end{bmatrix} = \begin{bmatrix}1.5\\0.69812\end{bmatrix} = \hat{f}_t^{-1}\left(\begin{bmatrix}\hat{x}_1\\\hat{y}_1\end{bmatrix}\right) \\ \hat{f}_r\begin{bmatrix}2.25\\0.75\end{bmatrix} = \begin{bmatrix}2.25\\0.69812\end{bmatrix} = \hat{f}_t^{-1}\left(\begin{bmatrix}\hat{x}_2\\\hat{y}_2\end{bmatrix}\right) \\ \hat{f}_r\begin{bmatrix}1.5\\0\end{bmatrix} = \begin{bmatrix}1.5\\0\end{bmatrix} = \hat{f}_t^{-1}\left(\begin{bmatrix}\hat{x}_3\\\hat{y}_3\end{bmatrix}\right) \end{cases}$$

From this set of equations the remaining parameters can be obtained. The result is

$$\begin{bmatrix}SKX^2\\SKY^2\end{bmatrix} = \frac{1}{(\hat{x}_2-\hat{x}_1)^2(\hat{y}_3-\hat{y}_1)^2-(\hat{x}_3-\hat{x}_1)^2(\hat{y}_2-\hat{y}_1)^2}\begin{bmatrix}(\hat{y}_3-\hat{y}_1)^2 & -(\hat{y}_2-\hat{y}_1)^2\\-(\hat{x}_3-\hat{x}_1)^2 & (\hat{x}_2-\hat{x}_1)^2\end{bmatrix}\begin{bmatrix}0.75^2\\0.69812^2\end{bmatrix}$$

$$\begin{bmatrix}x_{ko}\\y_{ko}\end{bmatrix} = \begin{bmatrix}SKX\cdot\hat{x}_1\\SKY\cdot\hat{y}_1\end{bmatrix}$$

For α, two solutions are obtained. The first

$$\alpha_1 = \tan^{-1}\left[\frac{SKY\cdot(\hat{y}_1-\hat{y}_2)}{SKX\cdot(\hat{x}_2-\hat{x}_1)}\right]$$

corresponds to making the x-axis of the camera system horizontal, and the second

$$\alpha_2 = \tan^{-1}\left[\frac{SKX\cdot(\hat{x}_3-\hat{x}_1)}{SKY\cdot(\hat{y}_3-\hat{y}_1)}\right]$$

corresponds to making the y-axis of the camera system vertical. If the axes of the camera system are not exactly perpendicular, α_1 and α_2 will differ. We will use the mean value of α_1 and α_2 as our estimate.

$$\alpha = \frac{1}{2}\left\{\tan^{-1}\left[\frac{SKY\cdot(\hat{y}_1-\hat{y}_2)}{SKX\cdot(\hat{x}_2-\hat{x}_1)}\right] + \tan^{-1}\left[\frac{SKX\cdot(\hat{x}_3-\hat{x}_1)}{SKY\cdot(\hat{y}_3-\hat{y}_1)}\right]\right\}$$

Results analogue to this apply for camera A.

When a calibration measurement has been done the program SEKAL calculates the parameters according to the above equations for both cameras. These parameters are then stored on a file on disc memory to be used for coordinate transformation of subsequently collected measurement data.

5.3. Force plate data

To measure the ground reaction forces a piezo-electric force plate made by Kistler is utilized. The signals are amplified in charge amplifiers. The discussion here will not include the characteristics of these components, but rather describe how they are integrated with the rest of the ENOCH system. For details of the Kistler's hardware the reader is referred to [Kistler, 1974], and [Kistler, 1972].

The force plate is hidden in the walkway by masonite that covers the entire surface of the walkway. The philosophy is that the subject does not know that the force plate exists, and if he misses it the measurement is restarted until finally the subject unconsiously steps on the force plate.

The force plate is located in the middle of the measurement area, according to figure 1, allowing space for the measurement of approximately one gait cycle before leaving the force plate and one gait cycle after entering the force plate.

The force plate measurement includes three variables; total horizontal force $F_x = F_{x_1} + F_{x_2}$, vertical force on front end of the force plate F_y and vertical force on rear end of the force plate F_{y_2}, according to figure 19.

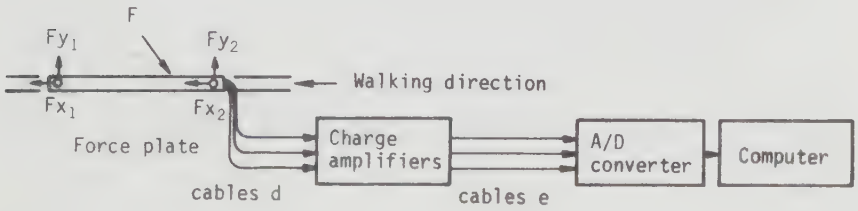

Figure 19. The force plate.

The piezoelectric crystals are charged with charges proportional to the applied forces. These charges are transformed into proportional voltages by the charge amplifiers. Finally, the voltages are digitized in a 10-bits A/D converter from which the data are transferred to the computer core memory by a routine called FOPLA. Each time FOPLA is called, the three channels of the A/D converter, containing force plate data, are stored in consecutive cells in the primary memory.

During a gait measurement, the coordinates of the light emitting diodes mounted on the subject and the force plate data are to be recorded simultaneously. However, the force plate data can, but does not need to be sampled with the same sampling frequency as the coordinate data. The high sampling frequency utilized for coordinate data is motivated by the noise sensitive numerical differentiation that must be performed to obtain estimates of velocities and accelerations. Once this differentiation is performed, only a fraction of the result is saved. This fraction is automatically chosen so that not more than 150 samples are saved over the entire measurement interval. This figure has been regarded sufficient for getting a reasonable time resolution, and at the same time keeping computing time and memory requirement within reasonable limits.

If for instance 400 samples of coordinate data are to be measured, then after differentiation only 1/3 of the resulting derivatives values will be saved. This fraction is determined by a variable, called NDT, which in this case is given the value 3. The sampling rate for the force plate data will in this case be set to 1/3 of that of the coordinate data.

The major principles of the measuring routine are illustrated by figure 20.

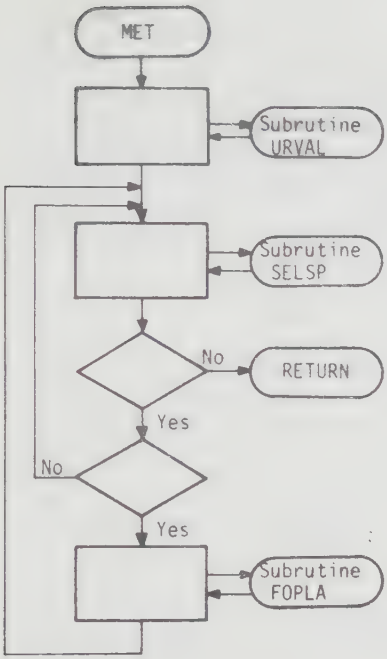
MET
Subrutine URVAL
Subrutine SELSP
No
RETURN
Yes
No
Yes
Subrutine FOPLA
The force plate sampling fraction, NDT, is calculated.
One cycle of Selspot data is measured and stored.
Has less than NT selspot cycles been stored?
Has NDT Selspot cycles been stored since the last force plate measurement?
Three channels of force plate data are measured and stored.

Figure 20. Subroutine MET for collection of measurement data.

As mentioned in section 5.2.1 the time for one measurement cycle is approximately 3.2 ms. When 6 diodes are used for each one of the two cameras, the computer is busy collecting coordinate data during the first 1.4 ms of this cycle time. The computer is then free for 1.8 ms and during that time the force plate data are registrated. The sampling and storing of the three force plate channels require approximately 0.1 ms.

5.4 Measurement control

This section deals with the parameters that are used to directly control a measurement and how they are determined. These parameters are:

- Starting time for the measurement.
- Measurement time.
- Measurement frequency.

As mentioned in section 5.2.1, measurement time and frequency are controlled by parameters of the program SELSP. Values of these parameters are fed into the computer from the graphic terminal immediately before a measurement is to take place.

To initiate a measurement one can choose between three different methods in the present version of the system:

1) Initialization from the main unit of the measuring equipment. Program SELSP must then be running on the computer and the measurement starts when the start mode switch is turned on the main unit.
2) Initialization from a photocell. Program SELSP must be running and the start mode switch must be in the "remote" position. The measurement is starting when a light beam across the walkway is interrupted by the subject.
3) Initialization from the computer. With the start mode switch in the "on" mode the measurement is starting when the computer operator starts to execute the routine SELSP.

Method 1) is the simplest starting method. Its major drawback is that it requires an operator.
Method 2) has been used with a phototransistor based triggering device and a torch as a light source. For normal gait, when the subject is not dragging his feet on the floor, the device can be positioned so that the measurement is started only if it is likely that the subject will step on the hidden force plate. This is achieved by estimating the step length prior to the measurement, and placing the torch and

phototransistor only one or two centimeters above the walkway at a distance from the force plate center of an integer number of step lengths.

Method 3), to start up the measurement from the computer, is not feasible in the present installation with the computer and the measurement equipment in different rooms.

6. ANALYSIS SUBSYSTEM

The most important parts of the analysis are described in this chapter. In 6.1 the computation of body segment parameters from body data is accounted for and in 6.2 a description is given of the method used for numerical differentiation of displacement data. Section 6.3 gives the criterion used for the determination of points of time for gait phase changes. Section 6.4 contains a description of the mechanical model and in section 6.5 a method is given for the testing of gait stationarity.

6.1 Computation of body segment parameters

The calibration of forces and moments require certain body segment parameters (BSP). These are mass (m), moment of inertia (j), length (l) and distance between proximal joint and center of mass (h) for each body segment. These four types of parameters are needed for the thighs, shanks and feet, and for the complex consisting of trunk, head and arms.

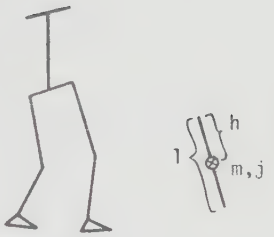

Figure 1. The four types of parameters are ascribed to each segment.

BSP varies from person to person in correlation to several factors such as sex, age, body type, eventual defects etc.

Determination of the BSP through direct measurements require special equipment and experience and is very time consuming. A relatively accurate determination is possible through statistical realtions which only requires some basic measurements, such as body weight and some distances and circumferences (see section 5.1). Below, such a method is presented which uses statistical results from Drillis and Contini [Drillis, Contini, 1966], [Contini, 1970, 1972]. Unfortunately Drillis and Contini do not deal with trunk and head why we fetch this information from [Chandler et al, 1975].

Method for the BSP determination

The method for determination of BSP is presented in figure 2 and explaned step by step. The numbers in figure 2 corresponds to the numbers in the text.

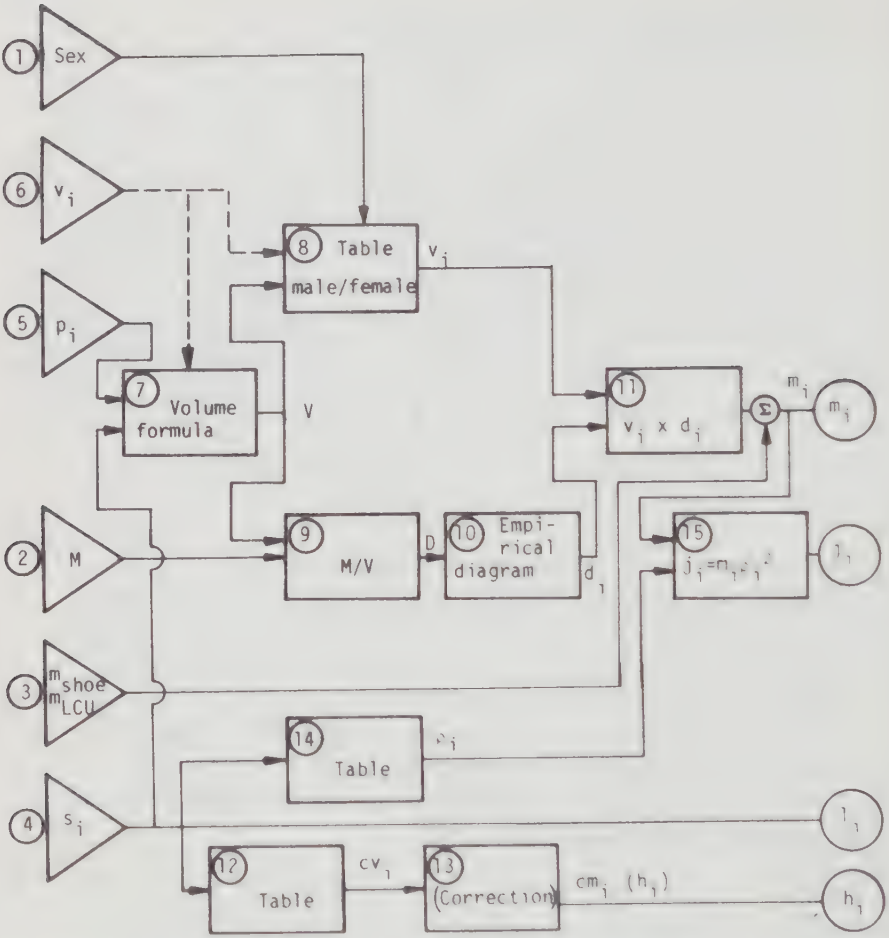

Figure 2. A method for determination of BSP from certain body data. Capital letters represent the total body. Small letters with index i represent a partial quantity, usually the i:th segment.

cm_i	center of mass	M, m_i	mass
cv_i	center of volume	p_i	circumference
D, d_i	density	S, s_i	distance
j_i	moment of inertia	V, v_i	volume
l_i	length of segment	ρ_i	radius of gyration

Input data

The input data, (most of them are described in section 5.1) are:

(1) The sex.

(2) The total mass is measured with a scale or the force plate.

(3) The mass of the shoes and the LCU-box which are carried during the measurement are registrated.

(4) Total height and seven other distances s_1 - s_7 are measured with a scale. If there are pathological differences between right and left,corresponding measurements are performed for both sides.

Notice also that all the segment lengths l_i are directly measured or can easily be obtained.

(5) The ten circumferences p_1-p_{10} are measured on the analogy of the distances.

(6) In the case of asymmetry, e.g. for an amputated subject, it is necessary to estimate the divergent or lacking volume separately and,if necessary,also to adjust the corresponding mass contribution. Methods for separate volume determination are body immersion or estimation with distance - circumference measurements. For normal subjects this point is excluded.

Computations

(7) The total volume V is estimated with Škerlj's modified formula presented in [Contini, 1970] pages 72-73. The coefficients of the formula have been estimated in an empirical way by Contini. If corrections under point (6) are made, these have to be included in the formula.

(8) Using the tables 1 and 2 we estimate the different segment volumes as a certain percentage of the total volume. Divergences from point (6) have to be regarded.

6.1

The tables separate men and women as well as right and left. C.V. in the last column is the relative standard deviation: $\frac{\text{s.d.}}{\text{mean}}$. As can be seen the variations are not very small. The tables are based on investigations of Americans which can also be a small source of error when applied to non Americans.

VOLUME OF BODY SEGMENTS (MALE) EXPRESSED IN PERCENTAGE OF WHOLE-BODY VOLUME

Segment	Range	Mean	S. D.	C. V. in Percent
Hand, right	0.43- 0.59	0.50	0.051	10.2
Hand, left	0.42- 0.59	0.51	.049	9.61
Forearm, r	1.46- 2.01	1.69	.167	9.9
Forearm, l	1.36- 1.97	1.73	.184	10.6
Upper arm, r	1.95- 2.58	2.17	.222	10.25
Upper arm, l	1.80- 2.54	2.18	.273	12.5
Whole arm, r	3.98- 5.05	4.37	.195	4.47
Whole arm, l	4.12- 4.78	4.38	.339	7.75
Foot, r	1.13- 1.38	1.24	.111	8.95
Foot, l	1.13- 1.39	1.26	.076	6.03
Shank, r	4.14- 5.39	4.64	.429	9.25
Shank, l	3.47- 5.00	4.41	.475	10.77
Thigh, r	8.41-11.08	9.22	.819	8.89
Thigh, l	8.68-10.99	9.17	.723	7.88
Whole leg, r	13.98-16.60	15.09	.848	5.62
Whole leg, l	13.38-16.66	14.84	0.925	6.24

VOLUME OF BODY SEGMENTS (FEMALE) EXPRESSED IN PERCENTAGE OF WHOLE-BODY VOLUME

Segment	Range	Mean	S. D.	C. V. in Percent
Hand, right	0.341- 0.600	0.497	0.087	17.5
Hand, left	0.320- 0.580	0.497	.082	16.5
Forearm, r	1.31 - 1.79	1.560	.137	8.8
Forearm, l	1.33 - 1.73	1.520	.132	8.7
Upper arm, r	1.70 - 2.40	1.955	.252	12.9
Upper arm, l	1.60 - 2.30	1.935	.263	13.6
Whole arm, r	3.59 - 4.80	4.00	.360	9.0
Whole arm, l	3.43 - 4.35	3.954	.314	7.94
Foot, r	1.17 - 1.70	1.31	.177	13.6
Foot, l		1.28		
Shank, r	4.40 - 5.96	5.18	.524	10.1
Shank, l		5.08		
Thigh, r	8.70 -10.80	9.87	.577	5.85
Thigh, l		9.72		
Whole leg, r	14.77 -17.80	16.42	0.921	5.61
Whole leg, l		16.10		

Tables 1 and 2 [Contini, 1972].

The tables give all the v_i. v(torso + arms + head) is derived by subtraction of the leg volumes.

(9) Mean density D is calculated as $\frac{M}{V}$.

(10) The segment densities d_i are estimated from D with the help of the figures 3 and 4.

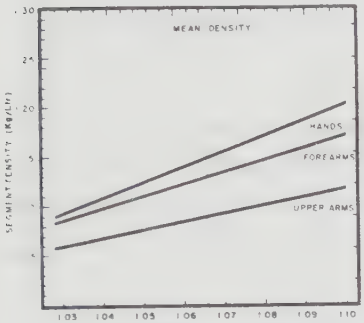

DENSITY OF UPPER EXTREMITY SEGMENTS

Figure 3. [Contini, 1972]

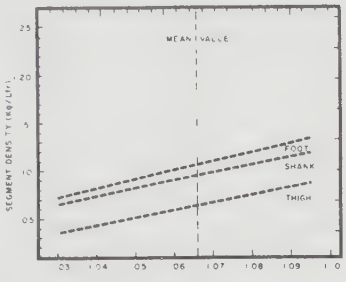

DENSITY OF LOWER EXTREMITY SEGMENTS

Figure 4. [Contini, 1972].

The relation $D = \frac{M}{V} = \frac{\Sigma v_i d_i}{\Sigma v_i}$ give us d(torso + arms + head).

(11) The segment masses are calculated as $m_i = v_i \cdot d_i$. The mass of the head is estimated from [Chandler et al, 1975]. The mass of the torso is the total mass minus the masses of arms, legs and head. The masses of the shoes are added to the masses of the feet and the LCU mass is added to the mass of the torso.

(12) Determination of the centers of volume are made with the help of table 3. Differences between males and females are not large. Different investigators have obtained results very similar to that in table 3.

Location of Centers of Volume Measured from the Proximal Joint Expressed in Percentage of Segment Length

Segment	Normal Males	Normal Females
Upper arm, right	46.4	46.9
Upper arm, left	46.0	45.9
Forearm, r	41.9	43.4
Forearm, l	42.2	43.5
Hand, r		
Hand, l		
Thigh, r	43.7	42.1
Thigh, l	43.4	42.5
Shank, r	42.0	42.6
Shank, l	41.5	41.3
Foot, r[a]	58.9	57.6
Foot, l[a]	59.5	58.0

[a] These values are measured vertically down from the ankle joint.

Table 3. [Contini, 1972].

(13) Centers of mass cm_i differ very little from centers of volume. In lack of good information we equalize them. Centers of mass for torso and head are taken from [Chandler et al, 1975].

Centers of volume and mass are given as distances from proximal joint for thigh, shank, foot, thigh and foot, upper arm, fore arm, hand and whole arm. For the trunk we use the hip joints as base-line, and for the head we give the center of mass as distance from the hollow of Sternum Manibrium. We have also assumed that the shoulder joints are placed 0.01·S below the hollow of Sternum Manibrium.

(14) The radii of gyration ρ_i are needed to calculate moments of inertia. They are derived as a percentage of the lengths of the segments. See table 4.

Ratio of Radius of Gyration (ρ) to Segment Length (L) in Percentage

Segment	Range	Mean	S.D.
Whole arm (normals)	24.2-26.0	25.0	0.79
Whole arm, males	24.0-26.0	24.9	0.93
Whole arm, females	24 -26	25.1	0.60
Whole arm, male amps.	24 -27	25.9	0.99
Whole arm, female amps.	24 -27	25.2	0.69
Whole arm, all amps.	24 -27	25.6	1.04
Whole arm, hemiplegics	25 -27	25.8	0.75
Upper arm, all amps.	19 -36	27.2	4.85
Forearm, all amps.	27 -31	29.2	1.23
Hand, all amps.	26 -29	26.7	0.67
Whole leg, males	31 -33	31.8	0.63
Whole leg, females	28 -30	29.6	0.73
Thigh	27 -29	28.1	0.74
Shank	27 -29	28.1	0.70
Shank & foot	32.0-34.0	33.4	0.66

Table 4. [Contini, 1972].

(15) The moments of inertia with respect to axes through the centers of mass are given through $J_i = m_i \cdot \rho_i^2$. For the torso we do not know the radius of gyration. Instead we take the moment of inertia directly from [Chandler et al, 1975].

Computer program

All the computations from input data to results, described above, are performed by a computer program named BSP. This program is listed in [Gustafsson, Lanshammar, 1977].

6.2 Numerical differentiation

In gait analysis an important problem is to find the derivatives of measured displacement data. The inaccuracies in the calculted internal forces and moments originate namely to a large extent from inaccurate estimates of the accelerations.

Whenever experimental data are to be numerically differentiated it is important that the measurement noise is kept down and the sampling frequency must be chosen with care. For example, it is not at all ascertained that it is sufficient to use a sampling frequency that exceeds the highest signal frequency with a factor 4 or 5, if one wants to use the data for the estimation of say the second order derivative. In section 6.2.1 a formula is presented that can be used for the determination of a suitable sampling frequency when the signal bandwidth, the variance of the measurement noise and the desired accuracy in the derivative are known.

Section 6.2.2 contains a review of methods for digital filtering in general with special emphasize on differentiation methods. Only methods within the "traditional" filtering theory will be treated. Methods like the Kalman-Bucy filter are not included because they require a dynamic model for the representation of the signal. The signal properties of gait data are different for different parts of the body, and they are also time varying. Using the Kalman-Bucy filter would therefore become very complex.

In section 6.2.3 a new method for numerical differentiation of noisy data is presented. The method is based on least squares minimization of the sum of the deterministic and the stochastic errors in the estimates of the derivatives. Derivatives of arbitrary order can be estimated. The resulting filters are narrowband, nonrecursive, differentiating filters with perfect phase characteristics. A state space model is formulated for the filter. This model makes it possible to implement the filter recursively and thereby to speed up the calculations considerably.

In section 6.2.4 the new method is evaluated and in 6.2.5 it is compared to two related methods.

The method will be further investigated in [Lanshammar, Söderström, 1977].

6.2.1 Some fundamental properties of numerical differentiation of noisy data

The purpose of numerical differentiation is to estimate the derivatives of a given time series with sufficient accuracy. In this section a result is given on the maximal obtainable accuracy in undistorted estimates of derivatives. Knowing this maximal accuracy (minimal variance), it is possible to tell if a specific numerical differentiation technique gives results with an accuracy that is sufficiently near to the limit value. From this one can judge whether it is wortwhile to try to improve the accuracy by changing the differentiation technique.

Another important aspect of this result on accuracy limit is that it becomes possible to decide whether a certain measurement technique is capable to produce measurement data that gives an acceptable accuracy limit.

Assumptions

The measurement data are assumed to be signals with added white noise

$$f(t) = s(t) + e(t) \qquad t = 0, T, 2T, \ldots, M \cdot T$$

where

s(t) is an at least k times differentiable signal and
e(t) is white noise

$$[E\ e(t) \cdot e(\tau)] = \begin{cases} \sigma_f^2 & t=\tau \\ 0 & t \neq \tau \end{cases}$$

T is the sampling interval (the inverse of the sampling frequency).

Further it is assumed that the signal s(t), the k:th order derivative of which is to be estimated from the measurement data, is strictly bandlimited with the bandwidth ω_s rad/s^2.

Result

It will be verified that inequality (1) applies for all undistorted linear estimates of the k:th order derivative.

$$\sigma_k^2 \geq \sigma_{k,min}^2 = \frac{\sigma_f^2 \cdot T \cdot \omega_s^{2k+1}}{\pi \cdot (2k+1)} \qquad (1)$$

where σ_k^2 is the variance of the estimate of the k:th order derivative and $\sigma_{k,min}^2$ is the minimal value of this variance.

With an undistorted estimate it is meant that the k:th order derivative of the signal should be reproduced exactly in the absence of measurement noise.

Proof of equation (1)

The k:th order derivative of s(t) is estimated from the measurement data by

$$\hat{s}^{(k)}(t) = H(z)f(t) = \sum_{i=-\infty}^{\infty} h_i f(t-iT)$$

where $H(z) = \sum_{i=-\infty}^{\infty} h_i z_i$ is the transfer function of the estimator and z is the shift operator. If the k:th order derivative is to be reproduced exactly in the absence of noise we must have

$$|H(e^{i\omega t})|^2 = \omega^{2k} \qquad \text{for } 0 \leq \omega \leq \omega_s$$

In the presence of noise the variance of $\hat{s}^{(k)}(t)$ for an undistorted estimate (σ_k^2) becomes

$$\sigma_k^2 = E\left[(\hat{s}^{(k)}(t) - E\,\hat{s}^{(k)}(t))^2\right] = E\left[\left(\sum_{i=-\infty}^{\infty} h_i(s(t-iT)+e(t-iT) - \sum_{j=-\infty}^{\infty} h_j\, s(t-jT)\right)^2\right] =$$

$$= E\left[\left(\sum_{i=-\infty}^{\infty} h_i\, e(t-iT)\right)^2\right] = \sigma_f^2 \sum_{i=-\infty}^{\infty} h_i^2$$

Parseval's equality gives

$$\sum_{i=-\infty}^{\infty} h_i^2 = \frac{T}{2\pi} \int_{-\frac{\pi}{T}}^{\frac{\pi}{T}} |H(e^{i\omega T})|^2 d\omega = \frac{T}{\pi} \int_0^{\pi/T} \left|H(e^{i\omega T})\right|^2 d\omega$$

since it can easily be shown that the function $|H(e^{i\omega T})|$ is symmetric around the origin $\omega = 0$

Thus we get

$$\sigma_k^2 = \frac{\sigma_f^2 \cdot T}{2\pi} \int_0^{\frac{\pi}{T}} |H(e^{i\omega T})|^2 d\omega = \frac{\sigma_f^2\, T}{\pi} \left[\int_0^{\omega_s} \omega^{2k} d\omega + \int_{\omega_s}^{\frac{\pi}{T}} |H(e^{i\omega T})|^2 d\omega\right]$$

$$\geq \frac{\sigma_f^2\, T \cdot \omega_s^{2k+1}}{\pi \cdot (2k+1)}$$

and equation (1) has been verified. Equality holds when and only when

$$|H(e^{i\omega T})| = 0 \qquad \text{for } \omega_s \leq |\omega| \leq \frac{\pi}{T}$$

Discussion

Equation (1) shows that the minimal variance in the estimate of the k:th derivative is a function of the measurement noise (σ_f^2), the sampling interval (T), and the signal bandwidth (ω_s).

Equation (1) can be used to answer several questions concerning numerical differentiation.

1) What is the minimal obtainable variance of an undistorted estimate of the k:th derivative?

The answer is given by equation (1).

Example: We want to estimate the second derivate of a measured signal. The sampling interval (T) is 0.02 s (50 Hz) and the standard deviation of the measurement noise (σ_f) is 0.001 m. The bandwidth of the signal (ω_s) is 4π rad/s (2 Hz). Equation (1) gives

$$\sigma_{2,min} = 2.00 \cdot 10^{-2} \text{ m/s}^2$$

Now if the bandwidth of the signal is doubled, the variance of the estimate will increase with a factor 2^5, which gives

$$\sigma_{2,min} = 1.13 \cdot 10^{-1} \text{ m/s}^2$$

2) What sampling interval should be used to obtain a specified maximal variance in the estimate of the k:th derivative of the signal? The signal bandwidth and the variance of the measurement noise is assumed to be known.

Equation (1) gives

$$T \leq T_{max} = \frac{\sigma_k^2 \cdot \pi \cdot (2k+1)}{\sigma_f^2 \cdot \omega_s^{2k+1}}$$

Example:

With
k=2 (second derivate)

$\sigma_k^2 = (3 \cdot 10^{-1})^2 \text{ m}^2/\text{s}^4$ (maximal variance in the estimate)

$\sigma_f^2 = (3 \cdot 10^{-3})^2 \text{ m}^2$ (measurement noise variance)

$\omega_s = 5 \cdot 2\pi$ rad/s (5 Hz) (signal bandwidth)

we get

$$T \leq 5.13 \cdot 10^{-3} s$$

This means that the sampling frequency, ν, must be at least

$$\nu = \frac{1}{T} \geq \frac{1}{5.13 \cdot 10^{-3}} = 195 \text{ Hz}$$

This frequency is much higher than that employed by most researchers working in the field of human gait analysis although 5 Hz is a typical bandwidth for gait data (99.7% of the signal power for a toe coordinate was below 4.8 Hz in a study reported in [Winter et al, 1974]) and the noise standard deviation 0.003 m means that the signal to noise ratio is roughly 1000:1 since the coordinates values are typically a few meters. A reason for using a lower sampling frequency might be the assumption expressed in [Capozzo, 1975] that the required sampling frequency is approximately six times the bandwidth of the signal. This indicates that the required sampling frequency is proportional to the signal bandwidth. However, according to equation (2), we have

$$\nu = \frac{1}{T} \leq \frac{\sigma_f^2 \cdot \omega_s^{2k+1}}{\sigma_k^2 \cdot \pi \cdot (2k+1)} \sim \omega_s^{2k+1}$$

Thus, for the estimation of the second derivative the required sampling frequency is proportional not to ω_s but to ω_s^5.

An explanation to the usable results reported by several researchers working with sampling frequencies far below 100 Hz, is that most of the signal power is contained in a band much narrower than 5 Hz. Our own experiments indicate that for the knee joint the signals corresponding to their cartesian coordinates have 99% of the power below 1.5 Hz.

3) What is the quality of a specific method employed for numerical differentiation?

The minimal variance in the estimate of the k:th order derivative according to equation (1) is obtained for an ideal differentiator with bandwidth ω_s. By an ideal differentiator is meant a filter, that is a perfect differentiator for $\omega < \omega_s$ and that gives zero as output for $\omega > \omega_s$. The phase shift of the ideal differentiator is $k \cdot \pi/2$ rad.

However, an ideal differentiator cannot be realized. For a realizable filter the variance in the output will be greater than $\sigma^2_{k,min}$ if the filter characteristics are to approach those of a perfect differentiator within the passband.

On the other hand, if we allow the filter characteristics to diverge from the perfect differentiators within the signal bandwidth, it is of course possible to obtain a smaller variance than $\sigma^2_{k,min}$. For instance, if the k:th derivative is always estimated with zero, the variance of the estimate will be zero. This estimate is of course quite meaningless.

If we allow the filter to diverge from the ideal differentiator in a transition band beginning before and ending after ω_s, some variance can be gained by the in-band distortion and some is lost by the out-of-band divergence from zero. Thus it is to be expected that the output variance for a good estimator of derivatives should not much exceed $\sigma^2_{k,min}$ as given by equation (1). If more a priori information about the signal characteristics than its bandwidth can be utilized one might be able to obtain estimates with a variance less than $\sigma^2_{k,min}$ but this case will not be discussed here.

4) What is the information retrieval capacity of a certain measurement technique?

Let

$$IRC = \frac{1}{\sigma^2_f \cdot T}$$

which could be called the Information Retrieval Capacity.

Equation (1) gives

$$\sigma^2_{k,min} = \frac{\omega_s^{2k+1}}{IRC \cdot \pi \cdot (2k+1)}$$

Thus, from the same type of data we can get better estimates of the signal derivatives if we have a higher value on IRC. We also notice that a doubling of the measurement noise variance can be compensated for, by a halving of the sampling interval. If two measurement equipments have the same IRC value, the one with the largest sampling interval is normally to be preferred, since a smaller sampling interval implies more data to store and process and more complex and time consuming routines for the numerical differentiation.

6.2.2 Review of some methods for digital filtering

The purpose of this section is not to provide a complete survey of existing methods for digital filtering but to give a rough classification of the different kinds of approaches that are in use. Extensive references to different methods can be found in the sources mentioned in this section and especially in chapter 7 of [Kuo, Kaiser, 1966].

The presentation will deal with different methods for the design of digital filters, followed by a brief discussion of methods for the filter implementation. Only linear filters will be considered and all specific methods that are described are merely intended as examples. Applications on differentiation have preferably been chosen.

Design methods

Depending on whether the impulse response of a filter is finite or infinite, the filter is often classified as an FIR (Finite Impulse Response) respectively an IIR (Infinite Impulse Response) filter.

FIR filters have two advantages. They have good stability properties. Further, it is possible to construct FIR filters with excellent phase characteristics. On the other hand IIR filters can often be realized with considerably fewer terms than a corresponding FIR filter, which makes the IIR filter more economic to use.

IIR filters

An IIR filter is usually formulated as a recursive filter. The transfer function of the filter can be written

$$H(z^{-1}) = \frac{\sum_{j=0}^{n-1} a_j z^{-j}}{1 + \sum_{j=1}^{n} b_j z^{-j}}$$

where z^{-1} is the unit shift operator;

$z^{-1} f(t) = f(t-T)$ T is the sampling interval

The filter design then consists of the determination of the parameters $a_0, \ldots, a_{n-1}, b_1, \ldots, b_n$. To achieve this, two basically different approaches are being used.

Direct methods. The parameters are determined directly from the specifications of the filter to be designed. The filter is often designed in the frequency domain by approximation of a desired amplitude function.

In a method proposed in [Steiglitz, 1969] the desired amplitude function is given for equidistant frequency values. The filter parameters are then given by minimization of the squared sum of the approximation errors for these frequencies. Nonlinear optimization is used to find the minimum.

In [Rabiner et al, 1974] a design algorithm is given that determines the parameters so that a given continuous amplitude function is approximated with the maximum error of approximation minimized. A varying accuracy demand for different frequencies can be accounted for by giving different error weights to different portions of the band. The optimization is formulated as a linear programming problem.

Both these methods are implemented in the form of computer programmes. They have been used for the design of for example low pass filters and wide band differentiators. They both have the drawback that the optimization does not include the phase characteristics of the filters.

Indirect methods. These methods are based on the digitalization of continuous filters, whose parameters are already known. Of these methods the standard z-transform, applied on samples of the impulse response of the continuous filter, has the serious drawback of not giving a digital filter with the same frequency response characteristics as those of the continuous filter, if the frequency characteristics of the continuous filter are not bandlimited to the Nyqvist frequency. The reason for this is that folding will occur. When the transfer function of the continuous filter, H(s), is a rational function in s,

it is not bandlimited and the frequency responses will thus not be equal. The situation is particularly severe for filters of low order and for wideband filters, [Kuo, Kaiser, 1965].

The bilinear z-transformation has been proposed as an alternative to the z-transform. This transformation has the advantage that no folding occurs. However, the frequency scale is nonlinearly changed (warping) but this effect can easily be compensated if the desired filter characteristics can be described by successive passbands and stopbands. The usefulness of this design method is demonstrated in [Golden, Kaiser, 1964]. However, for the design of digital differentiators this method will not be suitable due to the frequency warping.

Other transformations than the z-transform and the bilinear z-transformation have also been used for the digitalization of continuous filters.

FIR filters

FIR filters are often called nonrecursive filters because their transfer functions have all poles in the origin.

$$H(z^{-1}) = \sum_{j=0}^{n-1} a_j z^{-j}$$

which means that the filter has a finite memory. This type of filter is appealing because of its excellent phase characteristics and its intrisic stability. The length of the impulse response, n, is often called the number of taps. Depending on how the desired filter is specified, the different design methods can be classified as time domain design or frequency domain design.

Time domain design. The fomulae for interpolation and differentiation found in standard books on numerical analysis, for example [Scheid, 1968], can be regarded as FIR filters. They are often based on finite difference techniques or least squares polynomial fitting. The details of the different approaches are depending on the purpose which can be prediction, meaning that only historical data are used for the estimation,

filtering meaning that historical and the present values are used or smoothing, which implies the use of both historical and future data.

Lanczos proposes the use of least squares polynomial fitting for the estimation of the first derivate of a given time series [Lanczos, 1956]. To estimate the derivative for a certain sample, a parabola is fitted to the data points in a suitable neighbourhood of that sample. This neighbourhood is chosen so that the sample to be estimated is in the center of the fitted interval, which means that the result will be a smoother. The derivative of the parabola is then used as the desired estimate. The number of neighbouring data points to be used should be chosen so that the parabola can be fitted without the introduction of a large systematic error. This technique has the feature of giving a low noise transmission for differentiating filters (the noise transmission can be defined as the variance of the filter output divided by the input variance when the input is white noise).

In [Monroe, 1962] a similar approach is applied to the filtering problem. The difference is that Monroe is only using historical and the present value for the polynomial fitting which gives a greater noise transmission than the smoother proposed by Lanczos.

Allum uses a third order polynomial fitting to achieve an estimate of the first order derivate of time series [Allum, 1975]. The filter, that is intended for on line purposes, is using the derivative of the polynomial in the endpoint of the fitted interval. Allum demonstrates how the filter can be formulated recursively which considerably reduces the computer time. However, this recursive formulation is not numerically stable which was not pointed out by Allum.

Frequency domain design. The methods where the filter is characterized in the frequency domain are divided into two types, those based on Fourier series and others.

The Fourier series approach is based on Fourier series expansion of the frequency response of the desired filter. The problem with this approach is that the expansion will give an infinite number of terms in the filter

and mere truncation of the expansion often causes oscillating filter output (Gibb's oscillations). These oscillations are reduced by multiplication of the impulse response of the obtained filter with a suitable window function, which corresponds to a smoothing of the original frequency response. Several types of window functions can be found in [Kuo, Kaiser, 1965].

Among other methods several are based on the determination of the filter parameters by minimization, in least squares or minimax sense, of the deviation from desired frequency characteristics. A minimax error criterion is used, where different error weighting are allowed in different frequency band. The resulting filters are equiripple, and the filters will have narrow transition bands.

In [McClellan, Parks, 1973] and [McClellan et al, 1973] a computer program is presented for automatic FIR filter design. It is based on the fitting of the amplitude characteristics to a given continuous function according to a minimax criterion. Among other types of filters the program is capable of designing low pass, high pass, band pass filters and differentiators.

Methods for filter implementation

The IIR filters are suitable for direct implementation on digital computers since they are usually of relatively low order.

For the realization of FIR filters several methods are beeing used:

1) Direct convolution is the most direct approach. The impulse response of the filter must be known and the filter is realized by

$$y(i) = \sum_{j=0}^{n-1} a_j x(i-j)$$

where a_j represents the impulse response, x the filter input and y the filter output. For filters with few taps this is the natural approach to use.

2) Fast convolution is realized via the Fast Fourier Transform. The major drawback with this technique is that it can only be used in off line applications. The filter input is transformed and the convolution in the time plane is then exchanged for multiplication in the frequency plane with samples of the filter's frequency response. The inverse Fourier transform is then applied to produce the filter output. This technique is economic to use for large FIR filters. An example where this method is used for differentiation can be found in [Broman et al, 1975].

3) Frequency sampling is a technique for realizing the filter as a digital network. The signal is divided into frequency band by bandpass filters. The filter output is then given as a weighted sum of the amplitudes in the different bands. The weighting factor for a specific band is determined by the desired filter amplitude for the central frequency of the band. It follows that the filter characteristics must be given in the form of its amplitude values for the resonator frequencies. The digital network is realized by a comb filter followed by a set of parallel resonators. This technique is described in [Gold, Rader, 1969].

6.2.3 Description of a method for numerical differentiation

When noisy data are used for numerical differentiation, two types of errors will be present in the estimated values of the derivatives; stochastic errors due to the noise present in the given time series, and systematic errors due to imperfection in the algorithm used for the differentiation. An often used technique is to supress the noise by low pass filtering of the time series. The differentiation is then performed with a wideband differentiating filter, which gives a small systematic error but at the same time acts as a strong amplifier of white noise. With a wideband filter it is meant that the bandwidth of the filter is an appreciable fraction of the Nyqvist interval. Another technique is the one based on least squares polynomial fitting described in [Lanczos, 1956] (see also section 6.2.2). This technique can be viewed on as a constrainted least squares minimization of the stochastic error. However, since the objective normally is to make the total error sufficiently small, a more natural approach seems to be the minimization of a loss function containing both the systematic and stochastic errors.

The method for numerical differentiation that will be presented in this section is based on two principles.

The first principle is that one should minimize the total error in the resulting estimates. This method is therefore based on minimization, in the least squares sense, of the sum of one term representing the systematic error and another that represents the stochastic error.

The second principle is that a smoother should be used rather than a causal filter, which means that both historical and future values should be used instead of historical values only. This implies that the algorithm can not be used in a real time application whithout the introduction of a time delay. The advantages as compared to a causal filter are that we can achieve a filter characteristic that does not include any phase shift and it is of course possible to get better estimates when using both historical and future data as compared to using historical values only.

Before the method is described, the notations to be used as well as the basic assumptions will be given in 6.2.3.1. In 6.2.3.2 the method is derived. Section 6.2.3.3 presents a recursive formulation of the filter which makes it possible to speed up the calculations. In 6.2.3.4 suitable parameter values for the algorithm are given together with an analysis of the resulting errors when the algorithm is used for differentiation of gait data.

6.2.3.1 Notations and basic assumptions

Notations

T Sampling interval

$f(t)$ $t = 0, T, 2\cdot T, \ldots, M\cdot T$ Given time series

$\underline{f}(t)$ $[f(t-N\cdot T), f(t-(N-1)\cdot T, \ldots, f(t+N\cdot T)]^T$

k Order of the derivative to be estimated

$s(t)$ Differentiable, deterministic function defined for $0 \leq t \leq M\cdot T$

$s^{(k)}(t) = \frac{\partial^k}{\partial t^k} s(t)$ Derivative of $s(t)$ with respect to time

$\rho = \left[\frac{T^p}{p!} \cdot s^{(p)}(t)\right]^2$

$\hat{s}^{(k)}(t)$ Estimated value of $s^{(k)}(t)$

$\underline{s}(t) = [s(t-N\cdot T), s(t-(N-1)\cdot T, \ldots, s(t+N\cdot T)]^T$

$e(t)$ $t = 0, 2\cdot T, \ldots, M\cdot T$ White noise with zero mean and variance λ^2

$\underline{e}(t) = [e(t-N\cdot T), e(t-(N-1)\cdot T), \ldots, e(t+N\cdot T)]^T$

N Nonnegative integer (There will be $2N+1$ taps in the filter.)

h_i $i = -N, (-N+1), \ldots, N$ Filter weights

$\underline{h} = [h_{-N}, h_{-N+1}, \ldots, h_N]^T$

$\underline{u}_i = \left[(-N)^i, (-N+1)^i, \ldots, N^i\right]^T$

p Integer: $p > k$

$\underline{U}_{p-1} = \left[\underline{u}_0, \underline{u}_1, \ldots, \underline{u}_{p-1}\right]$

$V(h) = E[\hat{s}^{(k)}(t) - s^{(k)}(t)]^2$ Criteria function

$\underline{e}_k = [0, \ldots, 0, \underset{k}{1}, 0, \ldots, 0]^T$ (1 … k … p)

$\underline{\underline{I}}$ Unit matrix of appropriate order

Basic assumptions

The given time series

$$\left\{ f(i \cdot T) \right\}_{i=0}^{M}$$

are supposed to consist of a sufficiently differentiable and deterministic signal with added white noise

$$f(t) = s(t) + e(t) \qquad t = 0, T, 2 \cdot T, \ldots, M \cdot T \tag{1}$$

Here, $s(t)$ is the signal with derivatives

$$s^{(k)}(t) = \frac{\partial^k}{\partial t^k} s(t)$$

and $e(t)$ is white noise, $E\, e(t)\, e(\tau) = \begin{cases} 0 & t \neq \tau \\ \lambda^2 & t = \tau \end{cases}$ with zero mean and variance λ^2

The derivative $s^{(k)}(t)$ will be estimated by the linear estimate

$$\hat{s}^{(k)}(t) = \sum_{i=-N}^{N} h_i \cdot f(t+i \cdot T) = \underline{h}^T \cdot \underline{f}(t) \tag{2}$$

for some filter weights $\left\{ h_i \right\}_{i=-N}^{N}$ and some integer $N \geq 0$.

Figure 5 illustrates the data interval involved.

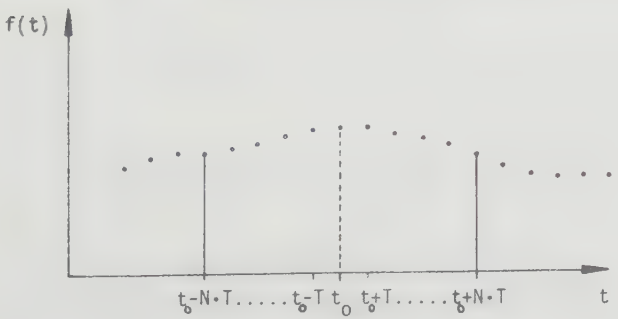

Figure 5. Data interval involved at the time t_o.

6.2.3.2 Derivation of the method

The filter weights are chosen so that the expected value of the mean squares error in the estimated derivatives is minimized. Thus, the criteria for finding the filter weights is

For a given N, find $\left\{h_i\right\}_{i=-N}^{N}$,

$$V^1(h)=E\left[\hat{s}^{(k)}(t)-s^{(k)}(t)\right]^2=E\left[\underline{h}^T\cdot\underline{f}(t)-s^{(k)}(t)\right]^2 \qquad (3)$$

is minimized.

This expression can be expanded in order to separate the deterministic and stochastic elements.

$$V^2(h)=E\left[\underline{h}^T\cdot\underline{f}(t)-s^{(k)}(t)\right]^2=E\left[\underline{h}^T\cdot(\underline{s}(t)+e(t))-s^{(k)}(t)\right]^2$$

$$=\left[\underline{h}^T\cdot\underline{s}(t)-s^{(k)}(t)\right]^2+\lambda^2\underline{h}^T\cdot\underline{h} \qquad (4)$$

In this expression the first term expresses the deterministic (systematic) error in the algorithm. It is the error in the estimate when there is no noise present in the time series.

The second term expresses the stochastic error. The variance of the noise in the time series is thus amplified by the factor

$$\underline{h}^T\cdot\underline{h}=\sum_{i=-N}^{N}h_i^2$$

called the noise transmission of the filter, which has already been mentioned in section 6.2.1.

We will now impose some constraints on the filter weights $\underline{h}$, namely that the estimates of the k:th order derivative must be unbiased when the signal, $s_{p-1}(t)$, is a polynomial of degree (p-1) where (p-1) $\geq$ k.

This implies that the deterministic error, given by equation (4), must be zero:

$$\left[\underline{h}^T \underline{s}_{p-1}(t) - s_{p-1}^{(k)}(t)\right]^2 = 0 \qquad (5)$$

Since $s(t) = s_{p-1}(t)$ is a polynomial of degree p-1 it is easy to see that

$$s(t+jT) = \sum_{i=0}^{p-1} \frac{(jT)^i}{i!} s^{(i)}(t)$$

and thus, using the vector $\underline{u}_i$

$$\underline{s}(t) = \sum_{i=0}^{p-1} \frac{T^i}{i!} s^{(i)}(t)\, \underline{u}_i \qquad (6)$$

Then (5) implies

$$0 = \underline{s}(t)^T \underline{h} - s^{(k)}(t) = \sum_{i=0}^{p-1} \frac{T^i}{i!} s^{(i)}(t)\, \underline{u}_i^T \underline{h} - s^{(k)}(t)$$

$$\underline{u}_i^T \underline{h} = \begin{cases} 0 & i \neq k \\ \dfrac{k!}{T^k} & i = k \end{cases}$$

Invoking the introduced notations $\underline{\underline{U}}_{p-1}$ and $\underline{e}_k$ this constraint can be written as

$$\underline{\underline{U}}_{p-1}^T \underline{h} = \frac{k!}{T^k} \underline{e}_k \qquad (7)$$

In general signals are not exactly of polynomial form. In such cases the signal will be approximated with the first (p+1) terms of its Taylor expansion, i.e.

6.2.3.2

$$s(t+jT) \approx \sum_{i=0}^{p} \frac{(jT)^i}{i!} s^{(i)}(t)$$

giving

$$\underline{s}(t) \approx \sum_{i=0}^{p} \frac{T^i}{i!} s^{(i)}(t)\, \underline{u}_i$$

Invoking the constraint (7) the loss function (4) then becomes (approximately)

$$V^1(h) \approx \left[\underline{s}(t)^T \underline{h} - s^{(k)}(t)\right]^2 + \lambda^2 \underline{h}^T\underline{h}$$

$$= \left[\sum_{i=0}^{p} \frac{T^i}{i!} s^{(i)}(t)\underline{u}_i^T\underline{h} - s^{(k)}(t)\right]^2 + \lambda^2 \underline{h}^T h$$

$$= \left[\frac{T^p}{p!} s^{(p)}(t)\, \underline{u}_p^T\underline{h}\right]^2 + \lambda^2 \underline{h}^T\underline{h}$$

with

$$\rho = \left[\frac{T^p}{p!} s^{(p)}(t)\right]^2$$

The loss function can be written as

$$V^1(h) \approx \rho\, \underline{h}^T \underline{u}_p\underline{u}_p^T \underline{h} + \lambda^2 \underline{h}^T\underline{h} \qquad (8)$$

Summarizing so far the following optimization problem has to be solved. Find the minimizing vector $\underline{h}_o$ of the function

$$V(\underline{h}) = \underline{h}^T \left[\rho\, \underline{u}_p^T \underline{u}_p + \lambda^2 \underline{\underline{I}}\right] \underline{h} \qquad (9)$$

under the constraint (7)

$$\underline{U}_{p-1}^T \underline{h} = \frac{k!}{T^k} \underline{e}_k$$

The estimate of the k:th order derivative is then to be taken as

$$\hat{s}^{(k)}(t) = \underline{h}_o^T \underline{f}(t) \qquad (10)$$

This optimization problem with a quadratic loss function and a linear constraint is straightforward to solve. The solution for a general case can be found e.g. in [Bryson, Ho, 1969]. For the present case the optimum is obtained for

$$\underline{h}_o = \left(\rho\, \underline{u}_p\, \underline{u}_p^T + \lambda^2\, \underline{\underline{I}}\right)^{-1} \underline{\underline{U}}_{p-1} \left[\underline{\underline{U}}_{p-1}^T \left(\rho\, \underline{u}_p \underline{u}_p^T + \lambda^2\, \underline{\underline{I}}\right)^{-1} \underline{\underline{U}}_{p-1}\right]^{-1} \frac{k!}{T^k}\, \underline{e}_k \qquad (11)$$

In order to proceed, the so called matrix inversion lemma, see e.g. [Aoki, 1967], will be used. Applied to the present case this lemma gives

$$\left(\rho\, \underline{u}_p\, \underline{u}_p^T + \lambda^2\, \underline{\underline{I}}\right)^{-1} = \frac{1}{\lambda^2}\, \underline{\underline{I}} - \frac{\rho}{\lambda^2} \cdot \frac{1}{\lambda^2 + \rho \underline{u}_p^T \underline{u}_p}\, \underline{u}_p \underline{u}_p^T \qquad (12)$$

Combining (11) and (12) we obtain

$$\underline{h}_o = \left[\frac{1}{\lambda^2}\, \underline{\underline{U}}_{p-1} - \frac{\rho}{\lambda^2} \frac{1}{\lambda^2 + \rho \underline{u}_p^T \underline{u}_p}\, \underline{u}_p\, \underline{u}_p^T\, \underline{\underline{U}}_{p-1}\right] \cdot$$

$$\cdot \left[\frac{1}{\lambda^2}\, \underline{\underline{U}}_{p-1}^T\, \underline{\underline{U}}_{p-1} - \frac{\rho}{\lambda^2} \frac{1}{\lambda^2 + \rho \underline{u}_p^T \underline{u}_p}\, \underline{\underline{U}}_{p-1}^T\, \underline{u}_p\, \underline{u}_p^T\, \underline{\underline{U}}_{p-1}\right]^{-1} \frac{k!}{T^k}\, \underline{e}_k$$

$$= \left[\left(1 + \frac{\rho}{\lambda^2}\, \underline{u}_p^T\, \underline{u}_p\right) \underline{\underline{U}}_{p-1} - \frac{\rho}{\lambda^2}\, \underline{u}_p\, \underline{u}_p^T\, \underline{\underline{U}}_{p-1}\right] \cdot$$

$$\cdot \left[\left(1 + \frac{\rho}{\lambda^2}\, \underline{u}_p^T\, \underline{u}_p\right) \underline{\underline{U}}_{p-1}^T\, \underline{\underline{U}}_{p-1} - \frac{\rho}{\lambda^2}\, \underline{\underline{U}}_{p-1}^T\, \underline{u}_p\, \underline{u}_p^T\, \underline{\underline{U}}_{p-1}\right]^{-1} \frac{k!}{T^k}\, \underline{e}_k$$

We finally get:

$$\underline{h}_o = \underline{\underline{U}}_p \cdot \underline{c} \qquad (13)$$

where

$$\underline{\underline{U}}_p = \left[\underline{\underline{U}}_{p-1}\, ,\, \underline{u}_p\right] = \left[\underline{u}_o, \underline{u}_1, \ldots, \underline{u}_p\right]$$

and $\underline{c}$ is a (p+1) - dimensional column vector given by

$$\underline{c} = \frac{k!}{T^k} \begin{bmatrix} (1 + \frac{\rho}{\lambda^2}\, \underline{u}_p^T \cdot \underline{u}_p) \cdot \underline{\underline{I}} \\ -\rho \cdot \underline{u}_p^T \cdot \underline{\underline{U}}_{p-1} \end{bmatrix} \cdot \left[(1 + \frac{\rho}{\lambda^2}\, \underline{u}_p^T\, \underline{u}_p) \cdot \underline{\underline{U}}_{p-1}^T \cdot \underline{\underline{U}}_{p-1} - \frac{\rho}{\lambda^2} \cdot \underline{\underline{U}}_{p-1}^T \cdot \underline{u}_p \cdot \underline{u}_p^T \cdot \underline{\underline{U}}_{p-1} \right]^{-1} \underline{e}_k \qquad (14)$$

For the estimation of a specified k:th derivative, the filter weights, h_i, will thus be depending on the parameters, N, p, and $\frac{\rho}{\lambda^2}$. How they can be chosen will be described in section 6.2.3.5.

6.2.3.3 Practical considerations

Recursive formulation of the algorithm

From equations (2) and (12) we have

$$\hat{s}^{(k)}(t) = \underline{h}_o^T \cdot \underline{f}(t) = \underline{c} \cdot \underline{\underline{U}}_p^T \cdot \underline{f}(t) =$$

$$= \begin{bmatrix} c_o, \ldots, c_p \end{bmatrix} \begin{bmatrix} 1 & 1 & \ldots & 1 \\ (-N)^1 & (-N+1) & \ldots & (N)^1 \\ (-N)^2 & (-N+1) & \ldots & (N)^2 \\ \vdots & \vdots & & \vdots \\ (-N)^p & (-N+1)^p & & (N)^p \end{bmatrix} \cdot \begin{bmatrix} f(t-N \cdot t) \\ f(t-(N-1) \cdot t) \\ \cdot \\ \cdot \\ \cdot \\ f(t+N \cdot t) \end{bmatrix} \qquad (15)$$

To calculate $\underline{\underline{U}}_p^T \cdot \underline{f}(t)$, $(p+1) \cdot (2 \cdot N+1)$ multiplications must be performed and the computation of $\hat{s}^{(k)}(t)$ requires $(p+1)$ additional multiplications. It will be demonstrated in the section on choice of filter parameters that N will typically be ≈ 20 and $p \approx 4$, which makes the filter very time consuming.

To overcome this problem we will show how the filter can be given a recursive formulation, i.e. the estimates for time t are used in the calculation of estimates for time (t+T).

The result will be a state space model for the calculation of $\bar{\underline{\underline{U}}}_p^T \cdot \bar{\underline{f}}(t)$, where the number of multiplications is $(p+1) \cdot (\frac{p}{2} + 3)$ and the number of additions is $(p+1) \cdot (\frac{p}{2} + 2)$. The time consumption is thus made independent on N, which reduces computing time considerably. For N=20 and p= 4, the recursive formulation gives a reduction in the number of arithmetic operations with approximately a factor 5 as compared to the nonrecursive algorithm, when the 0th, 1st and 2nd order derivatives are all calculated. The price that has to be paid to achieve this is that the algorithm will turn out to be unstable. When the recursive formulation has been presented, a way to overcome this problem is discussed.

Introduce now the variables

$$x_i(t) = \underline{u}_i^T \underline{f}(t) = \sum_{j=-N}^{N} j^i f(t+jT) \quad i=0, 1 \ldots p$$

It will now be shown that these variables can be computed recursively. We obtain by straightforward calculations

$$x_i(t+T) = \sum_{j=-N}^{N} j^i f(t+jT+T) = \sum_{j=-N+1}^{N+1} (j-1)^i f(t+jT)$$

$$= N^i f(t+NT+T) - (-N-1)^i f(t-NT) + \sum_{j=-N}^{N} (j-1)^i f(t+jT)$$

$$= N^i f(t+NT+T) - (-N-1)^i f(t-NT)$$

$$+ \sum_{j=-N}^{N} \sum_{\ell=0}^{i} \binom{i}{\ell} j^\ell (-1)^{i-\ell} f(t+jT)$$

$$= N^i f(t+NT+T) - (-N-1)^i f(t-NT) + \sum_{\ell=0}^{i} (-1)^{i-\ell} \binom{i}{\ell} x_\ell(t) \qquad (16)$$

Introduce now the notations

$$\underline{x}(t) = \left[x_0(t) \ldots \quad x_p(t) \right]^T$$

$$\underline{v}(t) = \begin{bmatrix} f(t-NT) \\ f(t+NT+T) \end{bmatrix}$$

$$\underline{\underline{A}} = \begin{bmatrix} 1 & & & & \\ -1 & 1 & & & \\ 1 & -2 & 1 & & \\ & & \ddots & \ddots & \\ & & & -p & 1 \end{bmatrix}$$

The i+1, j+1 the element of A is $(-1)^{i-j}\binom{i}{j}$ for $1 \leq j \leq i$

$$\underline{\underline{B}} = \begin{bmatrix} -1 & 1 \\ -(-N-1) & N \\ -(-N-1)^2 & N^2 \\ \\ -(-N-1)^p & N^p \end{bmatrix}$$

Then the equations (16) can be written

$$\underline{x}(t+T) = \underline{\underline{A}}\ \underline{x}(t) + \underline{\underline{B}}\ \underline{v}(t) \tag{17}$$

Finally (15) also implies

$$\hat{s}^{(k)}(t) = \underline{c}\ \underline{x}(t) \tag{18}$$

6.2.3.3

Stabilization of the algorithm

The recursive formulation (17), (18) of the filter is unfortunately not stable because the $\underline{A}$ matrix has all (p+1) eigenvalues in $\lambda = 1$. This causes an undesired growth of truncation errors when the algorithm is iterated many steps.

We now have two different realizations of the differentiating filter. The recursive (17), (18), that is computationally fast but can give large errors, and the original nonrecursive (11)-(13) that is slow but where the problem of error growth does not exist since a nonrecursive system is always stable.

In this section it will be described how the two realizations can be combined to obtain an algorithm that is both computationally fast and accurate.

The following scheme describes the principles by which the stabilized algorithm works.

1) The nonrecursive representation is used to provide initial values for the recursive representation.
2) The recursive filter is iterated L samples.
3) The nonrecursive filter is applied for the sample that was last calculated in 2).
4) The error due to instability is calculated as the difference between the result in 3) and the result for the last sample in 2).
5) The output from the nonrecursive filter are provided as new initial values for the recursive filter.
6) The error computed in 4) is compared to specified error bounds.
   a) If the error is within the error bounds, the computations proceed at 2).
   b) If the error is unnecessarily small, L is increased. The computations then proceed at 2).
   c) If the error is too large L is decreased. The computations are then restarted at 2) from the last sample that has previously

been tested and found to have an error that is not too large. Before proceeding to 2) the proper initial values are provided to the recursive algorithm.

Both upper and lower bounds are to be provided for the desired error. The lower bound is used for increasing the number of consecutive recursive iterations, L, when the actual error is smaller than the lower error bound. In this way the lower error bound makes it possible to increase the computing speed. The upper error bound, on the other hand, is preventing the error from becoming too large by causing a decrease in L when an error exceeding this bound is found.

For the application of the filters to gait analysis it is tolerable to let the instability error be 1% in the second derivative, since other sources give considerably larger errors. A lower error bound of 0.1% and an upper error bound of 1% have been used with satisfactorily results. With these error bounds L has been found to be approximately 5-10, which means that the time consuming, nonrecursive filter is being used only for about 10-20% of the samples. The recursive algorithm is about 5 times faster than the nonrecursive for the typical differentiation parameters, as was pointed out in the preceding section. This means that the computing time for the stabilized algorithm will be about 30-40% of the computing time for the nonrecursive algorithm.

This stabilized algorithm is implemented in subroutine DERAD, a list of which is found in [Gustafsson, Lanshammar, 1977].

To summarize, this stabilization technique has made it possible to keep the error due to instability within limits set by the user, and at the same time to keep the computing time within reasonable limits. The differentiation performed in ENOCH, including 24 variables and typically 400 samples of each variable, takes about 2-3 minutes on the HP 21MX computer.

6.2.3.4 Determination of filter parameters and estimation of the errors

The solution of the filter problem, given in section 6.2.3.2, is depending on several parameters, for which numerical values must be specified before the filter can be used. The parameters that will be discussed in this section are

$\frac{\rho}{\lambda^2}$ - Here, ρ is the square of the p:th term in the Taylor expansion of the signal, whose derivatives are to be estimated. Thus ρ is depending on the p:th derivative of the signal. λ^2 is the variance of the white noise that is assumed to be added to the signal. Since the derivatives of the signal are not known a priori, $\frac{\rho}{\lambda^2}$ will be treated as a parameter, to be given a suitable value.

p - The signal is approximated by the first p terms in its Taylor expansion. The filter is constrained not to give any systematic (deterministic) error, for polynomials of degree (p-1).

N - The number of filter weights (length of impulse response) is $(2 \cdot N+1)$.

First, the determination of $\frac{\rho}{\lambda^2}$ and p will be treated. The determination of N will be examplified with the application of the method to differentiation of gait data. In this context, the errors in the derivatives will also be analysed. It is suitable to make the error analysis simultaneously with the determination of the filter parameters, since the guideline for the choice of parameter values is to make the errors in the filter output as small as possible.

Determination of $\frac{\rho}{\lambda^2}$

Instead of trying to find a suitable value for $\frac{\rho}{\lambda^2}$ before the other parameters have been determined, the approach described below will be used.

A relation between all the parameters will be presented. This relation applies for parameter combinations that do not give a degenerated solution to the total error minimization problem (this will be further explained below). The relation is used to express $\frac{\rho}{\lambda^2}$ as a function of the remaining parameters p and N. In this way the number of independent parameters has been reduced to two.

The criteria function, equation (9) in section 6.2.3.2 is

$$V = \rho \cdot \underline{h}^T \cdot \underline{u}_p \cdot \underline{u}_p^T \cdot \underline{h} + \lambda^2 \cdot \underline{h}^T \cdot \underline{h}$$

and the minimization is subject to the constraints

$$\underline{h}^T \underline{u}_i = \begin{cases} 0 & i=0,\ldots,p-1 \quad i \neq k \\ \frac{k!}{T^k} & i=k \end{cases}$$

The two terms in V correspond to the systematic and the stochastic errors. It is important that p and N are chosen so that the systematic and stochastic errors are "balanced", i.e. have the same order of magnitude. Otherwise the criteria function will degenerate. What choice of p and N that will be suitable is depending on the signal and noise characteristics.

To clarify what will happen if they are not balanced, it will be assumed that the values of p and N are fixed, while $\frac{\rho}{\lambda^2}$ varies.

- $\frac{\rho}{\lambda^2} \to 0$

When $\frac{\rho}{\lambda^2}$ decreases, the systematic error term becomes less important, and in the limit the problem turns into:

6.2.3.4

Minimize

$$V = \underline{h}^T \cdot \underline{h}$$

where $\underline{h}$ is subject to the constraints

$$\underline{h}^T \cdot \underline{u}_i = \begin{cases} 0 & i=0,\ldots,p-1 \quad i \neq k \\ \dfrac{k!}{T^k} & i=k \end{cases}$$

This problem can be interpreted as least squares fitting of a polynomial of degree (p-1), and the use of its k:th derivative as an estimate of the signal's k:th derivative.

This effect occurs when p has become larger or N smaller than suitable. In both these cases the systematic error becomes small. Then the minimization problem essentially becomes a minimization of the stochastic error. The negative effect of this is that the stochastic error will often become larger than necessary; too large p implies unnecessarily many constraints on $\underline{h}$, while a small value on N means fewer degrees of freedom for the minimization.

$$\frac{\rho}{\lambda^2} \to \infty$$

When $\frac{\rho}{\lambda^2}$ increases, the systematic error is more heavily weighted. In the limit the problem becomes equivalent to:

Minimize

$$V = \underline{h}^T \cdot \underline{h}$$

where $\underline{h}$ is subject to the constraints

$$\underline{h}^T \cdot \underline{u}_i = \begin{cases} 0 & i=0,\ldots,p \quad i \neq k \\ \\ \dfrac{k!}{T^k} & i=k \end{cases}$$

Notice that in this case the systematic error term has turned into a constraint. In analogy with the above case this problem can be interpreted as the least squares fitting of a polynomial of degree p, and the use of its k:th derivative as an estimate of the k:th derivative of the signal.

This effect also occurs when p is smaller or N is larger than suitable. In these cases the true systematic error often becomes large, even if the systematic error term $\underline{h}^T \underline{u}_{p-p}^T \underline{h}$ has become close to zero. However, too small value on p means that it is not satisfactory to describe the systematic error with the p:th term in the Taylor series of the signal. There might well be higher order terms in the Taylor series corresponding to a systematic error much larger than the stochastic error, but they are not included in the model. Also, since the signal is approximated by the p first terms of its Taylor series over an interval including (2·N+1) samples, this approximation will of course become less accurate when N is increasing.

The two given examples had the purpose to emphasize the importance of obtaining a balance between the systematic and stochastic error terms in the criteria function. It is possible to achieve this by imposing a constraint on the parameters. This constraint will be used to define $\frac{\rho}{\lambda^2}$. From approximative calculations and from plots of the amplitude versus frequency characteristics of the resulting filters, it has been found that the following values for $\frac{\rho}{\lambda^2}$ are suitable for prevention of criteria function degeneration.

$$\frac{\rho}{\lambda^2} = 1.5 \cdot \frac{5}{2N^5} \qquad \text{for k=0, p=2}$$

$$\frac{\rho}{\lambda^2} = 2.5 \cdot \frac{7}{2\,N^7} \qquad \text{for k=1, p=3}$$

$\frac{\rho}{\lambda^2} = 15 \cdot \frac{9}{2N^9}$ for k=0, p=4

$\frac{\rho}{\lambda^2} = 5.5 \cdot \frac{9}{2N^9}$ for k=2, p=4

In figure 6 the amplitude responses for filters with k=2, p=4 and N=0 are plotted.

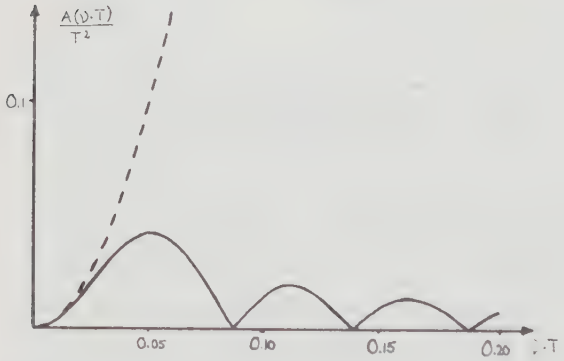

a) $\frac{\rho}{\lambda^2} = 0$

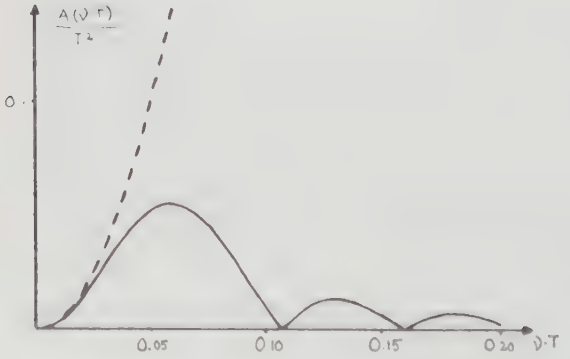

b) $\frac{\rho}{\lambda^2} = 5.5 \cdot \frac{9}{2N^9}$

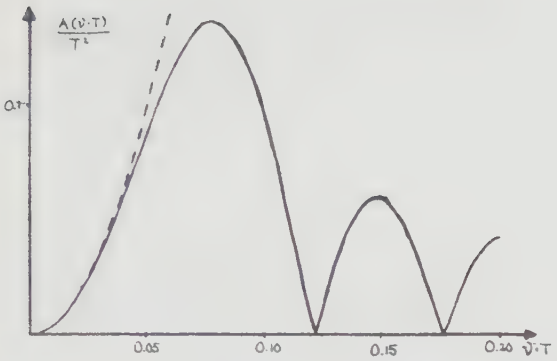

c) $\frac{\rho}{\lambda^2} = \infty$

Figure 6. Normalized amplitude versus normalized frequency. Parameters: k=2 (second derivative) p=4 N=10 (21 terms in the impulse response)

Figure 6 a), with $\frac{\rho}{\lambda^2} = 0$, is the degenerated case, which corresponds to the fitting of a second order polynomial. 6 b), with $\frac{\rho}{\lambda^2} = \frac{5.5 \cdot 9}{2\ N^9}$, is the case where it is ensured that the systematic and stochastic error terms will have the same order of magnitude, while figure 6 c), with $\frac{\rho}{\lambda^2} = \infty$, corresponds to the degenerated case equivalent to the fitting of a forth order polynomial.

Figure 6 c) has the best low frequency characteristics. This is because the minimization has forced the systematic error term to become zero. The price paid to achieve this is that the stochastic error has grown significantly (When the filter input is white noise, the standard deviation of the filter output can be roughly estimated by the area under the amplitude curve.).

An interesting feature of figure 1 is that the side lobes are much smaller in case b) than they are in the degenerated cases a) and c).

In b), the area of the first side lobe is 13% of the main lobe area, while it is 29% in a), and 23% in c). This will have the effect that the filter in b) will give better damping of high frequency noise than the filters in a) and c). This effect can also be seen in figure 7, which gives the amplitude characteristics of filters for estimation of the signal (k=0 p=4 N=10), the first derivative (k=1 p=3 N=10), and the second derivative (k=2 p=4 N=10).

We have now specified $\frac{\rho}{\lambda^2}$ as a function of N. This choice will make the minimization to produce a result where the terms corresponding to systematic and stochastic errors always have the same order of magnitude. Since no information regarding the signal characteristics has been used, there is of course no guarantee that the true systematic and stochastic errors will be balanced in this way. It is by variation of the remaining parameters, p and N, that this balance is to be accomplished.

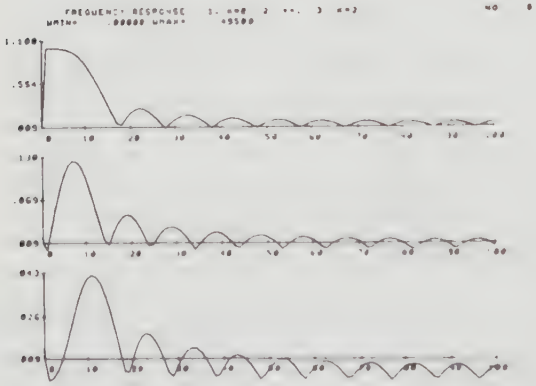

a) $\frac{\rho}{\lambda^2} = 0$

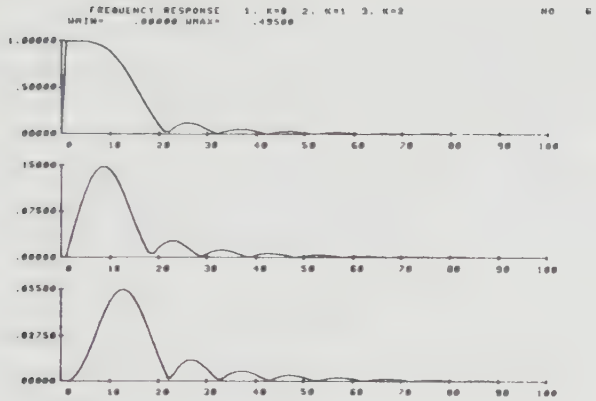

b) $\frac{p}{\lambda^2} = 15 \cdot \frac{9}{2 \cdot N^9}$ (upper curve), $2.5 \cdot \frac{7}{2N^7}$ (middle curve) respectively

$5.5 \cdot \frac{9}{2N^9}$ (lower curve)

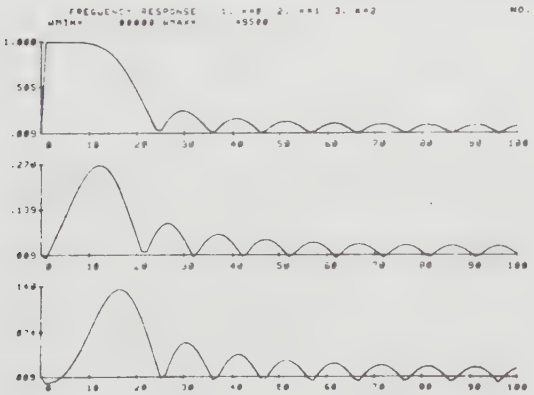

c) $\frac{p}{\lambda^2} = \infty$

Figure 7. Normalized amplitude versus frequency in percent of the Nyqvist frequency. Parameters: upper curves k=0,p=4,N=10, middle curves k=1,p=3,N=10, lower curves k=2,p=4,N=10.

Determination of p

The order of the recursive filter equals (p+1), so it is desirable to make p as small as possible to keep computation time down.

There are two constraints that must be met by the value chosen for p.

1) p must be greater than k. This follows directly from the problem formulation.

2) If k is odd, then p should also be odd, and if k is even, then p should be even. After some calculations it can be verified from equation (14) in section 6.2.3.2, that otherwise (p+1):th term in the Taylor expansion will not have any influence on the value of $\underline{h}$.

The natural starting point in the search for suitable parameter values is to choose p=k+2. If the following search for a suitable value on N shows that it is not possible to obtain a balance between the systematic and stochastic errors, because the systematic error is too large, then p can be increased two units.

Determination of N

By varying N, it is possible to change the filter characteristics so that the true systematic and stochastic errors obtain the same order of magnitude. If N is increased, the filter bandwidth will decrease, which results in a larger systematic error, while the stochastic error simultaneously will decrease. In the same way, a decrease in N will make the systematic error smaller and the stochastic error larger.

To make it feasible to find a suitable value for N, the filter bandwidth and noise transmission have been calculated for different values on N. The bandwidth, ω_b defined as that frequency for which the filters amplitude response equals $\frac{1}{\sqrt{2}}$ ·(the output from an ideal differentiator of the corresponding order), gives an idea of the systematic error to be expected when the frequency characteristics of the signal are known to some extent. The noise transmission, which equals $\underline{h}^T \cdot \underline{h}$, gives the

variance amplification of white noise in the filter. The formulas given in table 5 are approximate but usually they give ν_b and $\underline{h}^T \cdot \underline{h}$ within a few per cents. They have been obtained by frequency analysis of filters for different p and N values.

As an aid to computing the systematic error, the table also gives approximative upper error bounds for the systematic error within half and one quarter of the filter bandwidth.

The parameter combinations presented in table 5 are those that are used in ENOCH. Therefore the case k=0, p=2 has not been examined.

k	p	$\frac{c}{\lambda^2}$	ν_b	Upper bound for systematic error for signal frequencies less than			Noise transmission
				ν_b	$\frac{\nu_b}{2}$	$\frac{\nu_b}{4}$	$\underline{h}^T \cdot \underline{h}$
0	4	$15 \cdot \frac{9}{2 \cdot N^9}$	$\frac{0.60}{N \cdot T}$	29%	3%	0.2%	$\frac{1.2}{N}$
1	3	$2.5 \frac{7}{2 \cdot N^7}$	$\frac{0.33}{N \cdot T}$	29%	8%	3%	$\frac{2.0}{N^3 \cdot T^2}$
2	4	$5.5 \frac{9}{2 \cdot N^9}$	$\frac{0.38}{N \cdot T}$	29%	8%	3%	$\frac{2N+10}{N^5 \cdot T^4}$ $N \leq 10$ $\frac{30}{N^5 \cdot T^4}$ $N \geq 10$

Table 5. Approximative values for the relative systematic error and noise transmission of filters for the estimation of the signal and its first and second order derivatives.

The use of table 5 for the determination of the filter parameter N will now be examplified with gait data used in the ENOCH system.

6.2.3.4

Determination of parameters and error estimation for gait data

The kinematic data are dominated by the first few harmonics. According to [Winter et al, 1974a] 99.7% of the signal power is below 4.8 Hz when the signal is representing the toe coordinate. However, for other coordinates than the toe, the signal is probably more dominated by low frequency components and the high frequency components are present only for short periods, as for instance near heel strike. Our own preliminary frequency analysis indicates that more than 99% of the signal power for the knee is below 1.5 Hz for normal gait (two subjects have been examined).

The total noise from the kinematic measurement equipment and the A/D-converter gives a standard deviation of approximately 0.003 m.
The sampling interval will be assumed to be 0.00635 s, corresponding to half the maximum obtainable frequency with the Selspot equipment.

The second derivative will first be investigated.

Now, let us try with N=10 and calculate the resulting systematic and stochastic errors according to table 5.

The standard deviation of the output noise is calculated as the input noise standard deviation times the square root of the noise transmission.

$$\text{Stochastic error: } \sigma = \sqrt{\frac{30}{10^5 \cdot 0.00635^4}} \cdot 0.003 = 1.3 \text{ m/s}^2$$

$$\text{Systematic error: } \nu_b = \frac{0.38}{10 \cdot 0.00635} = 6.0 \text{ Hz}$$

The discussion above on the frequency content of gait data together with the filter bandwidth indicates that the systematic error will be less than approximately 3% most of the time. A typical value for the acceleration is 2 m/s^2, which means that the systematic error will be only a few cm/s^2 while the stochastic error, as calculated above, will be much greater. Figure 8 b) shows the resulting acceleration in horizontal direction for the knee when the parameter value N=10 was used.

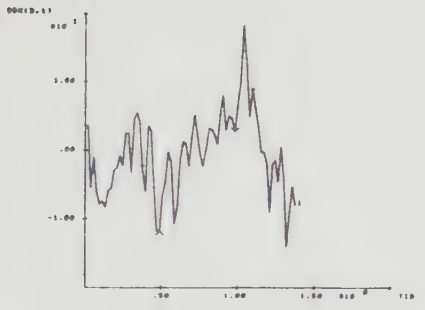

a) N=6

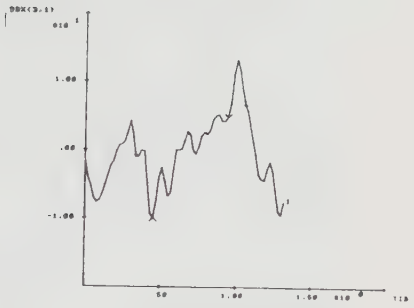

b) N=10

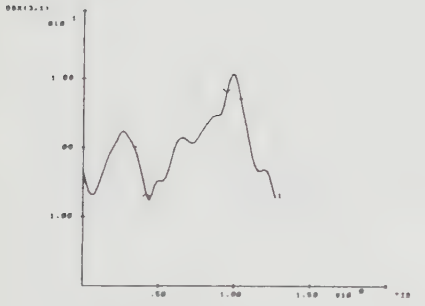

c) N=15

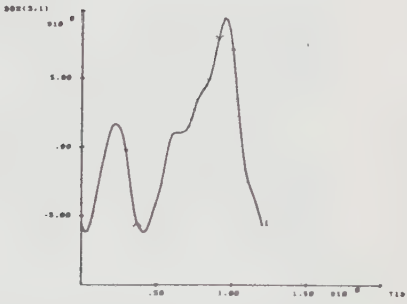

d) N=20

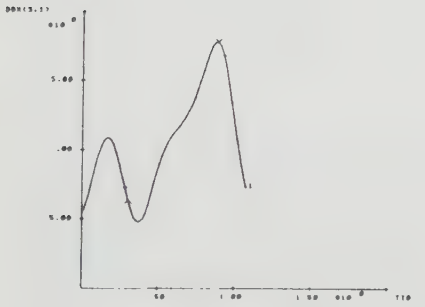

e) N=30

Figure 8. Second order derivative of the horizontal left knee coordinate, calculated with a varying number of taps in the differentiating filter
(The number of taps is 2N+1).

With N=30 the stochastic error becomes σ=0.08 m/s^2 and the bandwidth of the filter will be 2.0 Hz.

A typical systematic error will be perhaps 8% of a few m/s^2, which is greater than the stochastic error. The peak systematic error will occasionally be a few m/s^2 (notice that the peak values have decreased significantly in figure 8 e)).

Finally for N=20 we will get the stochastic error σ=0.23 m/s^2, while the bandwidth is 3.0 Hz. Most of the time the frequency content of the signal is essentially below half the bandwidth of the filter and the systematic error will be less than perhaps 5% of typically a few m/s^2. The systematic and stochastic errors will thus have the same order of magnitude. For short periods, however, there will be high frequency components in the signal that will not be accurately differentiated. In figure 8 d) the peak values have become too small.

In this described example we have found it reasonable to use N=20 for estimation of the second order derivative. The stochastic and systematic errors will then be of the same order, approximately 0.2 m/s^2, most of the time.

There are of course other error sources that are not included in this description. If, for instance, the diodes are not properly attached, they can move in a way that is not typical for the joint, the motion of which it is supposed to describe. This kind of error can be described with correlated noise and it will not be damped according to the noise transmission in table 1 since it often has a low frequency character.

A further error source is the instability in the recursive filter formulation. This error is limited to 1% in the stabilized algorithm.

The subroutine DERAD, in which the filter is implemented, is capable to produce simultaneous estimates of all deviatives up to the k:th order, which is the maximum as specified by the user. The same recursive algorithm (state space model) is used for all derivatives and only the

vector $\underline{c}$ (see section 6.2.3.2) differs. By this arrangement the 0th and 1st order derivatives are obtained simultaneously with the 2nd order derivative without any significant increase in the computation time. Different p and $\frac{\rho}{\lambda^2}$ values can be used but N must have the same value for all derivatives if this is to be feasible. Since the 2nd derivative is the most critical, we let it determine the N value to be used. With this in mind we will now present the parameters used for the 0th and 1st order derivatives together with the expected errors. The errors have been obtained analogously with what has been described above for the second derivative.

0th order derivative (coordinates):

Parameters: $\frac{\rho}{\lambda^2} = 15 \cdot \frac{9}{2\,N^9}$, p=4, N=20

Bandwidth of filter: 4.9 Hz

(The bandwidth has not been obtained from the formula in table 5 but from frequency analysis of the filter characteristics.)

Stochastic error: $\sigma = 8 \cdot 10^{-4}$ m

Systematic error: typically ~ 0.01 m

1st order derivatives (velocities):

Parameters $\frac{\rho}{\lambda^2} = 2.5 \frac{7}{2 \cdot N^7}$, p=3, N=20

Bandwidth of filter: 2.7 Hz

Stochastic error: $\sigma = 8\ 10^{-3}$ m/s

Systematic error: typically ~ 0.1 m/s

It should be noted that more accurate estimates for the 0th and 1st order derivatives can probably be obtained with other parameter combinations. Especially the 1st derivative has an unnecessarily large systematic error. The work done so far has mainly concerned the second order derivative, which is the important one as far as forces and moments are concerned.

For completeness the figures for the 2nd order derivative will finally be repeated.

6.2.3.4

2nd order derivative (accelerations):

Parameters: $\frac{\rho}{\lambda^2} = 5.5 \cdot \frac{9}{2 \cdot N^9}$, p=4, N=20

Bandwidth of filter: 3.1 Hz
(not obtained from table 1)
Stochastic error: 0.23 m/s^2
Systematic error: typically ~ 0.1 m
(the peak error can be much larger).

6.2.4 Evaluation of the differentiation method

The evaluation of the method described in section 6.2.3 will only consider second order derivatives which is the highest order needed in the ENOCH system and which is more difficult to obtain than the lower order derivatives.

First the properties of the presented method will be compared to those of the ideal filter presented in section 6.2.1. Then a comparison between differentiated data and accelerometer data will be presented. Finally, ground reaction forces measured with a force plate are compared to ground reaction forces estimated from accelerations (second order derivative of displacement data) and antrophometric data.

Comparison with an ideal differentiator

In section 6.2.1 it was verified that the output noise variance for an ideal differentiator is related to the input noise variance according to

$$\frac{\sigma^2_{k,min}}{\sigma^2_f} = \frac{T \cdot \omega_s^{2k+1}}{\pi \cdot (2k+1)}$$

which for estimation of the second order derivative becomes

$$\frac{\sigma^2_{k,min}}{\sigma^2_f} = \frac{T \cdot \omega_s^5}{\pi \cdot 5}$$

For our differentiator we have

$$\frac{\sigma^2_2}{\sigma^2_f} = \underline{h}^T \cdot \underline{h} \approx \frac{30}{N^5 \cdot T^4} \approx \frac{30}{\left(\frac{0.38}{\nu_b \cdot T}\right)^5 \cdot T^4} = 6 \frac{T(2\pi \cdot \nu_b)^5}{\pi \cdot 5}$$

where the parameter values and relations between bandwidth, ν and noise transmission found in table 5 in section 6.2.3.4 have been used. Theoretically, this means that it is possible to reduce the noise variance with a factor 6 by using a differentiator with a perfect cut off at the filters bandwidth. This corresponds to a reduction in the standard deviation of the noise with the factor 2.5. This ideal differentiator can be approached by an increase in the order of the filter. A negative consequence of doing this is increased computing time and there will also be an increased number of endpoint samples, for which no estimates of the derivatives are obtained from the basic algorithm.

Comparison of accelerations obtained by numerical differentiation with accelerometer data

In figure 9 b) a comparison is presented between accelerometer data (solid line) and estimated accelerations (crosses) obtained by differentiation of goniometer data. Figure 9 a) shows the corresponding goniometer data.

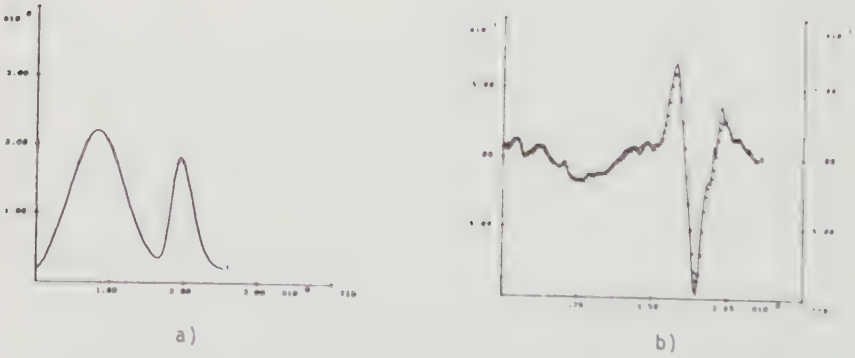

a) b)

Figure 9. Comparison between twice differentiated goniometer data and accelerometer data. a) Goniometer data. b) Accelereometer data (solid line) and differentiated goniometer data (crosses).

The data have been obtained from Dave Winter (personal communication).

For the differentiation the following parameter values were used

$$k=2 \quad p=4 \quad N=3 \quad \frac{\rho}{\lambda^2} = 5.5 \frac{9}{2 \cdot N^9}$$

This corresponds to the filter bandwidth ν_b=5.5 Hz.

The excellent agreement found in figure 9 b) has also been obtained by Winter by digital low pass filtering (4.8 Hz bandwidth) prior to numerical differentiation by finite differences.

This test shows that for these data, the new method works at least as good as the method used by Winter.

Comparison between calculated and measured floor reaction forces

In figure 10 the result from a comparison between calculated and measured floor reaction forces is presented

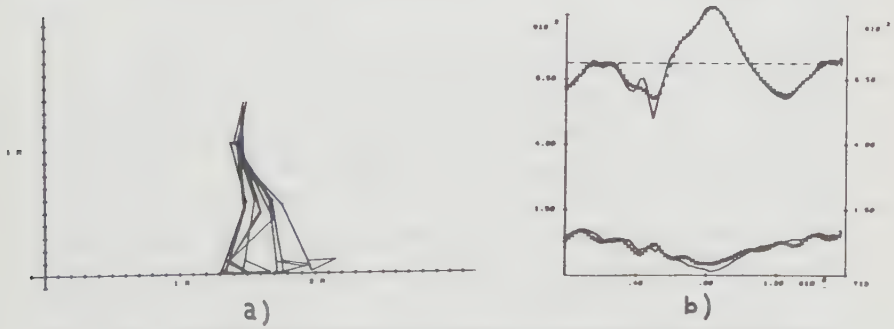

Figure 10. Comparison between calculated and measured vertical floor reaction forces. a) Experimental conditions. The left foot was on the force plate, while the rest of the body was in motion. b) Measured (solid lines) and calculated (crosses) forces, with vertical forces in upper curves and horizontal in lower curves.

The calculated forces have been obtained as

$$F_x = \sum_{i=1}^{5} m_i \ddot{x}_i$$

$$F_y = \sum_{i=1}^{5} m_i(\ddot{y}_i + g)$$

where x is horizontal and y vertical direction, m_i is segment mass and g is the gravitational constant. The summation is performed over the five segment that constitutes the human body according to the model described in section 6.4. The accelerations have been obtained by numerical differentiation of gait data, obtained from the Selspot equipment at the sampling frequency 157.5 Hz. For the differentiation, the parameters

$$\frac{\rho}{\lambda^2} = 5.5 \cdot \frac{9}{2N^9} \qquad p=4 \qquad N=20$$

was used, which means that the bandwidth was 3.1 Hz and that the filter had 41 taps.

The measured forces was obtained from a force plate.

During the experiment, the subject was standing with his left foot on the force plate while the rest of his body was moving.

In this context the force plate data can be considered to be exact while several types of errors enters into the calculated forces

- m_i is not exact
- The diode coordinates do not exactly represent the segment locations
- The measured coordinate values do not exactly correspond to the diode coordinates
- Errors are introduced in the differentiation

- Errors are introduced in the computation of the accelerations for the segments centers of mass from diode accelerations since the true locations of the centers of mass are not exactly known.

These different error sources are evaluated in chapter 9. Here we will only conclude that in spite of all these different types of errors the curves are fitting remarkably well. The deviations in the vertical force (upper curves) near the sharp peak can be attributed to the smoothing of the differentiating filter, while the deviations in the horizontal forces (lower curves) might be the result of diode motions that do not correspond to the motions of the segment centers of mass.

6.2.5 Comparison with two related methods

The differences between the new method and two related methods for numerical differentiation will be examined in this section.

The method described in [Lanczos, 1956] is based on least squares polynomial fitting to measurement data, and the use of the derivatives of this polynomial as estimates of the signal derivatives.

In the degenerated cases, when $\frac{\rho}{\lambda^2} \to 0$ or $\frac{\rho}{\lambda^2} \to \infty$, the results produced by our filter in fact become equivalent to those obtained from the method described by Lanczos. This has also been pointed out in section 6.2.3.4. However, when $\frac{\rho}{\lambda^2}$ assumes finite values, the method proposed here exhibits quite different characteristics. One important feature is the better damping obtained for high frequencies.

Another difference concerns the implementation. Lanczos results are non-recursive, while the recursive implementation of the new method (implemented in subroutine DERAD) has made it computationally faster.

In [Allum, 1975] a method is given for recursive implementation of a filter for estimation of the first derivative. The resulting algorithm is called CUBIC. The design is based on least square fitting of a third order polynomial. Among the important differences between Allum's filters and DERAD are:

- Allums design is for a filter, while DERAD is for a smoother. As a result of this, CUBIC exhibits phase errors, while DERAD gives perfect phase characteristics.
- CUBIC uses third order polynomial fitting, while DERAD allows an arbitrary order. DERAD also includes a remainder for the systematic error.
- In CUBIC, only the first derivative is estimated, while DERAD allows simultaneous estimation of all derivatives up to a specified order.

- The recursive formulation of CUBIC is done in a way, which is valid only for the special case of a third order polynomial, while the formulation used in DERAD is valid for all orders.
- CUBIC is unstable, while DERAD has been stabilized.

6.3 Determination of times for gait phase changes

Whenever a person is changing his stride length (covered distance during one gait cycle) or stride frequency (inverse of the time required for one gait cycle) his gait patterns will also change, a fact that is strongly emphasized in [Lamoreux, 1971]. Therefore it is important to know the stride length and stride frequency when analyzing the results from a gait measurement.

In this context the problem is important also from another aspect. To be able to calculate the resultant joint forces and torques it is necessary to know whether one or two feet are touching the floor, and if one foot is touching the floor (single limb support) one must also know if it is the right or the left foot that is swinging. This information is necessary for the force plate data to be properly used.

To determine the stride frequency a number of methods can be used. The simplest is to manually measure the time required for a certain number of gait cycles and then estimate the stride frequency by the number of cycles divided by the time required. Another method developed by Larry Lamoreux is to use foot switches that control a digital clock. This system displays the time required for a certain number of cycles. Simultaneously, this system also produces a display of the time required for the subject to walk a specified distance, defined as the distance between two parallel light beams guarded by photocells. From this registration, the gait velocity is obtained as the distance divided by the time required. The stride length can then be obtained as the velocity divided by the stride frequency.

We will, however, use a different approach for the determination of stride length and stride frequency, that does not require any extra hardware to be mounted on the subject. Before going into details on this method we will discuss the division of the gait cycle into different gait phases.

To meet the requirements of the gait model we have divided the gait cycle into four different phases:

- Right double stance phase, defined as double stance phase that is followed by right swing phase.

- Right swing phase occurs during single limb support when the right leg is swinging.
- Left double stance phase, defined as double stance phase that is followed by left swing phase.
- Left swing phase occurs during single limb support when the left leg is swinging.

The transitions between these gait phases are characterized by the four events:

1) Left heel strike
2) Right toe off
3) Right heel strike
4) Left toe off.

The concepts of "heel strike" and "toe off" are referring to normal gait but if defined as the events of transition between the different gait phases they can be used even when the actual gait pattern is characterized for instance by "toe strike" instead of "heel strike".

The division of a gait cycle into gait phases can go further than we have done here, but the four described phases are sufficient for our purposes, which are to determine stride length and stride frequency and to provide the gait model with proper information concerning the interaction between the subject and the floor.

If we assume that the gait is stationary, and if we know the point of time of the four events described above, then stride length and stride frequency can be determined as follows:

Stride length can be estimated by the difference in horizontal (x) coordinates of for instance the left heel between two adjacent left heel strikes (event 1). Stride time can be estimated by the time interval between two phase change events of the same kind, for example two left heel strikes (event 1). The stride frequency is then calculated as the inverse of the stride time.

When force plates are present in the measurement system, the most natural approach is to determine the point of time for a gait phase change from the force plate data. The transition from swing to stance phase occurs when the force plate data begin to deviate from zero, and vice versa. However, in the present installation there is only one force plate implemented, so it is only possible to determine the gait phase changes for the foot that steps on the force plate. To make it possible to determine the point of time for gait phase changes for both legs and for several steps another approach has been used.

The point of time for gait phase changes have been calculated from the velocities of the feet. For normal gait it is reasonable to assume that the velocity of a foot is much higher during swing phase than during stance phase. More precisely the velocity of either the heel or the toe ought to be nearly zero during stance phase, since the heel or the toe is in contact with the floor during this phase.

If we define the squared foot velocity as the smallest of the squared ankle velocity and squared toe velocity, i.e.

$$V^2_{foot} = \min(V^2_{ankle}, V^2_{toe})$$

we can use V^2_{foot} to determine whether the foot is in stance or swing phase. As a criterion we will use a constant V^2_{limit} in the following way

$$V^2_{left\ foot} \geq V^2_{limit} \Rightarrow \text{left leg is swinging}$$

$$V^2_{left\ foot} < V^2_{limit} \Rightarrow \text{left leg is in stance phase}$$

and an analogous criterion is used for the right leg. The criteria are evaluated for all the samples and if we for instance find that for time t we have left leg swinging and right leg in stance phase, we then have left swing phase for this point of time. During double stance phase we separate between right and left double stance phase using the fact that normally the foot that has the smallest horizontal coordinate is the one that will swing during the following swing phase.

Thus, we must find a suitable value for V_{limit}.

Figure 11 is a computer plot of the velocities in horizontal and vertical direction of the left heel and the left toe. This subject is a grown male with normal gait.

The phase shifts have here been calculated using the value

$$V^2_{limit} = 0.2 \quad m^2/s^2$$

The events are denoted by ⌄ for heel contact and ⌃ for toe off. Left leg is represented by small arrows and right leg by bigger arrows.

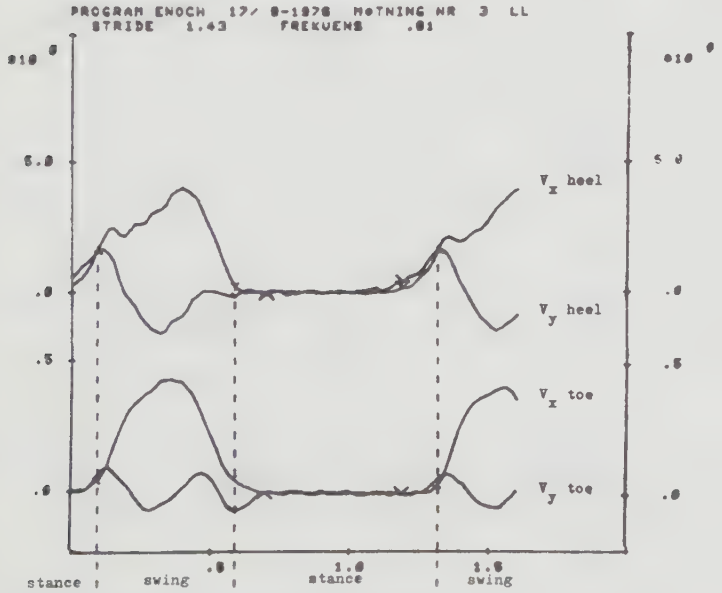

Figure 11. Velocities for the left heel and toe diodes.

Before the first transition from stance phase to swing phase we see that the heel curves have departed considerably from zero while the toe curves are still approximately zero. This means that the heel is leaving the floor before the toe. Shortly after the toe curves have also departed

from zero we have the small arrow that indicates that we have the event of left toe off and thus a transition from stance to swing phase. This means that the squared toe velocity has exceeded 0.2 π^2/s^2. The next time we get a small arrow is when the left heel velocity is approaching zero. We then get an arrow that represents left heel contact and a transition from swing to stance phase. At this time the left toe still has a velocity that is relatively far from zero.

One can argue that it would be better to let V^2_{limit} assume a smaller value and thus to get the phase shifts when the velocities are closer to zero than in the described example. Two reasons can be given for not decreasing V^2_{limit}:

i) If V^2_{limit} is much closer to zero, then there is a risk that deviations from zero in the velocities during stance phase, due to measurement noise, can cause the requirements for a phase shift to be fulfilled. This would give indications of phase shifts that have no correspondence in reality.

ii) The diodes are mounted, not at the front and rear edges of the shoes, but rather at the "toe base" and at a place a few centimeters in front of the rear shoe limit. This means that for instance in the transition from stance to swing phase the toe diode is beginning to move before the toe is actually leaving the ground and the actual toe off and heel down is probably very near to those indicated in Figure 11.

The value chosen for V^2_{limit} would perhaps not be suitable for irregular or slow gait. It is undoubtfully more reliable to determine the point of time for gait phase shifts by more direct methods, as for example from force plate data.

Another type of phase change criterion has also been used for the determination of heel off. For normal gait, heel off seems to coincide in time with maximum vertical heel velocity. Therefore the point of time for heel off might be determined by the point of time for zero vertical heel acceleration.

The calculation of times for gait phase changes are implemented in the subroutine FASTE.

6.4 The mechanical model

In this section the structure of the model used for the kinetic calculations will be described.

Our model does not differ in any important aspect from other models found in the literature. Our is based on a model found in [Jahnberg, 1972]. It consists of seven rigid bodies linked according to figure 12.

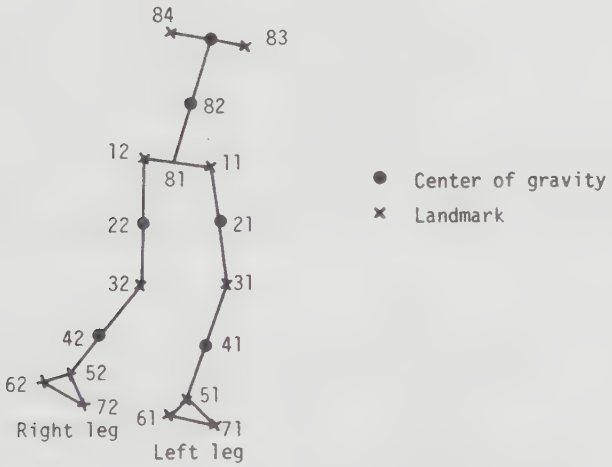

Figure 12. Structure of the gait model. With exception of the trunk, second index equal to one indicated left leg and second index equal to two indicates right leg.

The basic limitations of the model are

1) The model is two dimensional, i.e. only planar movement is studied.

2) The trunk, the arms and the head are considered as one rigid body.

3) Each leg is assumed to be composed of the rigid bodies, thigh, shank and foot which are linked together.

The foot has been included in the calculation of mass, segment, center of mass and moment of inertia for the model shank, while the model foot is weightless.

The joints and the center of gravity of the segments are indexed according to figure 12. Whenever a specific segment is refered to it is labelled by the index of its center of gravity. For instance, the mass of the right shank is called m_{22}, and in the computer programs it is called M (2,2).

The different kinds of variables in the models are body segment parameters, cartesian coordinates, velocities and accelerations, angles, angular velocities and angular accelerations, forces and moments.

Body segment parameters:
These parameters define the mechanical properties of the body segments. They are segment mass (m), segment length (l), location of center of mass (h), and moment of inertia (i) The variables are defined in Figure 13.

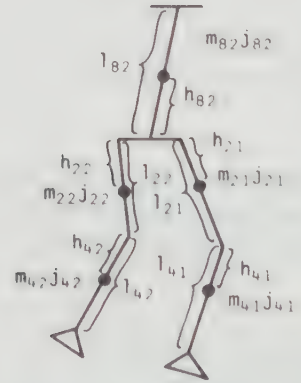

Figure 13. Body segment parameters.

The estimation of these parameters is described in section 6.1.

Kinematic variables:
The cartesian coordinates (x, y) are denoted according to figure 14. Their first and second order derivatives are denoted ($\dot{x}$, $\dot{y}$) and ($\ddot{x}$, $\ddot{y}$) respectively, and they are indexed in the same way as the coordinates.

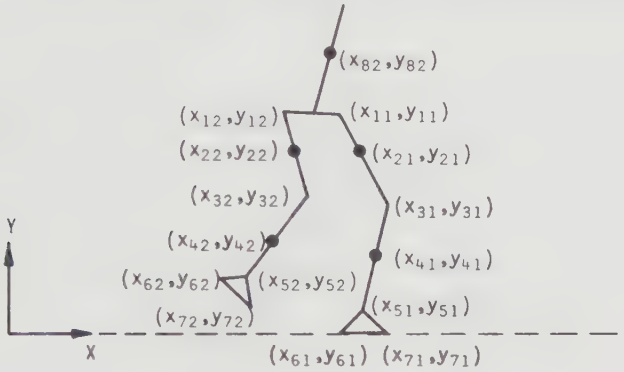

Figure 14. Cartesian coordinates.

The angles (φ) are defined by figure 15. Angles referring to joints are relative angles and those referring to segment centers are absolute angles. The same notations are used for the angular velocity, $\dot{\varphi}$, and the angular acceleration, $\ddot{\varphi}$.

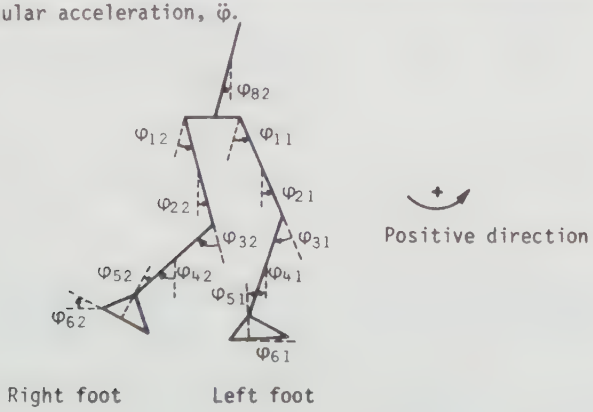

Figure 15. Definition of angles.

6.4

The estimation of angles and their derivatives is described in section 6.4.2.

Finally, forces and moments are defined by figure 16.

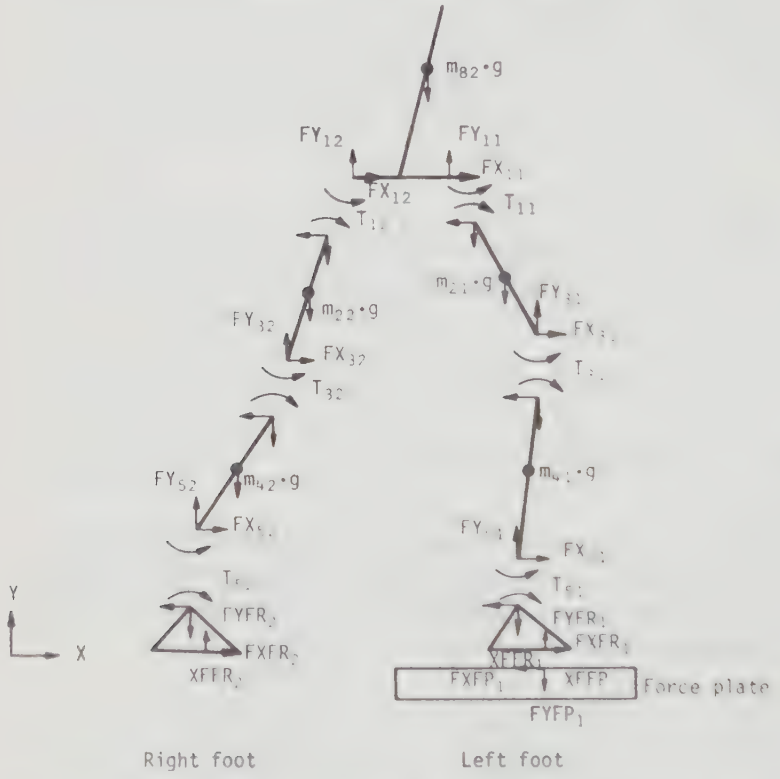

Figure 16. Definition of forces and moments. Example with left leg on the force plate.

Beside intersegment forces and moments, denoted (FX, FY) and T, figure 16, also illustrates the definition of floor reaction forces, (FXFR, FYFR) and their point of attack (x-coordinates XFFR, y-coordinate zero). The force exerted on the force plate (FXFP, FYFP) and its point of attack (XFFP, 0) is also shown.

The calculation of forces and moments is described in section 6.4.3.

6.4.1 Calculation of the displacements of the segments' centers of mass

For the determination of resultant joint forces and torques it is necessary to estimate the location of the center of mass for each one of the body segments included in the model, since the gravitation force acts at this point.

From the methods given in section 6.1 on body segment parameters we acquire an estimate of the distance (h) between the center of gravity and the proximal joint for each segment and of the segment length (l). If we assume that the center of mass is located along the straight line connecting the distal and proximal joints of the segment, we can calculate the coordinates of the center of gravity according to figure 17.

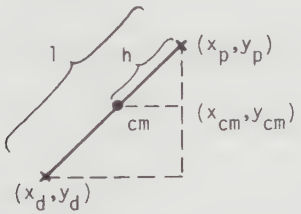

Figure 17. Center of gravity for one segment.

We get

$$x_{cm}(t) = x_d(t) + (l - h)\frac{(x_p(t)-x_d(t))}{l}$$

$$y_{cm}(t) = y_d(t) + (l - h)\frac{(y_p(t)-y_d(t))}{l}$$

where $(x_p(t), y_p(t))$ and $(x_d(t), y_d(t))$ are the proximal and distal joint coordinates that are estimated by the measured coordinates of the light emitting diodes.

For the trunk, we estimate $(x_p(t), y_p(t))$ and $(x_d(t), y_d(t))$ according to figure 18, as the mean value of the two shoulder diodes respectively the two hip diodes.

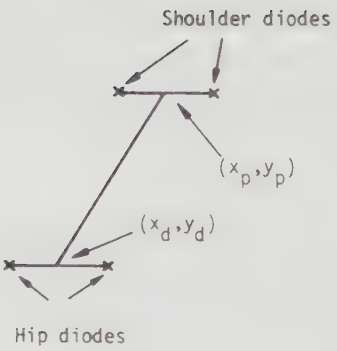

Figure 18. Estimation of the center of gravity for the trunk.

The calculations are done in subroutine TP.

6.4.2 Calculation of angles

The calculation of angles is straightforward. From figures 14 and 15 it is clear that

$$\varphi(2,i) = \tan^{-1}\left[\frac{X(3,i)-X(1,i)}{Y(1,i)-Y(3,i)}\right] \qquad i = 1,2$$

$$\varphi(4,i) = \tan^{-1}\left[\frac{X(5,i)-X(3,i)}{Y(3,i)-Y(5,i)}\right] \qquad i = 1,2$$

$$\varphi(6,i) = \tan^{-1}\left[\frac{Y(7,i)-Y(6,i)}{X(7,i)-X(6,i)}\right] \qquad i = 1,2$$

$$\varphi(8,2) = \tan^{-1}\left[\frac{X(8,1)-X(8,2)}{Y(8,2)-Y(8,1)}\right]$$

The relative angles are then obtained as

$$\varphi(1,i) = \varphi(2,i) - \varphi(8,2) \qquad i = 1,2$$

$$\varphi(3,i) = \varphi(4,i) - \varphi(2,i) \qquad i = 1,2$$

$$\varphi(5,i) = \varphi(6,i) - \varphi(4,i) \qquad i = 1,2$$

To calculate the first and second order derivatives of the angles the above expressions have been analytically differentiated twice. The resulting expressions give the angular velocities and accelerations in terms of the already estimated cartesian first and second order derivatives.

The described calculations of angles and their first and second order derivatives are performed by the subroutine VINKE.

6.4.3 Calculation of forces and moments

According to figure 16 the calculated forces and moments are the total intersegment forces and moments. There are 16 forces, 6 moments and 2 variables giving the horizontal coordinates of the point of attack of the floor reaction force on each foot.

For each one of the segments we use the Newtonian equations of motion

$$\sum_i FX_i = m \cdot \ddot{x}_{cm}$$

$$\sum_i FY_i = m \cdot \ddot{y}_{cm}$$

$$\sum_i T_i = j \cdot \ddot{\varphi}$$

where the summation is made over all forces and moments acting on the segment. Here

FX_i are horizontal

FY_i are vertical forces

T_i are moments acting perpendicular to the x-y-plane and calculated with respect to the segments center of mass.

m is the segment mass

$(\ddot{x}_{cm}, \ddot{y}_{cm})$ is the linear acceleration of the segments center of mass

j is the segment's moment of inertia

$\ddot{\varphi}$ is the angular acceleration of the segment.

We thus have 3 equations of motion for each segment. The model contains 7 segments which give a total of 21 equations from which forces and moments can be calculated. Since we have 24 variables that are to be calculated we are short of 3 equations.

The required extra information can be obtained by the use of force plates. With two force plates the forces applied on both feet can be measured. However, the present system installation only includes one force plate, so here we will present how the information obtained from this force plate have been used to calculate the joint forces and moments.

The three missing equations are obtained as follows:

1) During single limb support when only one foot is in contact with the floor, we know that the floor reaction forces (in x- and y-direction) on the swinging foot are zero. Assuming that the left foot is swinging (last index equal to 1) we then get for the floor reaction force

$$FXFR_1 = 0$$
$$FYFR_1 = 0 \qquad (1)$$
$$XFFR_1 = 0$$

We thus have 3 extra equations and a total of 24 equations, which makes it possible to calculate the 24 variables.

2) During double limb support it is necessary to measure 3 of the variables to make it possible to solve the equations of motion. The force plate is used to measure the floor reaction forces (FXFP, FYFP) and its point of attack (XFFP) for one foot. We get the following three extra equations (assuming that left foot is on the force plate)

$$FXFR_1 = FXFP$$
$$FYFR_1 = FYFP \qquad (2)$$
$$XFFR_1 = XFFP$$

Again we have 24 equations and the 24 variables can thus be calculated.

We will now list the equations of motion applying for the model. Index i = 1 means left leg and i = 2 means right leg.

Foot:

$$\left.\begin{aligned} 0 &= FXFR_i - FX_{5i} && i = 1,2 \\ 0 &= FYFR_i - FY_{5i} && i = 1,2 \\ 0 &= -T_{5i}+Y_{5i}\cdot FXFR_i+(XFFR_i-X_{5i})\cdot FYFR_i && i = 1,2 \end{aligned}\right\} \quad (3)$$

Shank:

$$\left.\begin{aligned} m_{4i}\cdot\ddot{x}_{4i} &\equiv FX_{4i} = FX_{5i} - FX_{3i} && i = 1,2 \\ m_{4i}\cdot\ddot{y}_{4i} &\equiv FY_{4i} = FY_{5i} - FY_{3i} - m_{4i}\cdot g && i = 1,2 \\ j_{4i}\cdot\ddot{\varphi}_{4i} &\equiv T_{5i}-T_{3i}+(x_{5i}-x_{4i})\cdot FY_{5i}-(y_{5i}-y_{4i})\cdot FX_{5i} + \\ &\quad + (x_{4i}-x_{3i})\cdot FY_{3i}-(y_{4i}-y_{3i})\cdot FX_{3i} && i = 1,2 \end{aligned}\right\} \quad (4)$$

Thigh:

$$\left.\begin{aligned} m_{2i}\cdot\ddot{x}_{2i} &\equiv FX_{2i}=FX_{3i}-FX_{1i} && i = 1,2 \\ m_{2i}\cdot\ddot{y}_{2i} &\equiv FY_{2i}=FY_{3i}-FY_{1i}-m_{2i}\cdot g && i = 1,2 \\ j_{2i}\cdot\ddot{\varphi}_{2i} &\equiv T_{2i} =T_{3i}-T_{1i}+(x_{3i}-x_{2i})\cdot FY_{3i}-(y_{3i}-y_{2i})\cdot FX_{3i} + \\ &\quad +(x_{2i}-x_{1i})\cdot FY_{1i}-(y_{2i}-y_{1i})\cdot FX_{1i} && i = 1,2 \end{aligned}\right\} \quad (5)$$

Trunk:

$$\left.\begin{aligned} m_{82}\cdot\ddot{x}_{82} &\equiv FX_{82} = FX_{11} + FX_{12} \\ m_{82}\cdot\ddot{y}_{82} &\equiv FY_{82} = FY_{11} + FY_{12} - m_{82}\cdot g \\ j_{82}\cdot\ddot{\varphi}_{82} &\equiv T_{82} = T_{11} + T_{12} + (x_{11}-x_{82})\cdot FY_{11}-(y_{11}-y_{82})\cdot FX_{11} + \\ &\quad + (x_{12}-x_{82})\cdot FY_{12}-(y_{12}-y_{82})\cdot FX_{12} \end{aligned}\right\} \quad (6)$$

In the above 21 equations m is segment mass, j is the segment moment of inertia and g is the gravitational constant (9.81 m/s^2)

We will now write down the equations as they are used in the calculations of forces and moments. These calculations are performed for each sample.

During double stance phase, the calculations will start with the foot on the force plate and the floor reaction forces and its point of attack is calculated from equation (2). During single limb support the calculation starts with the swinging leg, and equations (1) are first used.

In the following list of the equations, index i stands for the leg with which the calculation starts and index j stands for the other leg.

$FXFR_i$, $FYFR_i$, $XFFR_i$ are first calculated from equations (1) or (2). Equations (3)-(6) now give

$$FX_{5i} = FXFR_i \tag{7}$$

$$FY_{5i} = FYFR_i \tag{8}$$

$$T_{5i} = Y_{5i} \cdot FX_{5i} + (XFFR_i - X_{5i}) \cdot FY_{5i} \tag{9}$$

$$FX_{3i} = FX_{5i} - FX_{4i} \tag{10}$$

$$FY_{3i} = FY_{5i} - FY_{4i} - m_{4i} \cdot g \tag{11}$$

$$T_{3i} = T_{5i} - T_{4i} + (x_{5i} - x_{4i}) \cdot FY_{5i} - (y_{5i} - y_{4i}) \cdot FX_{5i} + (x_{4i} - x_{3i}) \cdot FY_{3i} - (y_{4i} - y_{3i}) \cdot FX_{3i} \tag{12}$$

$$FX_{1i} = FX_{3i} - FX_{2i} \tag{13}$$

$$FY_{1i} = FY_{3i} - FY_{2i} - m_{2i} \cdot g \tag{14}$$

$$T_{1i} = T_{3i} - T_{2i} + (x_{3i} - x_{2i}) \cdot FY_{3i} - (y_{3i} - y_{2i}) \cdot FX_{3i} + (x_{2i} - x_{1i}) \cdot FY_{1i} - (y_{2i} - y_{1i}) \cdot FX_{1i} \tag{15}$$

$$FX_{1j} = -FX_{1i} + FX_{82} \tag{16}$$

$$FY_{1j} = -FY_{1i} + FY_{82} + m_{82} \cdot g \tag{17}$$

$$T_{1j} = -T_{1i} + T_{82} - (x_{1i} - x_{82}) FY_{1i} + (y_{1i} - y_{82}) FX_{1i} - (x_{1j} - x_{82}) FY_{1j} + (y_{ij} - y_{82}) FX_{1j} \tag{18}$$

$$FX_{3j} = FX_{1j}+FX_{2j} \tag{19}$$

$$FY_{3j} = FY_{1j}+FY_{2j}+m_{2j}\cdot g \tag{20}$$

$$T_{3j} = T_{1j}+T_{2j}-(x_{3j}-x_{2j})FY_{3j}+(y_{3j}-y_{2j})FX_{3j} - \\ -(x_{2j}-x_{1j})FY_{1j}+(y_{2j}-y_{1j})FX_{1j} \tag{21}$$

$$FX_{5j} = FX_{3j}+FX_{4j} \tag{22}$$

$$FY_{5j} = FY_{3j}+FY_{4j}+m_{4j}\cdot g \tag{23}$$

$$T_{5j} = T_{3j}+T_{4j}-(x_{5j}-x_{4j})FY_{5j}+(y_{5j}-y_{4j})FX_{5j} - \\ - (x_{4j}-x_{3j})FY_{3j}+(y_{4j}-y_{3j})FX_{3j} \tag{24}$$

$$FXFR_j = FX_{5j} \tag{25}$$

$$FYFR_j = FY_{5j} \tag{26}$$

$$XFFR_j = (T_{5j}-Y_{5j}\cdot FXFR_j)/FYFR_j+X_{5j} \tag{27}$$

Note that during single limb support, force plate data are not used in the calculations, and equations (25)-(27) give the floor reaction forces and their point of attack.

If the corresponding foot is actually on the force plate, this gives an excellent method to check the results by comparison between the calculated data and the data directly measured on the force plate. Such a comparison is presented in chapter 9.

The calculations now described are carried through in the system ENOCH by the subroutines BEREK (calculate), KRAFT (force) and MOMEN (moment).

When two force plates are used instead of one, the forces and moments for both legs can be calculated from equations (7)-(15) by letting i assume the values 1 and 2. In this case the equations (16)-(18), representing the trunk, will not have to be used. By this arrangement the accuracy can be considerably improved since errors in the calculated coordinates and accelerations for the center of mass of the trunk is otherwise dominating over errors in the other segments due to the large mass of the trunk. The same calculations can also be performed during single limbs support when only one force plate is used, if the stance leg is on the force plate. We have not done this because the calculations would then become very unsymmetric with respect to left and right leg.

6.5 Estimation of gait stationarity

One of the experimental conditions is that the gait is stationary during the measurement, which means that the gait pattern during one gait cycle is the same as during others.

A way to test gait stationarity, proposed in [Cappozzo, 1975], is to calculate the time integral of the horizontal floor reaction forces during one gait cycle:

$$P = \int_0^{T_c} FX_{floor}(t)\, dt$$

where FX_{floor} is the horizontal floor reaction force

and T_c is the time required for one gait cycle.

Now, if P is not equal to zero it means that a net impulse has been transferred between the subject and the floor during the gait cycle and the condition of gait stationarity is thus not fulfilled.

For normal gait, there is a symmetry between the right and the left leg when the gait is stationary, and the integral of the horizontal floor reaction force on one foot during one gait cycle must then be zero.

To get a normalized value of the deviation from zero we will define the relative impulse as

$$Pr = \frac{\int_0^{T_c} FX_{foot}\, dt}{\int_0^{T_c} |FX_{foot}|\, dt}$$

where FX_{foot} is the force exerted by one foot on the floor.

6.5

Pr is estimated by

$$Pr \approx \frac{\sum_{i=1}^{N} FXFP(i)}{\sum_{i=1}^{N} |FXFP(i)|}$$

where FXFP(i) is the horizontal ground reaction force at sample No. i as measured by the force plate and N is the number of samples during one gait cycle.

Pr is calculated in the subroutine IMPUL and the resulting value is displayed shortly after a measurement on the raw data display. If Pr assumes a value that significantly deviates from zero, then we know that one of three possibilites is at hand:

1) The gait was not stationary

2) The gait was not symmetric

3) Something has failed in the measurement equipment.

For reasonably stationary and symmetrical gait it has been found that one should have $|Pr| < 0.2$.

This information is valuable for the system operator of the system when he is to decide whether the measurement has been successful or not.

7. RESULT PRESENTATION SUBSYSTEM

The major guidelines in the construction of the routines for presentation of the results have been to obtain flexibility, to make the results easy to understand and to make it easy for the operator to control the result-presentation.

These requirements have been met by using the following principles:

- All results are stored on disc memory, which means that the operator has access to all information at result output time.
- The operator gives instructions at result output time to the computer concerning the choice of output variables. This implies that the operator can change his mind concerning what variables he wants to study during the result output without having to do the analysis once again
- Whenever possible, the result presentation is in graphical form which is much easier to read than a table. The coordinate axes on the graphs are automatically chosen so that the entire axes correspond to 1, 2 or 5 times a multiple of ten of the proper physical unit. Metric units are always used, except for angles which are given in degrees. If the operator wants, he is free to manually give scaling factors for the axes.
- In the diagram form of result presentation the operator can plot any one of totally 178 result variables as a function of any one of the others (including time). This means that for instance he can get plots of a variable versus time, or one variable versus another (phase plane diagram) including symmetry diagram, i.e a variable versus another (phase plane diagram) including symmetry diagram, i.e. a variable for one leg is plotted versus the same variable for the other leg.
- If desired, the results can also be given in tabular form. The operator can then specify the variables he wants tabulated, or he can get tabular output of all available variables.

- When the operator specifies variables for plotting or printing he uses the same variable names that are used in this publication. These names are translated by a routine called VARLI into a number that makes it possible for the output routines to find the proper data location on the disc memory.

The following sections contain a more detailed description of the different types of result output available in system ENOCH.

7.1 Raw data display

To fully utilize the speed of the measurement system it is desirable to be able to look at the obtained data immediately after a measurement has been done.

To obtain this there is a special raw data display. This display, of which an example is given in figure 1, can be drawn on the graphic terminal directly after a measurement.

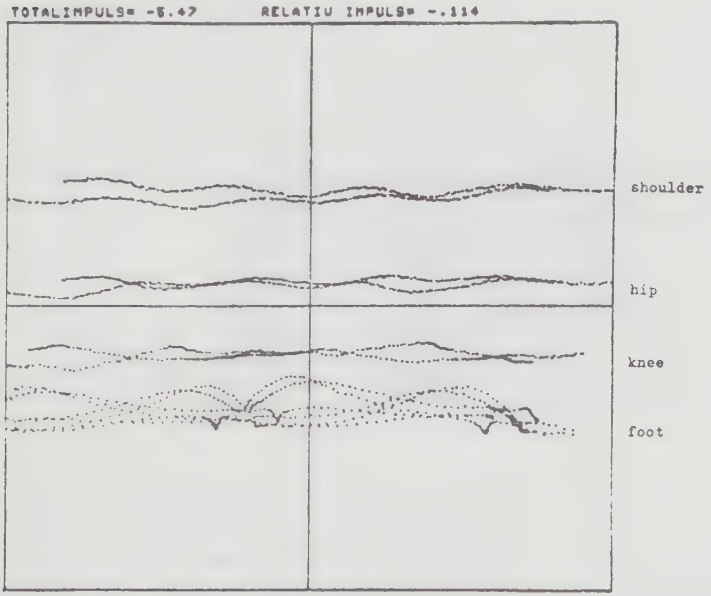

Figure 1. Raw data display

The big square represents the detector surface of the two cameras and the black dots show the postitions of the diodes images on the detectors. The diagram is drawn directly from measured data without coordinate transformation which implies that the diodes on the left half of the body move from right towards left, and the diodes on the right

half of the body will move from left towards right.

The operator specifies what fraction of the measurement cycles he wants displayed. In figure 1 one half of the measurement cycles are displayed, which in this case means that the time interval between two dots referring to the same diode is 0.013 seconds. From this display the operator can check that the kinematic data have been transferred properly to the computer and decide whether the data seem to be worth saving for analysis or if another measurement must be done.

As a check on the force plate data the total horizontal impulse, transferred from the force plate to the subject, and the relative impulse, as defined in section 4.3.6, are written on top of the raw data display.

From this point in the program the operator can either return to the beginning of program ENOCH to make further measurements or directly proceed with the analysis.

7.2 Display of the motion of the body in space

To get a visualization of the gait geometry there is a special diagram displaying the motion of the subject. In figure 2 an example of such a diagram is given.

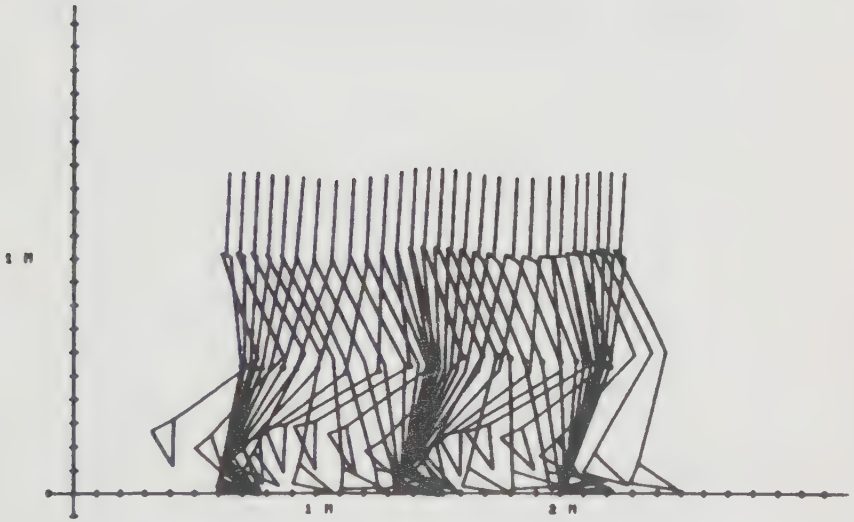

Figure 2. Display of the motion of the body in space.

The coordinates belonging to the same sample are linked together according to the structure of the gait model. While this diagram is drawn one can see how the body is moving, something that is harder to do in the resulting diagram. To make it easier to read the diagram, the right knee is marked with a small black square. When this diagram is to be displayed, the operator can specify how many samples he wants to be plotted and the program is then selecting a suitable fraction of the available samples.

This diagram is drawn by subroutine GUBBE.

7.3 Diagram output

The most flexible way to present the results from an analysis is to use a diagram where the values of a variable can be drawn as a function of any of the other 177 variables. We find it useful to divide the different possible diagrams into three categories:

1) Time diagram. The variable is plotted versus time to display the history of the variable.

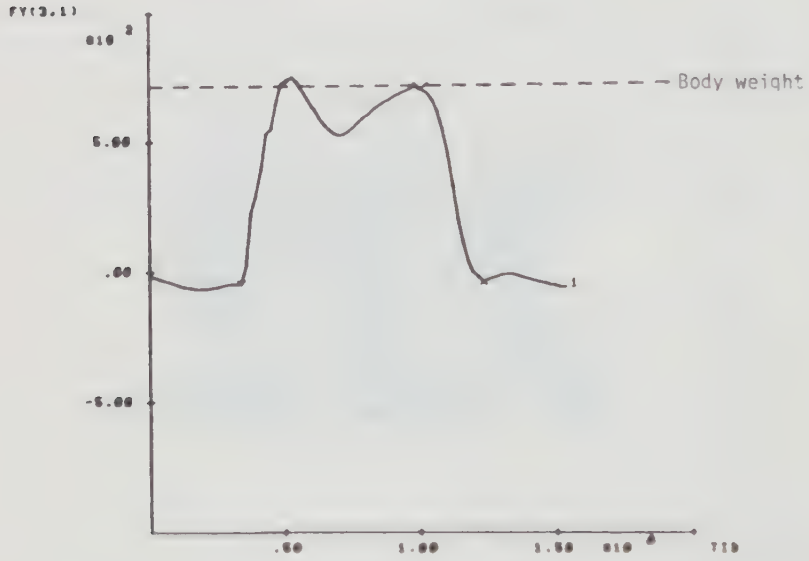

Figure 3. Time diagram. Example with vertical force at the left knee joint.

Figure 3 shows vertical force at the left knee joint plotted versus time. In the diagram one can also see the arrows indicating the event of a phase change. The notations are

- ˇ left heel strike
- ^ right toe off
- ˇ right heel strike
- ^ left toe off

The point of time for these events have been calculated according to section 6.3.

2) Phase plane diagram. One variable is plotted versus anyone of the other variables, time excluded. This type of diagram is useful when one wants to study the correlation between variables. Different types of phase plane diagrams have also been suggested for the evaluation of gait. As an example of a phase plane diagram, figure 4, shows left knee angular velocity plotted versus left knee angle. This diagram is interpreted in [Paul, 1967].

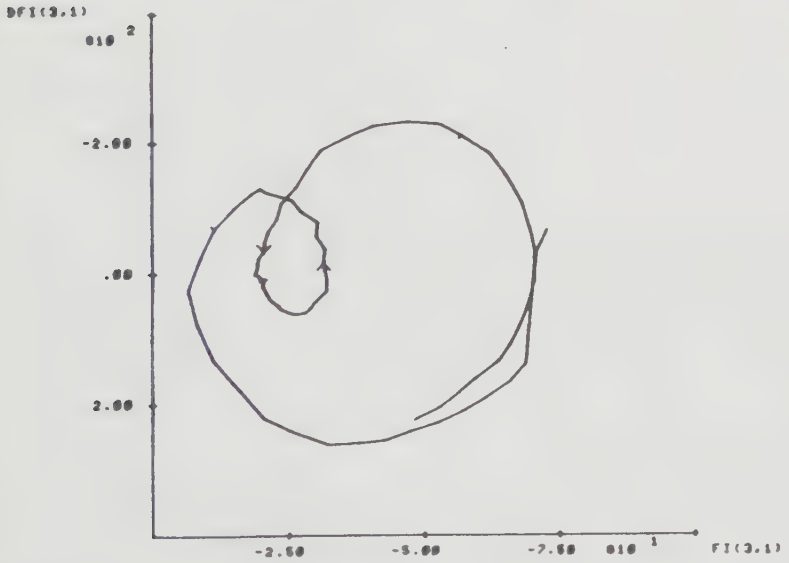

Figure 4. Phase plane diagram. Example with angular velocity at the left knee joint plotted versus left knee angle.

3) Symmetry diagram. When plotting a variable for one leg versus the corresponding variable for the other leg, the result is a curve that directly reveals any lack of symmetry between the legs with respect to the chosen variable. In figure 5 left knee angle is plotted versus right knee angle.

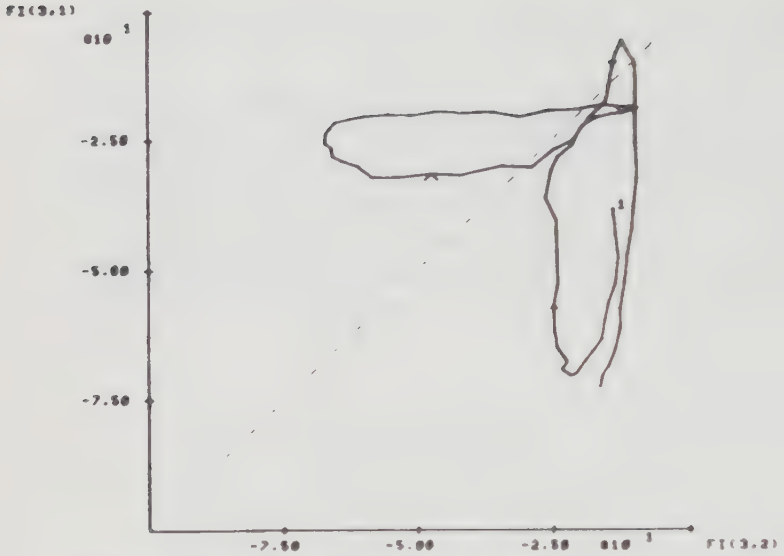

Figure 5. Symmetry diagram. Wxample with left knee angle plotted versus right knee angle.

It is easy to demonstrate that this type of curve is symmetric, with respect to a straight line with the slope 1 that is passing through the origin of the coordinate system, on the conditions that the gait is in steady state and symmetric.

The diagram part of ENOCH is controlled by subroutine DIAGR and several subordinate routines. Among them, subroutine VARLI translates variable names into storage numbers, which makes it possible for the operator to use the standard variable names when specifying output variables. The subroutines SKALF and IPOT calculate suitable scaling factors to the axes and the axes are then drawn by the subroutine DESIG.

Among implemented options in the diagram output, not already mentioned, are tics on the coordinate axis, grid on the diagram, manual scaling of the axis and drawing of several curves in one diagram.

7.4 Tabular output

Although diagrams mostly are superior to tables, there are also reasons for tabulating the output:

i) Some of the gait characteristics and also the measurement and analysis parameters are not time varying, and for them little is gained by a graphic representation.

ii) If the values of a variable are desired with high resolution, a table is better than a diagram.

iii) Sometimes the operator might want to know the values of all variables. In this case the graphical output is not suitable due to time and cost considerations.

After each analysis a table is printed on the line printer, where important information about the measurement and analysis is given. For example one can here find stride length, stride frequency, measurement time, measurement sampling frequency and parameter value used for the differentiation. This output is examplified in figure 6.

Figure 7 gives an example of the output for time depending variables.

The tabulating is controlled by the subroutine TABEL and performed by the subroutine PRINT.

```
EEEEE  H    H    000     CCC    H    H
E      H    H   0   0   C   C   H    H
E      HH   H   0   0   C       H    H
EEEE   H H H   0   0   C       HHHHH
E      H  HH   0   0   C       H    H
E      H    H   0   0   C   C   H    H
EEEEE  H    H    000     CCC    H    H
```

LOGGNING (1977-04-16)

MÄTNING

MÄTNING DEN 77 3-1977 NR

NAMN: HÖKAN LANSHAMMAR

ANTAL DIODER FÖR KAMERA A 5
ANTAL DIODER FÖR KAMERA B 5

MÄTFREKVENS SELSPOT 157 5 (KVARV= 2)
MÄTFREKVENS FORCEPLATE 52 5 (MDT= 3)

MÄTTID 2 62 (ANTAL MÄTCYKLER= 412)

BSPFIL BSPHL
RÅDATAFIL HLK12

STRIDE 1 54
FREKVENS 73
HASTIGHET 1 12

TOTALIMPULS -5 47
RELATIV IMPULS - 114

ANALYS

ANALYSERADE MÄTCYKLER 52 - 412 (TID= 2 29)
ANTAL UTVALDA OCH ANALYSERADE CYKLER (NTU) 187
TID MELLAN TVÅ UTVALDA ANALYSERADE CYKLER 0190

DERIVERING/SMOOTHNING N= 20 (FÖNSTER=2*N+1) (STANDARD N= 2
SPECIELL DERIVERING/SMOOTHNING AV KROPPEN NHPOP= 20

Figure 6. Output of information on measurement and analysis characteristics.

PROGRAM EMOCH 7/ 3-1977 MOTMING MR 3 ML

TIB	X(1,1)	X(2,1)	X(3,1)	X(4,1)	X(5,1)	X(6,1)
[illegible]	6118	6785	7648	5455	4142	3278
0190	6415	7124	8041	5915	4642	3863
0381	6624	7400	8405	6483	5204	4571
0571	6743	7588	8680	6806	5683	5018
0762	6983	7857	8987	7294	6281	5586
0952	7192	8096	9264	7739	6825	6308
1143	7372	8305	9512	8249	7492	7033
1333	7613	8536	9729	8675	8043	7611
1524	7734	8700	9949	9160	8688	8313
1714	7974	8931	1 0169	9610	9276	9052
1904	8157	9116	1 8358	1 0070	9897	9672
2095	8339	9274	1 8484	1 0510	1 0526	1 0359
2285	8552	9478	1 8675	1 0955	1 1123	1 1049
2476	8767	9682	1 8866	1 1325	1 1599	1 1618
2666	8980	9859	1 8994	1 1672	1 2078	1 2190
2857	9166	1 0047	1 1187	1 2004	1 2494	1 2637
3047	9382	1 0253	1 1379	1 2278	1 2816	1 3021
3237	9598	1 0501	1 1669	1 2587	1 3089	1 3214
3428	9878	1 0800	1 1993	1 2730	1 3171	1 3279
3618	1 0128	1 1084	1 2319	1 2893	1 3236	1 3311
3809	1 0348	1 1322	1 2581	1 3032	1 3301	1 3311
3999	1 0632	1 1597	1 2845	1 3191	1 3398	1 3375
4190	1 0919	1 1874	1 3110	1 3371	1 3528	1 3375
4380	1 1142	1 2131	1 3409	1 3483	1 3528	1 3343
4571	1 1401	1 2379	1 3643	1 3591	1 3560	1 3343
4761	1 1594	1 2590	1 3878	1 3679	1 3560	1 3407
4951	1 1853	1 2795	1 4013	1 3750	1 3593	1 3375
5142	1 2016	1 2960	1 4181	1 3813	1 3593	1 3343
5332	1 2245	1 3133	1 4283	1 3851	1 3593	1 3375
5523	1 2473	1 3321	1 4418	1 3902	1 3593	1 3343
5713	1 2704	1 3495	1 4519	1 3939	1 3592	1 3375
5904	1 2968	1 3659	1 4553	1 3952	1 3592	1 3375
6094	1 3101	1 3749	1 4587	1 3965	1 3592	1 3407
6285	1 3267	1 3857	1 4621	1 3977	1 3592	1 3375
6475	1 3433	1 3966	1 4655	1 4011	1 3625	1 3375
6665	1 3599	1 4074	1 4689	1 4003	1 3593	1 3343
6856	1 3799	1 4187	1 4689	1 4003	1 3592	1 3407
7046	1 3999	1 4329	1 4756	1 4028	1 3592	1 3407
7237	1 4167	1 4439	1 4790	1 4041	1 3593	1 3375
7427	1 4333	1 4562	1 4858	1 4087	1 3625	1 3375
7618	1 4501	1 4671	1 4892	1 4079	1 3592	1 3375
7808	1 4702	1 4829	1 4994	1 4137	1 3625	1 3407
7998	1 4836	1 4934	1 5061	1 4163	1 3625	1 3343
8189	1 5037	1 5077	1 5129	1 4188	1 3625	1 3406
8379	1 5205	1 5202	1 5197	1 4193	1 3592	1 3375
8570	1 5407	1 5359	1 5266	1 4231	1 3592	1 3407
8760	1 5541	1 5479	1 5399	1 4269	1 3592	1 3375
8951	1 5742	1 5622	1 5467	1 4315	1 3625	1 3407
9141	1 5943	1 5765	1 5534	1 4340	1 3624	1 3407
9332	1 6111	1 5869	1 5602	1 4365	1 3624	1 3406
9522	1 6312	1 6046	1 5703	1 4407	1 3624	1 3407
9712	1 6512	1 6203	1 5804	1 4461	1 3656	1 3406
9903	1 6711	1 6360	1 5905	1 4498	1 3656	1 3374
1 0093	1 6911	1 6531	1 6040	1 4549	1 3655	1 3405
1 0284	1 7109	1 6701	1 6174	1 4639	1 3720	1 3405
1 0474	1 7307	1 6846	1 6241	1 4743	1 3785	1 3404
1 0665	1 7537	1 7069	1 6508	1 4805	1 3785	1 3404
1 0855	1 7799	1 7324	1 6709	1 4920	1 3849	1 3435
1 1046	1 8027	1 7568	1 6975	1 5060	1 3913	1 3434
1 1236	1 8255	1 7812	1 7279	1 5240	1 4043	1 3530
1 1426	1 8482	1 8069	1 7536	1 5473	1 4238	1 3592
1 1617	1 8739	1 8385	1 7928	1 5722	1 4400	1 3687
1 1807	1 8964	1 8602	1 8317	1 6031	1 4662	1 3880
1 1998	1 9155	1 8986	1 8768	1 6384	1 4957	1 4074
1 2188	1 9283	1 9240	1 9184	1 6726	1 5253	1 4367

Figure 7. Tabulator output. Example with time in the first column and horizontal coordinates for the left leg in the other columns.

8. ADMINISTRATION SUBSYSTEM

This chapter gives a short description of some parts of the computer program that are not necessary from the gait analysis point of view, but important for making the system work, to simplify for the user and to localize errors whenever something goes wrong.

In section 8.1 the user-system communication is described. Section 8.2 deals with data management in the program, and in section 8.3 a short account is given of measurement failure tests and corrections implemented in the system.

PROGRAM EMOCH 7/ 3-1977 MOTMING MR 3 ML

TIB	X(1,1)	X(2,1)	X(3,1)	X(4,1)	X(5,1)	X(6,1)
0000	6118	6785	7648	5455	4142	3278
0190	6415	7124	8041	5915	4642	3863
0381	6624	7480	8405	6483	5204	4571
0571	6743	7588	8680	6806	5683	5018
0762	6983	7857	8987	7294	6281	5586
0952	7192	8096	9264	7739	6825	6308
1143	7372	8305	9512	8249	7492	7033
1333	7613	8536	9729	8675	8043	7611
1524	7734	8700	9949	9160	8688	8313
1714	7974	8931	1 0169	9610	9276	9052
1904	8157	9116	1 0358	1 0070	9897	9672
2095	8339	9274	1 0484	1 0510	1 0526	1 0359
2285	8552	9478	1 0675	1 0955	1 1123	1 1049
2476	8767	9682	1 0866	1 1325	1 1599	1 1618
2666	8980	9859	1 0994	1 1672	1 2078	1 2190
2857	9166	1 0047	1 1187	1 2004	1 2494	1 2637
3047	9382	1 0253	1 1379	1 2278	1 2816	1 3021
3237	9598	1 0501	1 1669	1 2587	1 3009	1 3214
3428	9878	1 0800	1 1993	1 2730	1 3171	1 3279
3618	1 0128	1 1084	1 2319	1 2893	1 3236	1 3311
3809	1 0348	1 1322	1 2581	1 3032	1 3301	1 3311
3999	1 0632	1 1597	1 2845	1 3191	1 3398	1 3375
4190	1 0919	1 1874	1 3118	1 3371	1 3528	1 3375
4380	1 1142	1 2131	1 3409	1 3483	1 3528	1 3343
4571	1 1481	1 2379	1 3643	1 3591	1 3568	1 3343
4761	1 1594	1 2598	1 3878	1 3679	1 3568	1 3407
4951	1 1853	1 2795	1 4013	1 3750	1 3593	1 3375
5142	1 2016	1 2960	1 4181	1 3813	1 3593	1 3343
5332	1 2245	1 3133	1 4283	1 3851	1 3593	1 3375
5523	1 2473	1 3321	1 4418	1 3902	1 3593	1 3343
5713	1 2704	1 3495	1 4519	1 3939	1 3592	1 3375
5904	1 2968	1 3659	1 4553	1 3952	1 3592	1 3375
6094	1 3181	1 3749	1 4587	1 3965	1 3592	1 3407
6285	1 3267	1 3857	1 4621	1 3977	1 3592	1 3375
6475	1 3433	1 3966	1 4655	1 4011	1 3625	1 3375
6665	1 3599	1 4074	1 4654	1 4003	1 3593	1 3343
6856	1 3799	1 4187	1 4689	1 4003	1 3592	1 3407
7046	1 3999	1 4329	1 4756	1 4028	1 3592	1 3407
7237	1 4167	1 4439	1 4790	1 4041	1 3593	1 3375
7427	1 4333	1 4562	1 4858	1 4087	1 3625	1 3375
7618	1 4501	1 4671	1 4892	1 4079	1 3592	1 3375
7808	1 4702	1 4829	1 4994	1 4137	1 3625	1 3407
7998	1 4836	1 4934	1 5061	1 4163	1 3625	1 3343
8189	1 5037	1 5077	1 5129	1 4188	1 3625	1 3406
8379	1 5205	1 5202	1 5197	1 4193	1 3592	1 3375
8570	1 5407	1 5359	1 5265	1 4231	1 3592	1 3407
8760	1 5541	1 5479	1 5399	1 4269	1 3592	1 3375
8951	1 5742	1 5622	1 5467	1 4315	1 3625	1 3407
9141	1 5943	1 5765	1 5534	1 4340	1 3624	1 3407
9332	1 6111	1 5869	1 5602	1 4365	1 3624	1 3406
9522	1 6312	1 6046	1 5703	1 4407	1 3624	1 3407
9712	1 6512	1 6203	1 5804	1 4461	1 3656	1 3406
9903	1 6711	1 6360	1 5905	1 4498	1 3656	1 3374
1 0093	1 6911	1 6531	1 6040	1 4549	1 3655	1 3405
1 0284	1 7109	1 6701	1 6174	1 4639	1 3720	1 3405
1 0474	1 7307	1 6846	1 6241	1 4742	1 3785	1 3404
1 0665	1 7537	1 7089	1 6508	1 4805	1 3785	1 3404
1 0855	1 7799	1 7324	1 6709	1 4920	1 3849	1 3435
1 1046	1 8027	1 7568	1 6975	1 5060	1 3913	1 3434
1 1236	1 8255	1 7812	1 7279	1 5240	1 4043	1 3530
1 1426	1 8482	1 8069	1 7536	1 5473	1 4238	1 3592
1 1617	1 8739	1 8385	1 7920	1 5722	1 4400	1 3687
1 1807	1 8964	1 8682	1 8317	1 6031	1 4662	1 3888
1 1998	1 9155	1 8986	1 8768	1 6384	1 4957	1 4074
1 2188	1 9283	1 9240	1 9184	1 6726	1 5253	1 4367

Figure 7. Tabulator output. Example with time in the first column and horizontal coordinates for the left leg in the other columns.

8. ADMINISTRATION SUBSYSTEM

This chapter gives a short description of some parts of the computer program that are not necessary from the gait analysis point of view, but important for making the system work, to simplify for the user and to localize errors whenever something goes wrong.

In section 8.1 the user-system communication is described. Section 8.2 deals with data management in the program, and in section 8.3 a short account is given of measurement failure tests and corrections implemented in the system.

8.1 User-system communication

The communication between the operator and the computer has been programmed in a dialogue-form. Whenever possible the computer puts simple questions to the operator that only require a yes or no as an answer. This makes it possible for a person, not at all familiar with computers and with a minimum of knowledge about the ENOCH system, to operate the system. Whenever the communication concerns more complex issues, e.g. determination of parameters needed for numerical differentiation, the user is first asked whether standard parameter values are to be used. Only if he does not want standard values he will have to face the problem of specifying parameter values.

The communication between the system and the operator can be divided into the following groups:

1) Structural questions. This type of communication concerns what parts of the ENOCH system that shall be used. If, for instance, the user is interested in the cartesian coordinates only, there is no point in going through the numerical differentiation and the kinetic analysis parts of the programs. This type of communication is programmed in the administrative parts of the ENOCH program, namely the routines S1 - S7.

2) Parameter questions. Several of the functions, performed by the different routines in ENOCH, can be done in many different ways. To determine the exact operation, parameter values must then be given to the subroutine. As a rule, the operator can choose between using standard values given in the program, or he can specify parameter values. In the program, this communication is located at a hierarchically lower level, usually in the subroutine that needs the information.

3) Information to the operator. Beside the output of results there is another kind of information that is useful for the operator and that is presented for him on the graphic terminal.

An example of this kind of information is concerning errors detected by the different routines. If for instance a light emitting diode has been covered during parts of a measurement this will be detected by the measurement error testing routine DAFEL and presented to the operator.

Error tests are also implemented in the various analysis routines and messages are given to the operator when something has gone wrong.

To enable the user to follow the program execution the name of the running part of the program is also written on the graphic terminal.

8.2 Data management

To handle the large number of data produced by the measurement and analysis system a disc memory unit is used. Several types of data files are used by the programs to make the data management effective. The major guidelines in the work have been that it must be possible to permanently store all data from a measurement, and also that the data management must be arranged so that the time required for an analysis is kept within reasonable limits, which is a couple of minutes.

Before the data files are described some factors that have influenced the file arrangement will be mentioned.

- The primary memory available for programs and data is 18k words, while the result variables occupy approximately 60k words. Therefore, the data must be resident on the disc memory most of the time. Due to this an appreciable fraction of the total time required for an analysis is used by data transfer between the primary and the secondary memory.
- After a measurement, the data are ordered in a time sequence, i.e. first the values corresponding to sample number 1 for all diodes, then the values for sample number 2, etc.. In contrast to this the differentiation is working on a variable basis; All samples corresponding to a specific diode are used for the calculations. In this case the data are most suitably ordered in a variable sequence, i.e. first all samples corresponding to diode number 1, then all samples corresponding to diode number 2, etc.. The analysis that follows after the differentiation is again best performed if the variables are ordered in a time sequence. These calculations are namely utilizing the values of several different variables for a specific point of time. Examples of this kind of analysis are the calculation of forces and moments.
- The differentiation requires a high sampling frequency if it is to give good estimates, while the subsequent calculations can be performed for the number of samples that is to be presented in the result output.

We will now list the different data files used in the system.

1) Camera calibration file (file name KAL00). This file contains the parameters describing the present orientation of the cameras. Whenever the cameras are moved a new calibration must be made. Program KALIB is then automatically storing the parameters in this file.

2) Body segment parameter files. In a file of this type, the BSP of the subject are stored.

3) Measurement data files. The data collected from the Selspot and the force plate are stored in a file of this type immediately after a measurement. The data in the camera calibration file are also transferred to this file to insure that the Selspot data will always be compensated with the camera calibration parameters valid at the time of the measurement.

4) Compensated displacement data file (file name KON00). In this file the compensated displacement data are stored. As a preparation for the differentiation the data are here stored in a variable sequence.

5) Differentiation output file (file name DER00). The results from the differentiation are stored here. A variable sequencing is still used. In this file, as well as in the result file, only a fraction of the original number of samples are stored.

6) Result file (file name RES00). In this file all the result variables are stored in a time sequence. The routines for calculation of angles, center of mass coordinates and their derivatives, forces and moments are all using this file as input and output file. The result output routines are also collecting the values of the variables from this file.

8.3 Measurement data error tests

The kinematic measurement data obtained from the optoelectronic device are represented in the computer by 16 bits words, one word for each data item. Each word has the content according to figure 8.

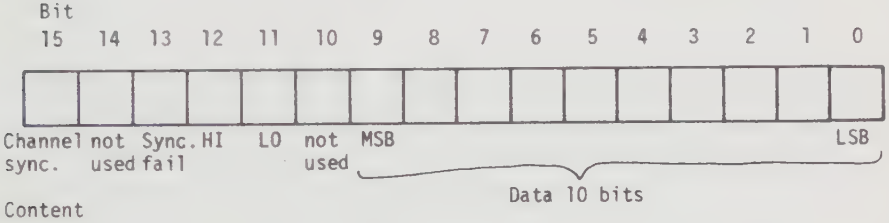

Figure 8. Content of the measurement data words collected from the Selspot equipment.

In subroutine DAFEL all the data words are tested with respect to errors indicated by bit 11-13. Detected errors are written on the line printer and on the graphic terminal. Bit 13 = 0 indicates a syncronization failure in the measurement equipment. Bit 12 = 0 indicates that the detectors have been saturated. Normally this will not occur on the distance that we use between the diodes and the cameras. Bit 11 = 0 indicates that not enough light has reached the detectors from the diodes to separate the signal from the background noise. This will occur when a diode is not within the scope of the camera or when a diode is covered.

Sometimes this error test shows that some samples in the beginning or at the end of a measurement contain errors, because the subject is not entirely within the scope of the cameras. The analysis can then be performed for the part of the measurement that does not contain any errors, simply by excluding the erroneous samples from analysis. If errors occur in the middle of the measurement interval one can not exclude these samples from the analysis. Instead one can either correct the errors by interpolation, which can be done automatically by the program KOREK, or manually with the file editing routine FIHED, or one can choose to do a new measurement immediately, since the errors are detected within some seconds after a measurement.

PART III · EVALUATION OF THE SYSTEM

In chapter 9 the accuracy of the system is investigated. The evaluation is made for the different parts of the system and also with respect to the overall accuracy obtained for the result variables. The time for the investigation of a subject is also examined.

9. EVALUATION

A system for the determination of gait parameters and gait varibles has now been presented. These quantities are obtainable from a combination of measurements and models. However, measurements are never exact and models are based on simplifying hypotheses. Therefore we have to estimate the reliability and accuracy of our results. In the cases of bad estimates we also want to find the cause of it, so we can eliminate the underlying errors, change bad hypotheses or in other ways make the system better. Thus there are two main reasons for the evaluation.

- To illuminate weak links of the system.
- To estimate the reliability and accuracy of the results.

This evaluation is described in sections 9.1 - 9.3. In section 9.4 a brief description of the time consumption for investigation of a subject is given.

9.1 Description of the system from the evaluation point of view

To make it possible to analyse how and where different errors effect our estimates we need an internal description of the whole measurement context containing the subject, his purpose, experimental conditions, measurements, and data processing. This is presented in figure 1.

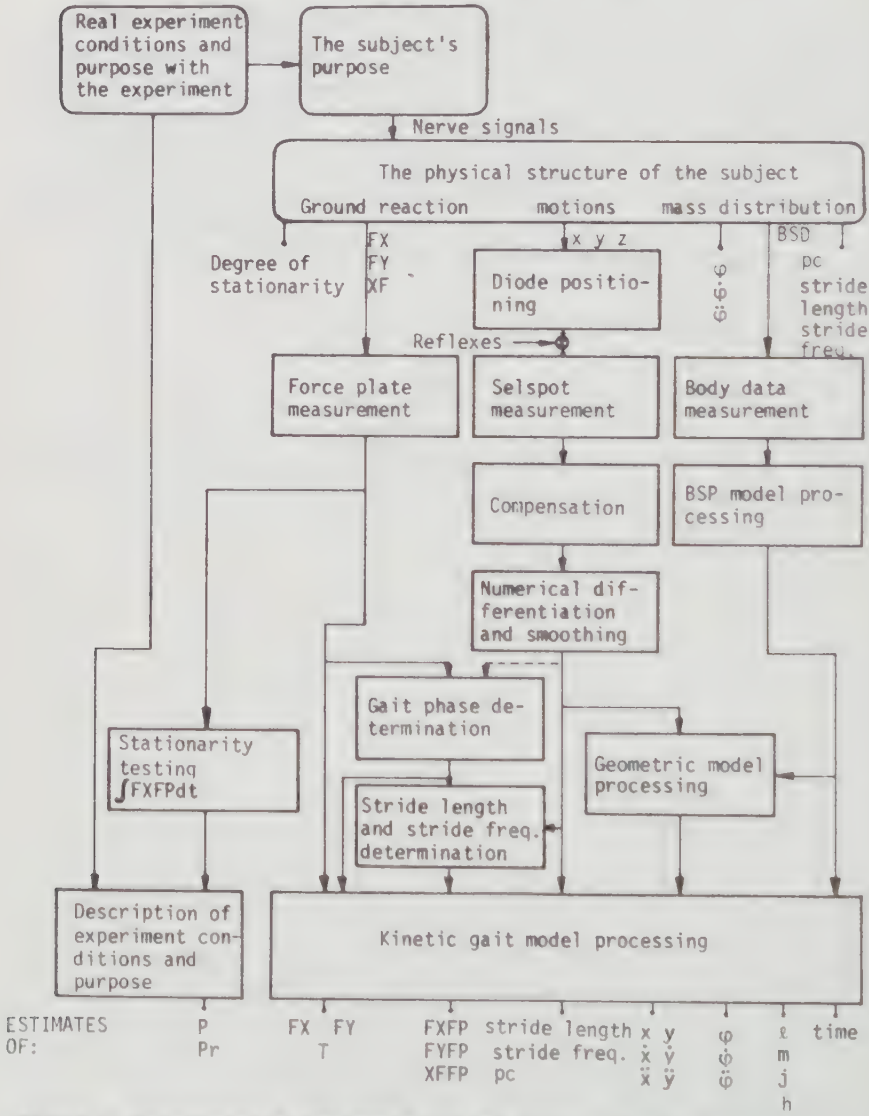

Figure 1. Description of the system and its context from the evaluation point of view.

The purpose of the figure is to illustrate the following points:

Behind an experiment there are an experiment purpose and experiment conditions. Some of the experiment conditions can be controlled but in any case they all affect the results of the experiment. Some important experiment conditions are perhaps not even known. For example it can be important if the measured gait is stationary or not.

The subject is informed about his role. He then gets his perception of what to do and tries to perform this. This makes him use his muscles to realize the forces and moments that generate the motions we call gait.

We want to study the resultant joint forces and moments. To realize this we have to perform three kinds of measurements, namely mass distribution, kinematic, and ground reaction measurements.

The measured quantitites contain noise and other errors of different kinds. Which are used as input data to different imperfect models.

The results are presented together with the experimental purpose and the conditions of the experiment.

Now the questions are: what is the value of these results in terms of the accuracy of the result? Which are the sources of the errors?

9.2 Types of errors in the system

To prepare an evaluation of the system we try to find out what kind of errors that might exist, by separating the errors into three types.

Errors from disturbances

To this type of errors, all measurement errors independently of their nature, including noise and other electronic or optical disturbances, are assigned

Examples:
- Incorrectly placed diodes
- Errors due to limited accuracy
- Reflexions of the light from the diodes
- Noise
- etc.

Method and model errors

Models are simplified and incomplete pictures of reality. They are based on hypotheses which can be put in question. Also methods have their restrictions.

Examples:
- The model of the subject is two-dimensional
- The body model is composed of rigid links
- The linearizations of the lenses and detectors are not perfect
- The best diode positions do not perfectly coincide with the real joints during the gait
- The numerical differentiation is not ideal
- etc.

Also incomplete or erroneously specified purposes or conditions of the experiment belong to this type, e.g. hypotheses about the stationarity, about the nature of the ground, and about what the subject is striving at.

Implementation errors

This group contains different types of technical errors made during the implementation. Because of the fact that they are unintentional, they are also hard to find. The best way to find them is to use different kinds of validation tests.

Examples: Programming errors
Wrong electronic connections
etc.

9.3 Error evaluation from two different aspects

Two purposes of evaluation have already been mentioned, namely:

- To illuminate the weak links of the system.
- To estimate the realability and the accuracy of the result quantities.

The first point requires an analysis of the internal structure of the system (See figure 1). We perform this analysis by investigating how the information is transformed through the different parts of the system. With this approach we illuminate how well the different links are functioning, and we also search for implementation errors. But to add the errors from different parts in order to give an ovarall evaluation about the prestanda is not a possibly way to go, because several important factors are not known.

The second point above deals with evaluating the reliability and accuracy of the resulting quantities. This is most effectively performed through a comparison with what is known in other ways, for examples through comparisons with independent measurements. With this approach we try to achieve a result evaluation. Of course this gives no explanation to eventual errors because we here consider the system as a black box.

In the following of this section we will handle the branches of figure 1, one by one.

9.3.1 The BSP branch

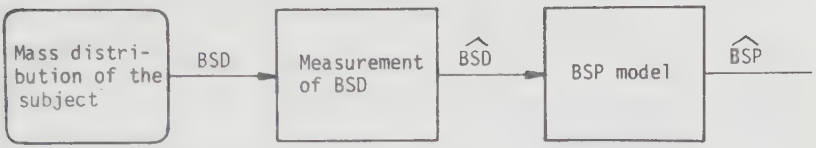

Figure 2. The BSP branch.

A subject has a set of body segment parameters, (See section 6.1), which are not directly measurable in a realizable way. Therefore they have to be determined from more easily attainable body segment data. (See section 5.1).

Our BSD are the bodyweight, M, some characteristic distances s_i, and circumferences p_i. Through measurements we obtain estimates of the BSD denoted $\widehat{BSD}$. These estimates are then fed into a model which we have constructed from results of [Drillis, Contini, 1966], [Contini, 1970,] [Contini, 1972] and of [Chandler et al, 1975]. With this model we estimate the BSP of the subject, denoted $\widehat{BSP}$.

The errors are due to

- Measurement errors ($\widehat{BSD} \neq BSD$)
- Model errors ($\widehat{BSP} \neq BSP$ even when $\widehat{BSD} = BSD$).

Several reasons make it very difficult to give good estimates of the accuracy of the BSP estimates. We have to use a model based on different investigators, who build their reports on a statistical material, which of course includes variations. The investigated groups were Americans. The model described in section 6.1, includes several steps, but although a single step is often statistically evaluated we cannot get statistical results from the whole model, because we do not know the covariation between the errors in the different steps.

Even if it is not possible to get a high accuracy of the BSP estimates we still have to perform an estimation. Notice also that the BSP

variables are used in the system only for force and moment computations and it will be shown in 9.3.7 that these calculations are rather insensitive to variations in the BSP.

The remaining of this section is devided in the parts: Measurement errors, model errors and total errors.

Measurement errors

To get some idea of the accuracy of the measurement an experiment to measure the BSD of the same subject twice was performed on two different subjects. This can be regarded as two independent measurements except that it is the same person who performed.

BSD	Subject 1	Subject 2
$\frac{\Delta M}{M}$ for the total mass	< 0.3%	< 0.3%
$\overline{\frac{\Delta S}{S}}$ for the 7 distances	2.6%	1.0%
$\overline{\frac{\Delta p}{p}}$ for the 10 circumferences	1.1%	2.0%

Table 1. Relative deviations of BSD measurements.
- The symbol Δ is the difference between the two measurements.
- For $\frac{\Delta M}{M}$ which is estimated from the force plate, 0.3% is due to the resolution of our A/D-converter.

From the table 1 it is concluded that the accuracy of the mass is very good. The average relative errors for distances and circumferences are about 2%. Notice also that this is not an estimate of the deviations from the true values. Systematic errors are not included.

It can also be interesting to see how the $\widehat{BSP}$ differ when based on the two sets for each subject of $\widehat{BSD}$-data presented above (see tables 2 and 3).

Subject 1

$\widehat{BSP}$	Segment length (l)	Distance:proximal joint - center of mass (h)	Mass (m)	Moment of inertia (j)
$\frac{\Delta(\text{Trunk+head+arms})}{\text{Trunk+head+arms}}$	1.0%	1.3%	0.1%	2.8%
$\frac{\Delta\text{Thigh}}{\text{Thigh}}$	3.2%	3.2%	0.2%	6.7%
$\frac{\Delta(\text{Shank+foot})}{\text{Shank+foot}}$	0.2%	0.1%	0.2%	1.2%

Table 2. Relative deviations of estimated BSP.

respectively:

Subject 2

$\widehat{BSP}$	Segment length (l)	Distance:proximal joint - (h)	Mass (m)	Moment of inertia (j)
$\frac{\Delta(\text{Trunk+head+arms})}{\text{Trunk+head+arms}}$	0.0%	0.6%	0.1%	0.6%
$\frac{\Delta\ \text{Thigh}}{\text{Thigh}}$	0.8%	0.8%	0.2%	1.4%
$\frac{\Delta\ \text{Shank+foot}}{\text{Shank+foot}}$	0.4%	0.5%	0.2%	1.7%

Table 3. Relative deviations of estimated BSP.

9.3.1

We see that $\hat{BSP}$ are not very sensitive for errors in $\hat{BSD}$. Most sensitive are the moments of inertia, which can be expected, since they contain a product of the mass and the square of the radie of gyration.

Model errors

Even if the estimated BSD were equal to the true values, there would still be errors in the model that relate the $\hat{BSD}$ to the $\hat{BSP}$. Let us now regard this model.

Drillis and Contini have based their investigations on adult Americans of both sexes (21 males and 8 females). The males for example were between 1.65-1.86 m tall and had a weight between 63-87 kg. This excellent investigation does not deal with the head and trunk so we have supplemented it with an investigation of [Chandler et al, 1975]. This report is based on six American Cadavers with height between 1.65-1.82 m and weight between 51-89 kg.

In their investigations Drillis and Contini have derived relations between measured data and body segment parameters and other quantities involved. They also give estimates of the variations in these relations. From the work of Chandler et al we supplement with similar relations for the trunk complex.

Now the question is: How accurate is the constructed model? The main sources of errors in the model are the following:

1) The investigations are based on a relatively small group of Americans.
2) Two subjects with the same BSD can differ in BSP which illustrates that there are intrinsic errors in the statistical method
3) The results from the investigations have a limited accuracy due to limitations in the investigations.
4) The estimated BSP are assumed to be independent of the motion.

We shall discuss these points although some of them are difficult to quantify.

1) The fact that the investigations are based on a relatively small group of Americans has two aspects. Firstly, how representative is this group for the whole population? Secondly, does it matter that the investigation is based on Americans?

In [Drillis, Contini, 1966] chapter 2, it is described how the sample of the population is taken, but we have no estimates of the representativity of the results. Notice also, that even if a sampled subject in the average have a height, weight, density etc. different from the average of the whole population, the relations between his BSD and BSP do not differ very much from the average relations. Accordingly we do not think that this problem give any large errors.

About the second part of the question we have the following arguments. The fact that the investigations are based on Americans does not mean that the errors will be large when used on people with "non-american body constitution". It just means that the curve fitting is performed on Americans, but still the method takes most variables into consideration. We can also add that the differences in length, weight and other body constitution parameters vary largely among Americans as well as among Swedes. Most of these variations are certainly much larger than the variations among Americans or among Swedes. Perhaps the density distribution can be rather different for different nationalities. Part of this problem has been taken care of by calculating the body density D from the mass M and the volume V which is the way we have implemented the calculation of D.

Of these reasons we would strongly guess that the errors in point 1) are very small. It would hardly effect the results more than a few percent, and probably much less.

2) and 3) The effect of having a statistical BSP distribution for subjects with the same BSD, and that investigations have a limited accuracy shall now be estimated. These two effects are contained in Drillis' and Contini's estimates. We place together estimates of the relative accuracy from the investigations mentioned. The relative accuracy defined from standard deviation/average value is called coefficient of variability and abreviate C.V. in the reports of Drillis and Contini. These figures are presented in table 4.

Estimates (Averages for the segments)	C.V. in percent	Comments
Total volume V (from p_i, s_i)	2	a)
Segment volume v_i (from V, table)	10	b)
Segment density d_i (from D, table)	2	c)
Distance:proximal joint-center of mass h_i (from l_i)	2	d)
Segment radious of gyration ρ_i (from l_i)	4.5	e)

Table 4. Relative accuracy of some estimates.

Comments:

a) The accuracy of Šerlj's formula [Contini, 1970] p 62 gives the surprisingly low error of 0.1 liter which means C.V. ≈ 0.15%. But as said in [Drillis, Contini, 1966] p. 54, the volume changes due to the lung volume. We would rather estimate the relative accuracy to let us say 2%. Note also that we use Šerlj's revised formula from [Contini, 1970] p. 73, the accuracy of which Contini gives no new estimate.

b) Segment volumes in percent of the whole body volume are surprisingly different for different subjects in the population. It is possibly that the estimates would be better if we instead use our distance and circumference measurements in connection with a formula (see [Contini, 1970] p. 73).

c) For determination of the density of the whole body, D, Drillis and Contini used a body index ($c = S/\sqrt[3]{M}$), and had the relative accuracy of D to about 1%. From D and M they then got V = M/D. But the figures are based on Americans and [Contini, 1970]p. 64, 67 stress that differences in D between e.g. Russians and Americans are about 3%. (The body index perhaps partly handles these problems, but how much?) Instead of this way of calculation we utilize M and V for computation of D. Then we use the same method as Drillis and Contini in deriving d_i from D.

Unfortunately, we have no accuracy estimates of the segment densities d_i when derived from D. One guess is that the individual differences in segment densities within a poluplation are about the same as the differences in the total density. $\left(\text{I.e. that } \frac{\Delta d_i}{d_i} \approx \frac{\Delta D}{D}\right)$. This last realitve accuracy $\frac{\Delta D}{D}$ we estimate to about 1%. (From [Drillis, Contini, 1966] p. 56). If the relation between $\frac{\Delta d_i}{d_i}$ as a function of D is of the same order this means about 1%. But then we have not included differences between different populations.

To inspect this problem we look at [Drillis, Contini, 1966] p. 62 where old estimates by Harless on Germans are presented. Typically $\frac{|d_{Harless} - d_{NYU}|}{d_{NYU}}$ is in the average less than 2%, though it does not use the information of total density explicitely. (NYU stand for the investigations of Drillis and Contini.) Without going deeper into the problem, 2% error seems to be reasonable when d_i is determined from D.

d) The distances between proximal joints and centers of volume are taken from [Contini, 1970] p. 45-47 where we have used the normal subjects. Then we have assumed the centers of mass to coincide with the centers of volume. On page 73 in [Drillis, Contini, 1966] it is written "... it is assumed that the segment volume and mass centers are coincident; these, according to Bernstein, are in very close agreement.". We therefore ignore this error in comparison with the variance between the subjects.

For the trunk we get a relative error of 1.5% from [Chandler et al, 1975].

e) The relation between segment radius of gyration , ρ, and its length is presented in [Contini, 1972] p. 13. The definition of segment length is not clearly specified nor do we know the best boundaries between body segments during gait. An average error of a centimeter in a segment length means about 2% in l_i. This number we add to the estimates.

For the trunk Chandler et al present similar figures from which we get $\frac{\Delta\rho}{\rho}$ to about 4%. On the other hand here we do not have the problem with the definition of segment length.

4) Finally the estimated BSP are assumed to be independent of the motion. Of course this is not exactly true. But on the other hand the differences in segment length and mass must be minimal. The mass distribution which effects the location of the center of mass and the radius of gyration ought to be a little changed. A guess could be 2%. (In the model there exists a case where ρ and h change a bit more, namely for the thigh and foot which, in this respect, are regarded as one unit.)

Total errors

Now we have identified different types of errors that cause our BSP estimates to differ from the real BSP. To see what the total effect will be, we have to "sum up" the errors in the same structure as the model in which the BSP are estimated. We then utilize the analysis just performed. One problem remains. We do not know the correlation between the errors of the different quantities. Since we have no arguments for neither a strong positive nor negative correlation, we assume that it is zero.

In figure 3 we give a graphical display of the total relative errors.

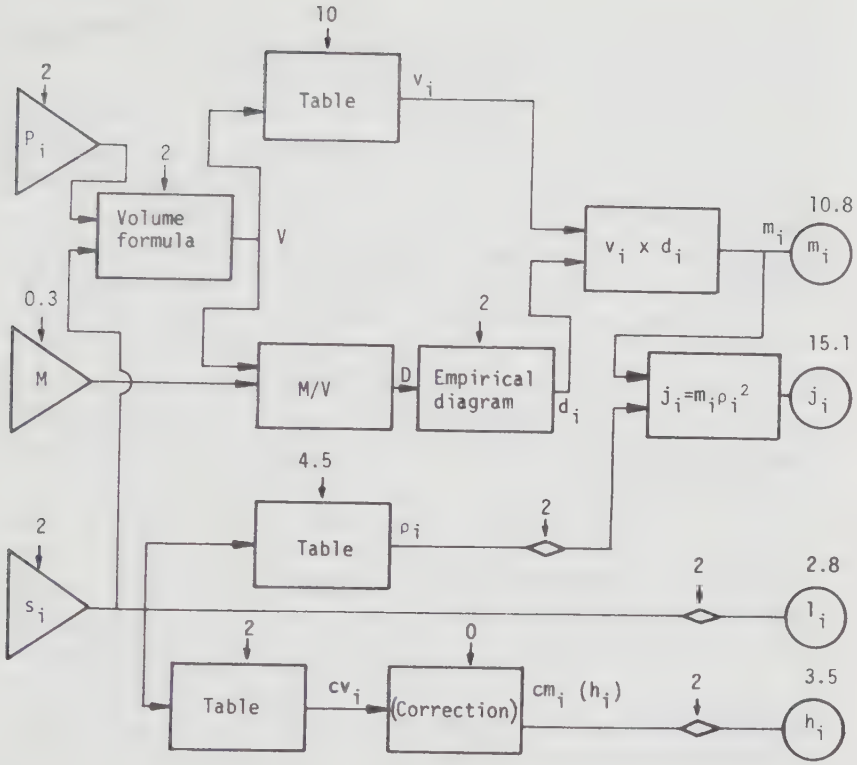

Figure 3. Calculation of relative errors in the BSP model
◇: BSP errors due to the motion. For designations see section 6.1.

Some symbols and assumptions ought to be explained.

- The symbol ε ▭ — means that a block receives an input quantity with an estimated relative error of ε%.
- The symbol ▭ with ε means that the block includes a relative model error of ε%.
- When two uncorrelated quantities with relative erorrs of ε_1 respectively ε_2 are multiplied or divided we get a relative error of approximately $\sqrt{\varepsilon_1^2 + \varepsilon_2^2}$, since the term $\varepsilon_1 \cdot \varepsilon_2$ can be neglected because all $\varepsilon_i \ll 1$.

9.3.1

For the case of moment of inertia: $j = m \cdot \rho^2$, of course ρ is completely correlated with itself, why we here get $\sqrt{(2\varepsilon_\rho)^2+\varepsilon_m^2}$.

Results:

Relative accuracy	Relative accuracy (C.V.)
Segment length l_i	3%
Segment distance: proximal joint - center of mass h_i	4%
Segment mass m_i	11%
Segment moment of inertia j_i	15%

Table 5. Relative accuracy of BSP estimates.

It shall also be stressed again that these figures do not claim to give a complete description of the BSP-accuracy. We just need the order of magnitude in the errors to see if the estimates are sufficiently accurate for our purpose in this project.

9.3.2. The time variable

The accuracy of time (t) is of special importance because most of the variables are time functions. In this section the relative time (t_r) will also be treated.

Our time base originates from the crystal controlled electronic clock, located in the Selspot equipment. The task of the computer is to keep track of the pulses from this clock and to sample and store measurement data.

One measurement cycle consists of 32 clock pulses. To estimate the cycle frequency, which is very stable we measured the time with a chronometer for 189 500 cycles which took 602 ± 0.5 seconds. (The experiment was performed twice with nearly the same result.) This gives a frequency of 314.8 ± 0.3 Hz and a cycle time of 3.174• ± 0.003 ms.

However, the diodes are not sampled simultaneously, because each cycle is divided into 32 intervals during which all 12 Selspot channels and all 3 force plate channels are sampled. The 12 diodes are sampled during interval 1 and 4 to 14. The intervals 2,3 are used for synchronization purposes. The 3 force plate channels are measured during the 0.1 ms following the last diode sample, see figure 4.

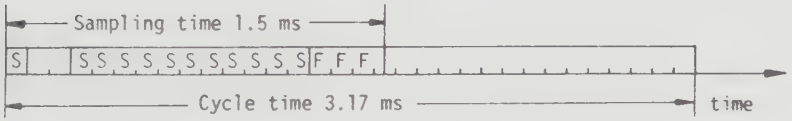

Figure 4. The sampling of the Selspot (S) and the force plate (F).

From figure 4 we see that we have a time discrepancy between the first diode channel and the last forceplate channel of ± 0.75 ms. This is easy to compensate for numerically but the errors are so small that we find it unnecessary. Compensation would also increase the computation time a little.

The main reason why this error is neglectable is that we need the high frequency to get good derivatives but all primary derivatives contain

one variable obtained from one diode only. This means that the only effect is that the whole derivative function is translated at most 0.75 ms which is harmless.

The relative time is normed to 1 for one gait cycle. Linearity of t_r is of course the same as for t. The accuracy in the normation is the same as the accuracy of the time between two successive phase changes (pc) of the same kind. In stationary gait this time interval remains correct even with a bad gait phase criterion. But a bad criterion means a linear translation of t_r so that the starting point is too early or too late. For more information about the accuracy of pc see section 9.3.6.

9.3.3 The kinematic branch

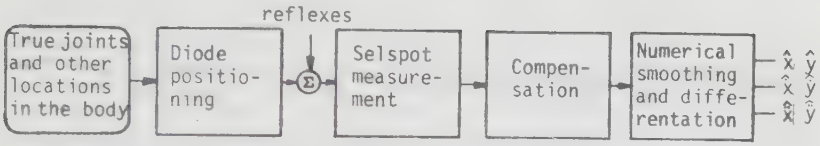

Figure 5. The coordinate branch.

This branch deals with the relation between the displacement of selected points inside the body and the corresponding estimated quantities expressed as motions, velocities and accelerations.

When the information is transferred from the subject to the results it passes several processes which affect the information. In this section we shall first investigate the different sources of error that we have recognized. Then we will present test results of the accuracy of the whole branch. Unlike the result evaluation in the BSP - branch, we are here able to perform direct tests by comparing known diode positions with the estimated results. This comparison includes the whole branch except the relation between the abstractly defined points inside the subject and the diode positions during gait, which have to be estimated separately.

Sources of errors

We recognize the following sources of errors:

1) Relation between a defined point and a diode position
2) Parallax errors
3) Errors due to the sampling
4) Errors originating from the measurement and remaining after compensation
5) Effects of the numerical differentiation.

1) Relation between a defined point and a diode position

We want to estimate the motions of the coordinates in x- and y-directions of some selected points. These points, e.g. the abstract joint axes, do not necessarily correspond to a physically point in the subject.

To approximate these points diodes are attached on the surface of the subject. The diodes therefore will differ i z-direction from the aimed points. This effect causes no error when the aimed point, the diode and the camera lie on a straight line, but will otherwise cause an error in x- or y-direction.

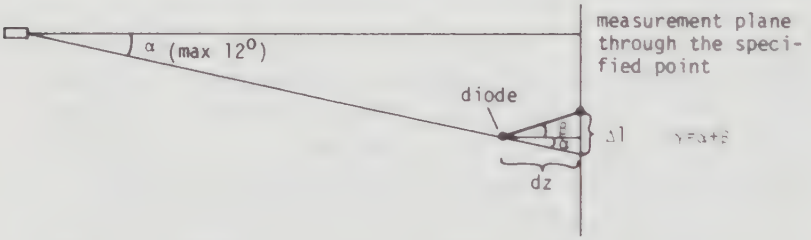

Figure 6. Difference in z-direction causes errors in x- and y-directions.

As figure 6 shows the error in the xy-plane depends on both the distance between the diode and the defined point,and the angle γ of the broken line through the camera, diode and specified point.

The angle γ is the sum of the angle α between the optical axes and the line camera-diode, and the angle β which is the angle of rotation of the subject as shown in figure 6.

The error is $\Delta l = dz \cdot (tg\alpha + tg\beta)$ where dz is the difference in z between the diode and the defined point.

We can estimate this error in different ways. First let us see how large dz, α and β can be.

The largest dz occurs for the hip where perhaps 6 cm can be typical.

The angle α is limited to 12^{o}.
The angle β is typically $< \pm 4^{o}$. Substituting the maximal errors would give $dz \cdot tg\ \beta \approx 4$ mm.

In practice tne errors of α and β do not add together in this way. During a measurement of one gait cycle the person moves about 1.5 m and starts and ends in the same position why the β angle is the same on these occasions. During such a measurement the α angle varies $\pm 3^{o}$ which gives $dz \cdot tg\alpha \approx \pm\ 0.06 \cdot 0.05 = \pm\ 3 \cdot 10^{-3}$ m. The variation of $dz \cdot tg\beta$ probably is somewhat larger.

Errors in x- and y-directions also origin due to incorrect placements of the diodes, and because there is no point on the skin which follows the internal motion of e.g. the hip joint. We lack estimates of this effect, but we think that the error has the magnitude of about 1-2 cm.

2) Parallax errors

A more serious error of the same kind as above occurs because we assume the whole motion to take place in a plane halfway between the cameras. In reality the body has an extension in the z-direction. The gait also has a variating z-component, and the error is increased if the gait is not centered around the measurement plane.

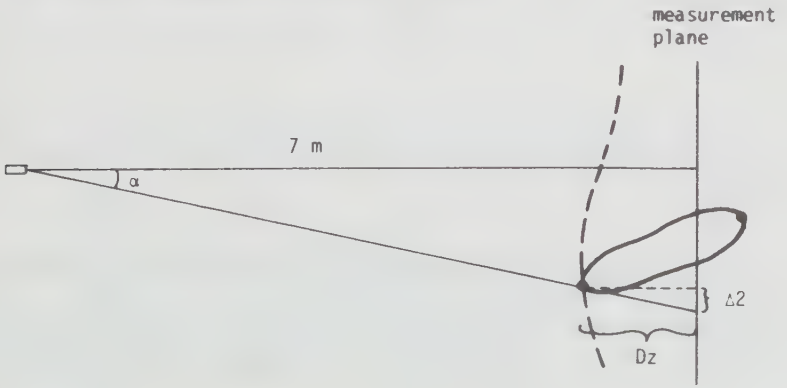

Figure 7. Parallax effect.

9.3.3

This in connection with the angle α defined in 1) causes an error which is largest in x-direction.

The angle α is limited to $\pm 12^{\circ}$ but varies only about 6° in total during a gait cycle. The Dz-distance, due to the extension of the body and a rocking gait, varies with the subject. A typical value of Dz for hips or axes ought to be about 30-40 cm.

This would give: $\Delta 2 = Dz \cdot tg\alpha$ a maximum value of 9 cm. A more realistic estimate for one gait cycle with stride length 1.5 m would give $\Delta 2 \approx \pm 0.4 \cdot tg6^{\circ} = \pm 4$ cm.

It shall also be mentioned that this error can be reduced by e.g. using two measurement planes, one through each side of the body. Although it would also effect the calibration procedure, there seems to be a good reason to perform such a change.

3) Errors due to the sampling

All the diodes are sampled during 1.3 ms. The maximum speed which occurs for the swinging foot is about 4 m/s. This gives a maximum error between the left shoulder (diode no. 1) and the right toe (diode no. 12) of $5 \cdot 10^{-3}$m which is neglectable. For adjacent diodes the time distance never exceeds 0.2 ms which gives an error less than approximately 1 mm. The most important question is whether the derivation process is effected. Since the derivatives are computed on one and the same diode it is not effected.

It shall also be mentioned that our sampling frequency of 315 or 157.5 Hz is far above the frequencies we wish to detect, why we have no aliasing problems.

4) Errors originating from the measurement and remaining after compensation

The information of the diode location is distorted in several ways during its transmission to and through the Selspot equipment. The main effects are:

- Reflexes from for example the floor add a false component to the position information.

- The lens exhibits distortion in form of a circular symmetric nonlinearity.
- Changes in distance,between diode and camera, causes blurring of the image in a way that distort the information.
- The detector is not perfectly linear.
- The detector and the electronics scale the x-and y-coordinates differently.
- The x- and y-axes are not perfectly orthogonal.
- Noise of different kinds enter into the system.

In section 5.2, the analysis and the compensation of the most important of these errors are described. Here we will focus on the remaining errors after that compensation.

To estimate these errors, the following experiment is performed. Five diodes were placed in a row on a vertical stick 40 cm above each other. The five diode set was sampled with 100 samples. We then translated the stick 40 cm horizontally and repeated the measurement. Through seven such measurements we got a 5 x 7 matrix. (This matrix is of course another than that, we once used to estimate the compensation factors.)

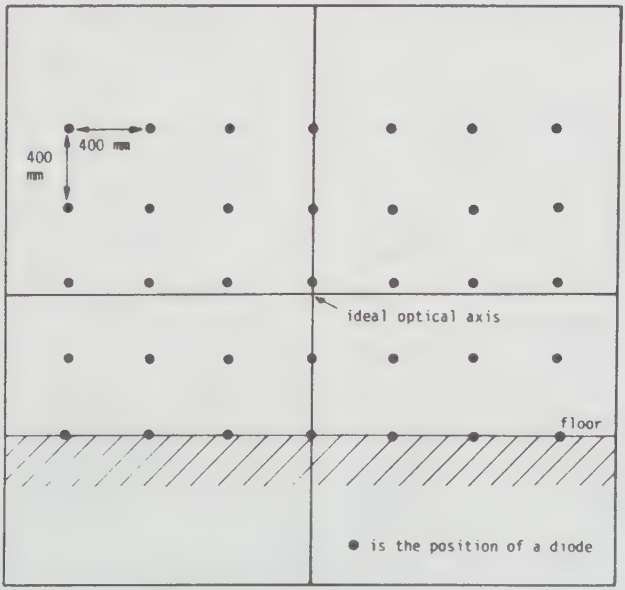

Figure 8. The diode matrix placed in the measurement plane.

9.3.3

This matrix covers the central measurement area of 1.60 m x 2.40 m, see figure 8.

The sampling of each diode 100 times gave the following results without compensation. (Only a translation and rotation of the coordinate system was performed.)

x-direction

Maximum error	87. mm	$(\max \lvert x_{true} - \hat{x} \rvert)$
Root mean square (RMS) deviation over the whole matrix	25. mm	$\sqrt{\frac{1}{34} \sum_{1}^{35} (x_{true} - x)^2}$

y-direction

Maximum error	117.mm
RMS deviation over the whole matrix	34.mm

After full compensation we got:

x-direction

Maximum error	31.mm
RMS deviation over the whole matrix	10.mm

y-direction

Maximum error	26. mm
RMS deviation over the whole matrix	14. mm

We can see that the compensation have been reduced to about 1/3 by the compensation. The remaining errors after compensation partly originate from the imperfect diode locations in space of the real matrix. The error of positioning a diode in space can be estimated to about 3-5 mm. The noise in the measurement had a standard deviation of typically 0.2 mm.

Figure 9. The estimated diode positions after compensation.

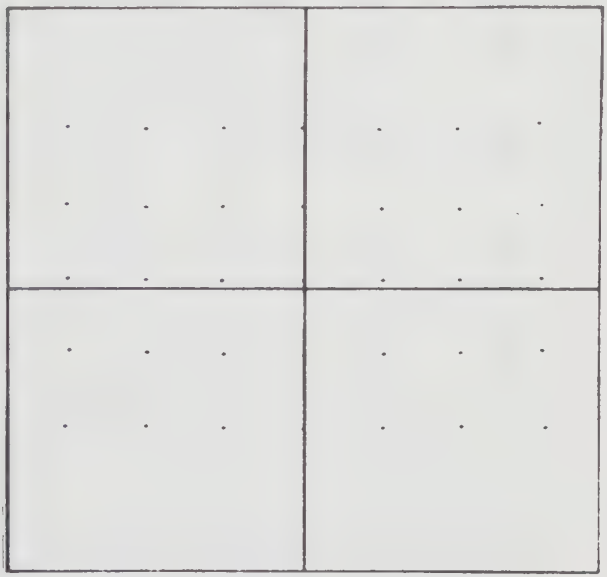

Table 6. The same as figure 6 in numbers.

LOCATIONS OF THE DIODES

Upper figures: x-coordinates
Lower figures: y-coordinates

-1.20	-.802	-.485	-.012	.382	.781	1.195
.858	849	.849	.849	843	845	876
-1.21	-.804	-.411	-.007	.398	.796	1.212
.450	435	.438	.439	.426	425	446
-1.20	-.804	-.412	-.003	.407	.801	1.212
058	.049	.046	.047	.045	.048	.068
-1.20	-.808	-.487	.000	.408	.802	1.215
-.325	-.334	-.344	-.353	-.344	-.335	-.324
-1.21	-.805	-.485	-.001	.405	.806	1.231
-.725	-.725	-.736	-.741	-.737	-.728	-.738

9.3.3

Table 7 shows the standard deviations of the measurement.

STANDARD DEVIATION IN X- RESP. Y-DIRECTIONS

.004	.004	.001	.002	.003	.004	.005
.004	.003	.003	.003	.003	.003	.004
.002	.002	.001	.002	.002	.003	.003
.002	.002	.003	.001	.002	.002	.002
.003	.002	.001	.002	.002	.003	.004
.002	.002	.001	.002	.002	002	.001
.003	.002	.001	.002	.002	002	.004
.002	.002	.002	.001	.002	.002	.002
003	.002	.002	.002	.002	003	.004
.003	.002	.002	.003	.002	.003	.003

Table 7. Standard deviations in x-direction (upper figure) and in y-direction (lower figure), calculated over 100 samples.

In the average we get σ_x = 2.5 mm and σ_y = 2.3 mm.

It can also be interesting to look at the variation of the distances between neighbour diodes. The chosen distances are rather typical for the distances between diodes during gait measurement.

DISTANCES TO NEIGHBOUR DIODES

401	397	.392	.395	.399	.416
.582	.567	.572	.589	.588	.587
.408	.414	.411	.411	.417	.420
.403	.393	.404	.405	.398	.417
.568	.552	.565	.571	.553	554
.392	.386	.392	.392	.382	.377
398	.392	.409	.409	.394	.411
.561	.559	.574	.567	.548	.556
.384	.383	.390	.400	.389	.383
.396	.393	.407	.408	.394	.413
.559	.563	.567	.558	.553	.583
.400	.391	.392	.388	.392	.393

Table 8. Distance to the neighbour to the right, -45° to the right, and below. The true distances are 0.400, 0.566 respectively 0.400 m.

From table 8 we can calculate some statistical values.

x-direction

Average distance (True distance = 0.400 m)
$$\hat{d}_x = \frac{1}{24} \sum_{1}^{24} d_{xi} = 0.402 \text{ m}$$

Standard deviation
$$\hat{\sigma}_x = \sqrt{\frac{1}{23} \sum_{1}^{24} (d_{xi} - \hat{d}_x)^2} = 0.008 \text{ m}$$

xy-direction (-45°)

Average distance (True distance = 0.566 m)
$$\hat{d}_{xy} = \frac{1}{24} \sum_{1}^{24} d_{xy_i} = 0.568 \text{ m}$$

Standard deviation
$$\hat{\sigma}_{xy} = \sqrt{\frac{1}{23} \sum_{1}^{24} (d_{xy_i} - \hat{d}_{xy})^2} = 0.012 \text{ m}$$

y-direction

Average distance (True distance = 0.400 m)
$$\hat{d}_y = \frac{1}{24} \sum_{1}^{24} d_{yi} = 0.395 \text{ m}$$

Standard deviation
$$\hat{\sigma}_y = \sqrt{\frac{1}{23} \sum_{1}^{24} (d_{yi} - \hat{d}_y)^2} = 0.012 \text{ m}$$

We see that the estimate in the x-direction has a random component of about 1 cm.

In 45°-direction the systematic error is about 0.2 cm and the random error about 1.2 cm.

In y-direction we have a systematic error of 0.5 cm and a random component of 1.2 cm.

Table 8 also shows that if we would use the center of the window, omitting the first and last column, the figures would have been even better.

From the same experiment we have also tested the angular accuracy. This is presented in section 9.3.4.

5) Effects of the numerical differentiation

The numerical differentiation is described in section 6.2. To describe the errors of the differentiation, we start with recognizing problems originating from the input of the filter, and from the filter itself, see figure 10.

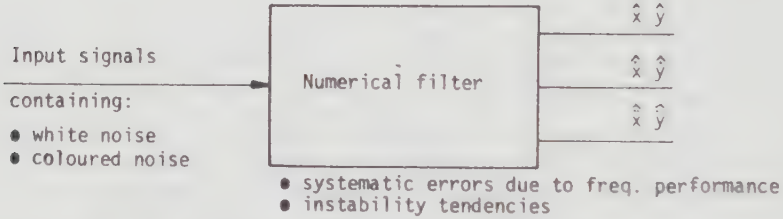

Figure 10. Some problematic points in filtering noisy data.

The input signal is processed through the filter to produce smoothed displacement data, and first and second derivatives of the displacement. The intrinsic problem of numerical differentiation is the large noise amplification. Therefore the noise present in the input signal is of crucial importance.

Diodes moving with the skin can be regarded as generating noise of mainly correlated nature, while for example electronical noise can be regarded as uncorrelated. Thus the noise can be regarded as the sum of:

- white noise (uncorrelated in time)
- coloured noise (correlated in time)

The filter, though constructed to handle the noisy data, necessarily has some fundamental limitations.

- The amplitude characteristics have a certain bandwidth.
- The recursive form of the filter gives a small and controlled round off error.

Before we analyse the effects of these points, som conditions and assumptions have to be specified.

We assume that the subject performs one gait cycle on 1.3 s.

The white noise on the input estimated from table 7 is for σ_x = 2.5 mm and for σ_y = 2.3 mm. But because of investigations, already performed with σ = 3 mm, we also here assume $\sigma_x = \sigma_y$ = 3 mm. In the remaining of 5) we will only consider σ_x since $\sigma_y = \sigma_x$.

We use a filter window of 2N+1 samples where N=20 if the measurement is performed with half frequency (157.5 Hz) and N=40 if full frequency (315 Hz).

In the way we use the filter, the bandwidth ν_B is set to 4.9 Hz for smoothing, to 2.7 Hz for the first derivative and to 3.1 Hz for the second derivative.

o Estimates of effects due to white noise with σ=3mm are given in table 9. (For deduction see section 6.2.3.4)

Cycle frequency [Hz]	Filter window 2N+1 samples	Smoothing ν_B[Hz]	Smoothing $\hat{\sigma_x}$[m]	First derivative ν_B[Hz]	First derivative $\hat{\sigma_{\dot{x}}}$[m/s]	Second derivative ν_B[Hz]	Second derivative $\hat{\sigma_{\ddot{x}}}$[m/s]
157.5	41	4.9	$0.8 \cdot 10^{-3}$	2.7Hz	$8 \cdot 10^{-3}$	3.1	0.23
315	81	4.9	$0.54 \cdot 10^{-3}$	2.7Hz	$5.4 \cdot 10^{-3}$	3.1	0.17 (≈0.02 g)

Table 9. The effect of the white noise.

The bandwidth for the first derivative is 2.7 Hz due to the formula used, which gives the advantage of fast calculations. This is because many calculations for zeros, first and second derivative are in common. Reasons exist to double this bandwidth to 5.4 Hz. For the same order of filter as that presently used, this would give $\hat{\sigma_{\dot{x}}} \approx$ 20 mm/s (for 2N+1=41) respectively 15 mm/s (for 2N+1=81) which is acceptable.

- Coloured noise can originate from the diodes, moving with the skin in a way that do not desribe the motion of the aimed points.

  Unfortunately we have no investigation of the velocity and acceleration for this effect, why we have to leave this question open.

  Another source of coloured noise is local nonlinearities from discontinuities in the Selspot detectors. Detector tests, however, indicates that this effect is unimportant.

- Now to the filter. In section 6.2.3.4 the characteristics of the filter are described. From investigations in this section we get an estimated relative error of approximately 2% of the accelerations. Near heel strike or other sudden peaks in the acceleration, the relative error is probably much larger during a very short time.

- The last source of error is the instability of the recursively implemented filter. To prevent this error from growing too much, the recursive algorithm is restarted when this error exceeds 1% of the estimated value (typically about 0.01 m/s^2).

We end up with table 10 over the error sources of the differentiation.

Source of errors	Error in the second derivative
White noise	0.2 m/s^2
Coloured noise	Unknown
Systematic error	2% (Near e.g. heel strike much larger during avery short time.)
Instability of the filter	1%

Table 10. Error sources of the differentiation.

To relate these figures: Typical accelerations during gait are for most of the body about 0.5 m/s^2 and for a swinging foot about 5 m/s^2. (Near heel strike it is about 20 m/s^2.)

Summary

We end this section with placing the different errors together in table 11. The errors can be separated into three groups, depending on if they effect the accuracy of; one point in time, the distance between different points at the same time or the derivatives.

Type	Coordinate errors with resp to one diode	Distance errors between different diodes	Influence of the derivatives
1) Diode positioning	1-2 cm	1-2 cm	No
2) Parallax	4 cm	< 4 cm	No
3) Sampling effects	---	0.5 cm	No
4) Incomplete compensation	1-1.5 cm	1-1.5 cm	No
5) Numerical differentiation	0.3 cm	0.3 cm	Yes

Table 11. A short summary of the errors.

We know very little about how the different types of errors add together during gait. Of this reason and because of having performed much stronger tests in evaluation of the angles, (which are directly determined

from the coordinates), through independent measurements wi' an exosceletal goniometer system, we will not try to evaluate the total errors during gait. If the accuracy of the derivatives are sufficient will be answered in connection to the force and moment evaluations in section 9.3.7.

9.3.4 The geometrical model

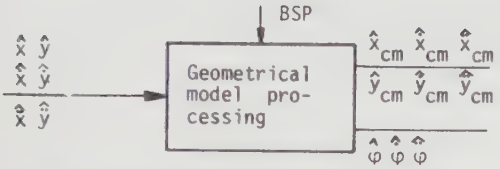

Figure 11. The geometrical gait model.

The geometrical model relates the different measured locations into a geometrical pattern. It has the purpose to deduce the motions of the centers of mass in terms of coordinates, velocities and accelerations as functions of time. It also has the purpose to deduce both the absolute and relative angles for the segments. Finally it deduces the angle derivatives of the segments. We enumerate these tasks I, II and III.

I. Centers of mass

The center of mass for a segment is constructed from the diodes on it and from the body segment parameter h. For most segments the center of mass is determined from two points, as in figure 10 a, and for the trunk from four points as in figure 10 b.

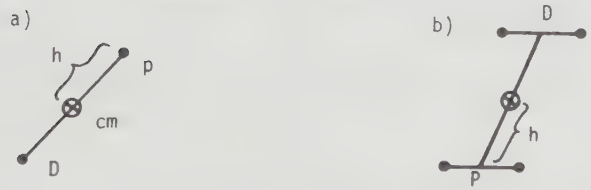

Figure 12 a,b. The location of the center of mass. P= proximal joint, D= distal joint.

It should also be noticed that we have lumped trunk, arms and head into one unit and that the same is done to shank and foot.

For a segment determined by the two points z_p and z_D we have:

$$z_{cm} = f(z_p, z_D) = z_p + \frac{h}{T}(z_D - z_p) = (1 - \frac{h}{T})z_p + \frac{h}{T} z_D$$

we can assume that var z_D = var z_p = var z

This gives

$$\text{var } z_{cm} = \left[\frac{\partial f}{\partial z_p} \frac{\partial f}{\partial z_D}\right] \begin{bmatrix} \text{Var } z_p & (\text{Cov}(z_p, z_D)) \\ \text{Cov}(z_p z_D) & \text{var } z_D \end{bmatrix} \begin{bmatrix} \frac{\partial f}{\partial z_p} \\ \frac{\partial f}{\partial z_D} \end{bmatrix}$$

$$= \text{var } z \left[(1 - \frac{h}{T}) \quad \frac{h}{T}\right] \begin{bmatrix} 1 & \rho \\ \rho & 1 \end{bmatrix} \begin{bmatrix} 1 - \frac{h}{T} \\ \frac{h}{T} \end{bmatrix}$$

$$= \text{var } z \left[(1 - \frac{h}{T})^2 + (\frac{h}{T})^2 + 2\rho \frac{h}{T} (1 - \frac{h}{T})\right]$$

Since $0 \leq \frac{h}{T} \leq 1$ and $-1 \leq \rho \leq 1$ we have:

$$\text{var } z_{cm} \leq \text{var } z \left[(1 - \frac{h}{T})^2 + (\frac{h}{T})^2 + 2 \frac{h}{T} (1 - \frac{h}{T})\right] = \text{var z}$$

If the noise of z_p and z_D are uncorrelated, which is reasonable to assume since the diodes are located so far apart, we get:

Var $z_{cm} = (1 - 2\frac{h}{T} + 2(\frac{h}{T})^2) \cdot$ var z which is less than var z for any value of $h < 1$.

Since $\frac{h}{T} \approx \frac{1}{2}$ we have approximately:

$$\text{var } z_{cm} \approx \frac{1}{2} \text{ var z.}$$

A similar argumentation is valid when z_{cm} for the trunk is determined from four diodes. In this case the resulting noise will be even more damped.

Of this reason, all that is said about the coordinates in section 9.3.3 is also valid for the mass centers if we just add the effect of errors in h.

The error in h was evaluated in section 9.3.1 to about 3.5% of the segment length (of which we guessed that 2% were caused by redistribution of mass during the gait). 3.5% would typically mean about 1.5-2 cm.

The total error then consists of the sum of coordinate and h errors in some statistical way depending what is assumed about their correlation.

For the derivatives we get

$$\Delta \dot{z}_{cm} = \frac{\partial \dot{z}_{cm}}{\partial \dot{z}_P} \Delta \dot{z}_P + \frac{\partial \dot{z}_{cm}}{\partial \dot{z}_D} \Delta \dot{z}_D$$

respectively

$$\Delta \ddot{z}_{cm} = \frac{\partial \ddot{z}_{cm}}{\partial \ddot{z}_P} \ddot{z}_P + \frac{\partial \ddot{z}_{cm}}{\partial \ddot{z}_D} \Delta \ddot{z}_D$$

$\dot{z}_{cm}$ and $\ddot{z}_{cm}$ are calculated from $\dot{z}_P$, $\dot{z}_D$ respectively $\ddot{z}_P$, $\ddot{z}_D$, by the same formula as that z_m was calculated from z_P, z_D. Therefore the same argumentation is valid for $\Delta \dot{z}_{cm}$ and $\Delta \ddot{z}_{cm}$ as for Δz_{cm}, and we can obtain the desired results from the discussion of derivatives in section 9.3.3 and from h in section 9.3.1.

II Angles

The angles are of two kinds; absolute angles, which means the angle to a reference fix in space and relative angles i.e. the angle between segments. See figures 13 a and b.

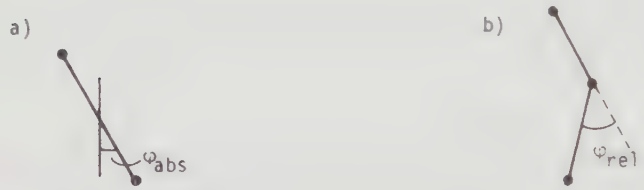

Figure 13 a, b. Absolute and relative angles.

The relative angle is computed as the difference between the absolute angles of two joining segments.

To evaluate the accuracy of the angles we have performed three different experiments:

1) Measurement and calculation of angles between fixed diodes on a diode matrix
2) Angles measured during gait from diodes mounted on Larry Lamoreux's exoskeletal system and compared with the results from this system.
3) Angles measured during gait from diodes mounted on the subject in the usual way and compared with angles obtained from the exoskeletal system.

1) The first experiment is from the measurement of the diode matrix in 9.3.3. We have calculated the averages and standard deviations of the absolute angles of the lines connecting neoighbouring diodes. The result from the measurement is presented in table 12.

ANGLES TO NEIGHBOUR DIODES

-1.4	.1	.0	-.9	.3	4.2
-46.7	-46.4	-45.9	-45.9	-45.3	-42.7
-90.6	-90.3	-90.8	-89.3	-87.9	-88.8
-2.2	.5	.1	-1.8	-.2	2.9
-44.9	-44.8	-43.8	-43.7	-43.2	-41.3
-89.2	-90.0	-90.2	-89.4	-88.7	-89.2
-1.6	-.4	.1	-.3	.5	1.7
-44.4	-44.7	-44.1	-43.6	-43.8	-41.9
-89.2	-89.5	-89.2	-89.6	-89.8	-89.8
-1.3	-1.4	-1.3	1.2	1.4	1.5
-45.7	-45.5	-44.4	-43.4	-44.0	-42.7
-92.7	-90.7	-89.8	-90.2	-90.4	-89.4

Table 12. Absolute angles to neighbour diodes.

The first value is the angle to the neighbour to the right. Theoretical value 0^{o}.

The second value is the angle to the diode one step to the right and one step downward. Theoretical value -45^{o}.

The third value is the angle to the diode below. Theoretical value -90^{o}.

In table 13 the averages and standard deviations of the 24 triplets are given

Measured angle in:	Average error	s.d.
x - direction	0.01^{o}	1.5^{o}
xy - direction	0.7^{o}	1.4^{o}
y - direction	0.3^{o}	1.0^{o}

Table 13. Measured angles in three directions

2) The second experiment was performed in cooperation with Larry Lamoreux during his visit to us in the summer 1976. He was wearing his exosceletal goniometric system, described in [Lamoreux, 1971], on which was applied two diodes on each bar, according to figure 14.

It shall also be pointed out that the goniometer calibration, which means translation and linear scaling of the goniometer curve, was performed afterwards. This means that the result do not show how accurately this sytem was calibrated.

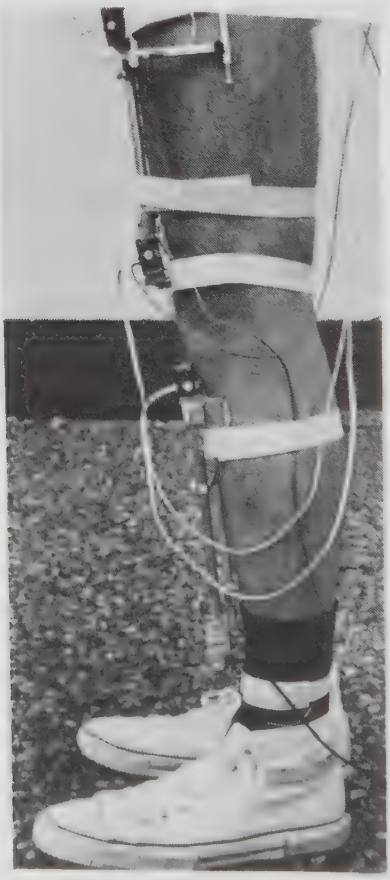

Figure 14. Diodes on the exoskeletal system.

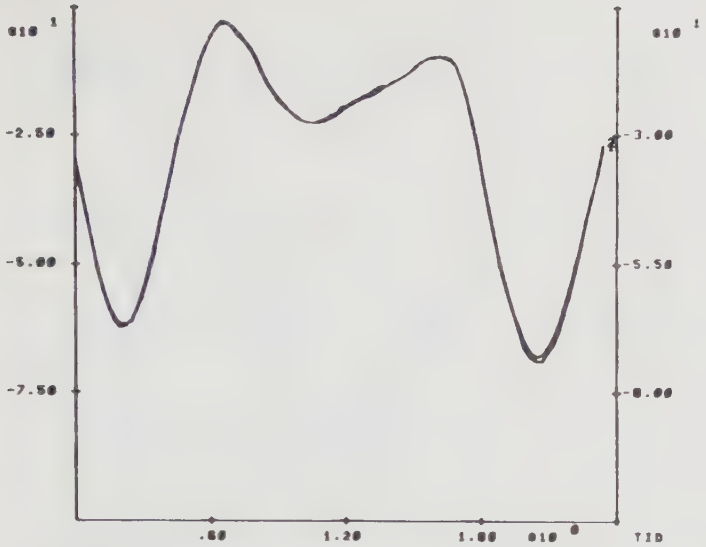

Figure 15. The knee angle measured independently with diodes and goniometers.

The result shows that the maximal difference is about 1^{o}, and most of the time the difference is much less.

3) The previous experiment did not include errors due to the diodes being placed on the skin. For this reason we performed an ordinary gait measurement on Larry Lamoreux simultaneously with sampling his exoskeletal system. The calibration of the exoskeletal system. (See figure 16.) The calibration of the exosceletal system was performed in the same way as in the previous experiment.

Th result of this experiment is shown in figures 17 and 18.

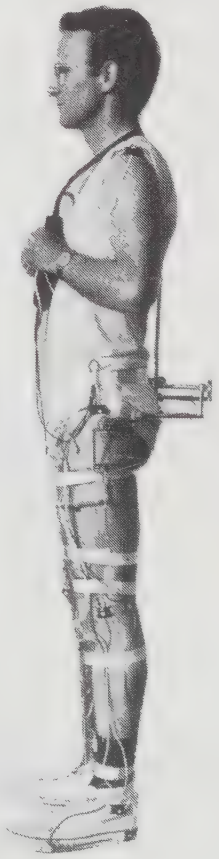

Figure 16. The ordinary diode configuration and the exoskeletal system

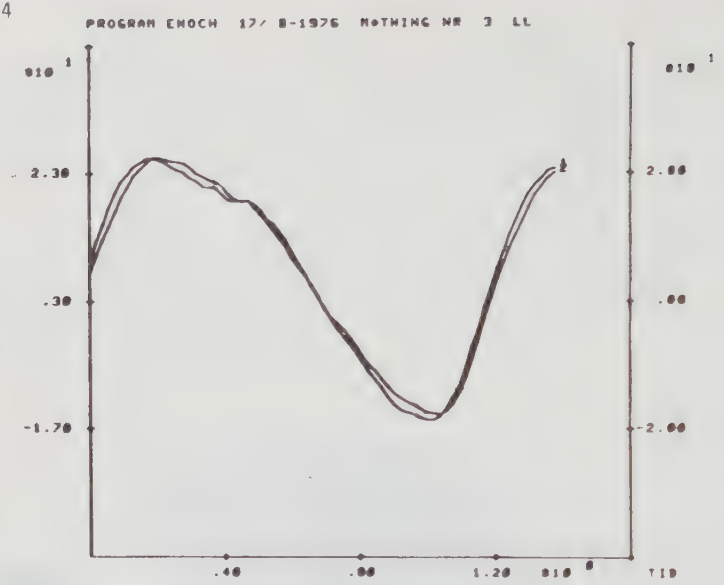

Figure 17. The hip angle measured with the ENOCH system and the exoskeletal system.

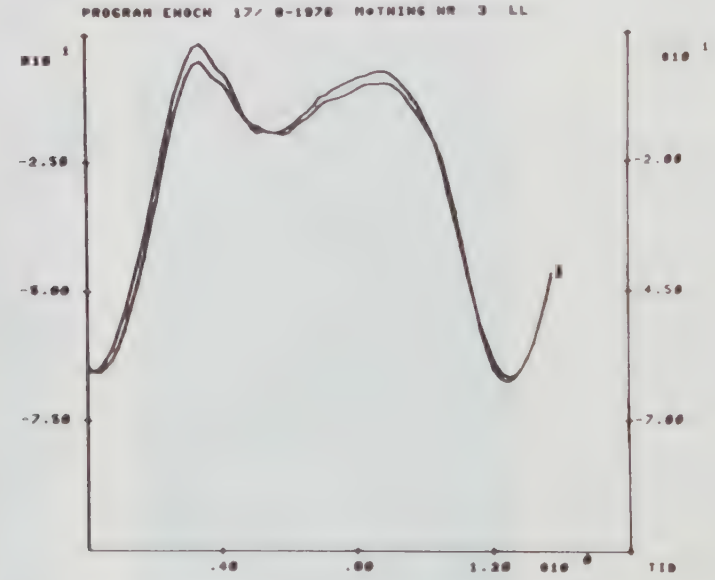

Figure 18. The knee angle measured with the ENOCH system and the exoskeletal system.

The maximum deviation is for the hip angle less than 2^{o} and for knee angle approximately 3^{o}.

Summary of the three angle experiments

These experiments give us important information about the errors. The first experiment tells us that the errors from a static measurement over most of the measurement window gives typical errors about 1 ± 1^{o}.

The second, when skin effects are abscent, give errors less than 1^{o}, usually much less (calibration errors are not included).

The third experiment where skin effects and anatomical differences of angle specifications are included, qive deviations of less than $2\text{-}3^{o}$. (Calibration errors are not included.)

III Angular derivatives

The angular derivatives are calculated from the coordinates and their derivatives.

The following investigation will only consider the effects of uncorrelated noise which due to its high frequency components is very serious for the differentiation.

A rectangular coordinate system fix in space and a polar system fix with respect to the measured diode locations are used according to figure 19.

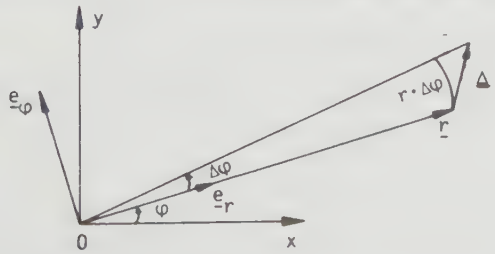

Figure 19. $\underline{r}$ is a vector defined by the measured locations of two diodes on a segment, in the absence of measurement noise. The vector $\underline{\Delta}$ corresponds to the measurement noise of one of the diodes.

9.3.4

The following relations apply for the unit vectors.

$$\begin{cases} \dot{\underline{e}}_r = \underline{e}_\varphi \cdot \dot{\varphi} \\ \dot{\underline{e}}_\varphi = -\underline{e}_r \cdot \dot{\varphi} \end{cases}$$

Differentiation of $\underline{r} = \underline{e}_r \cdot r$ gives

$$\underline{v} = \dot{\underline{r}} = \underline{e}_r \cdot \underbrace{\dot{r}}_{v_r} + \underline{e}_\varphi \cdot \underbrace{r \cdot \dot{\varphi}}_{v_\varphi}$$

$$\underline{a} = \ddot{\underline{r}} = \underline{e}_r \cdot \underbrace{(\ddot{r} - r\,\dot{\varphi}^2)}_{a_r} + \underline{e}_\varphi \cdot \underbrace{(r\ddot{\varphi} + 2\dot{r}\dot{\varphi})}_{a_\varphi}$$

To investigate the errors in these quantities we write

$$\Delta v_\varphi = \Delta r \cdot \dot{\varphi} + r \cdot \Delta \dot{\varphi}$$

$$\Delta a_\varphi = \Delta r \cdot \ddot{\varphi} + r \cdot \Delta \ddot{\varphi} + 2\Delta \dot{r} \cdot \dot{\varphi} + 2\dot{r} \cdot \Delta \dot{\varphi}$$

which gives

$$\Delta\dot{\varphi} = (\Delta v_\varphi - \Delta r \cdot \dot{\varphi})/r$$

$$\Delta\ddot{\varphi} = (\Delta a_\varphi - \Delta r \cdot \ddot{\varphi} - 2\Delta\dot{r} \cdot \dot{\varphi} - 2\dot{r} \cdot \Delta\dot{\varphi})/r$$

For $\Delta\dot{\varphi}$ we have

$r \approx 0.5$ m (segment lenght)

$|\Delta r| \approx 2.5 \cdot 10^{-3}$ m (standard deviation of measurement noise)

$|\dot{\varphi}| < 2.5$ rad/s (angular velocity)

$|\Delta v_\varphi| \approx 8 \cdot 10^{-3}$ m/s (standard deviation of velocity due to measurement noise)

why we get $\Delta\dot{\varphi} < 0.03$ m/s.

For $\Delta\ddot{\varphi}$ we have $|\Delta a_\varphi| \approx |\ddot{x}|$ or $|\ddot{y}|$ which is approximately 0.2 m/s^2.

The sum of the absolute values of the other terms of the right hand side are less than Δa_φ Setting this sum equal to Δa_φ gives

$$|\Delta\ddot{\varphi}| \approx 2\,\frac{\Delta a_\varphi}{r} \approx 2\,\frac{0.2}{0.5} = 0.8 \text{ rad/s}^2$$

In this discussion, only the errors due to one diode are regarded. The errors from two diodes with, independent errors, are $\sqrt{2}$ times larger, if they give the same amount of noise.

This means that $|\Delta\varphi_{abs}| \approx 1.1 \text{ rad/s}^2$

A relative angle is calculated as the differences between two absolute angles. Since the relative angle is determined from the positions of three diodes where the middle one is included in the calculations of both the absolute angles, we can regard the relative angle as described from four diodes where two are completely correlated. With the same assumptions as above and assuming the same length of the two segments, it can be shown that the error of $\ddot{\varphi}_{rel}$ will be $\sqrt{6}$ times larger than that for one diode.

Consequently:

$$|\Delta\ddot{\varphi}_{rel}| = \sqrt{6} \cdot 2\frac{\Delta a_\varphi}{r} \approx 2 \text{ rad/s}^2$$

9.3.5 The force plate branch

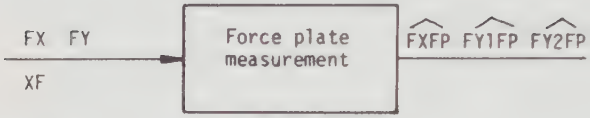

Figure 20. The force plate branch.

During the gait the force plate becomes loaded with a force which for our purpose is described by its x- and y-components and its point of attack.

The force plate, a Kistler 9261 A has a resonance frequency of 200 Hz and a high accuracy. The sources of errors are:

- Nonlinearity and hysteresis effects which we have tested up to a load of 72 kg, had a total difference from a linear relation less than 3 N. In x-direction this error is neglectable due to the small load.
- Crosstalk is specified to less than 1 , which is also what our tests give. This means that a load from a person of 700 N in y-direction gives an error of less than 7 N in x-direction. The influence of x- on y is much less due to the much smaller load in x-direction. Typically about 3 N.
- The calibration error is about ± 2 N.
- Noise gives fluctuations of about ± 1 N.
- The A D-converter has 10 bits which in our case gives a resolution of ± 1 N.

These effects are all assumed to be mutually independent. Therefore we estimate a maximum error as:

$$|\Delta FXFP| = \sqrt{3^2 + 7^2 + 2^2 + 1^2 + 1^2} \approx 8N$$

$$|\Delta FY1FP| = |\Delta FY2FP| = \sqrt{3^2 + 2^2 + 1^2 + 1^2} \approx 4N$$

why $|\Delta FYFP| < 8N$, since FYFP = FY1FP + FY2FP.

Due to the two components of the vertical force, the point of attack of the ground reaction force can be calculated. When estimated from the force plate it is denoted XFFP. The error of XFFP due to the errors in the vertical forces is a few mm. There is still another source of error, namely the positioning of the force plate in the camera system. This error is estimated to less than 1 cm. The total error $|\Delta XFFP| \approx 1$ cm.

9.3.6 The gait parameter branch

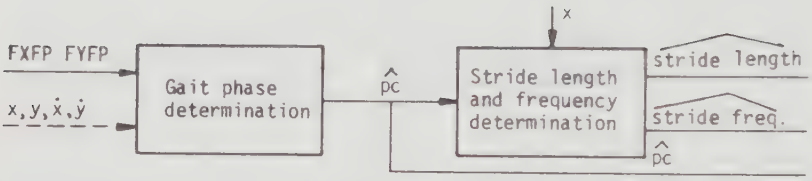

Figure 21. The gait parameter branch.

This branch deals with phase changes of the gait (pc) in time, with stride frequency, and with stride length determination. To have a criterion of when a new gait phase occurs is fundamental for all these three gait parameters. The phase changes of the gait considered are heel strike and toe off for left respectively right foot. The straightforward way to determine these changes is to use a foce plate and see when it becames loaded respectively unloaded. Two force plates are needed for a complete system, but during the development stage we have had one. Therefore we have designed a geometrical criterion based on positions and velocities of the foot.

Gait phase change

With a force plate criterion the accuracy of pc will be nearly the same as the sampling frequency we use for the force plate. In the present configuration the force plate is sampled with a frequency of about 100 Hz, or in the slower mode, about 50 Hz. This means that the accuracy of pc will be 0.01 s respectively 0.02 s, why

$pc = pc \pm 0.005$ s respectively $pc = \hat{pc} \pm 0.01$ s.

Due to the fact that one force plate has been used we have chosen to use a geometric criterion instead. The time of heel strike was computed from a measurement with this criterion. The result from the same measurement of a foot switch from Larry Lamoreux was compared. The result of this test is presented in figure 22.

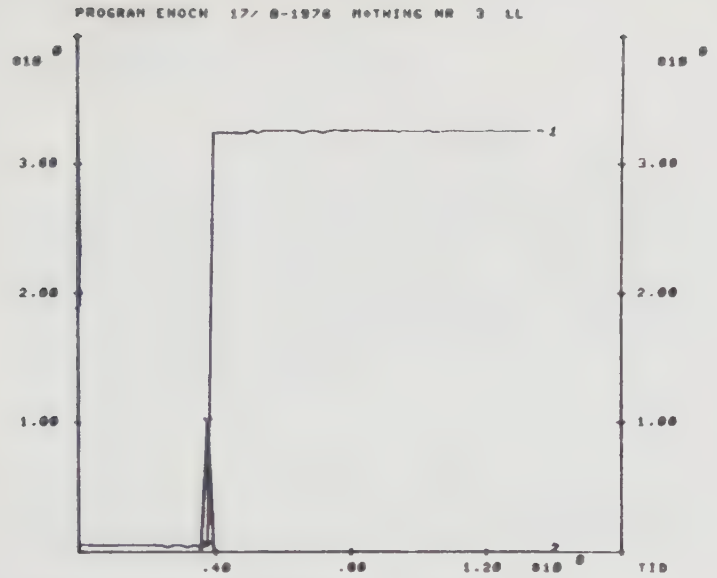

Figure 22. Test of the geometrical criterion.

This test only give an example where the criterion worked very good. It is also the only test we have performed. Still it seems reasonably that another type of gait could cheat the criterion.

If our effort to implement an algorithm have been successful for different types of gait, or how a good such geometrical algorithm should be constructed is not investigated sufficiently.

Through looking at tables of positions and velocities we believe that it is possible to estimate when a phase change of the gait occurred within about ± 5 Selspot samples, which means about 0.015 seconds. This means that it is easy to modify the criterion for a certain measurement.

Stride frequency

The stride frequency is derived from the inverse of the time between two phase changes of the same type. For reasonably stationary gait this means that it can be even more accurate than the determination of pc, since with the same criterion, the error between two pc of the same type is strongly correlated. The estimated error in stride time is < 0.015 s.

Estimated error for the stride frequency is approximately 0.01 Hz.

9.3.6

Stride length

The stride is calculated from the difference in position for two successive gait phase changes of the same type. Therefore the accuracy is determined from the accuracy of the coordinates of these instants. The fact that the foot velocity is nearly zero at phase changes makes it almost independent of errors in the time for pc.

From our discussions about the accuracy in coordinate determination we estimate the error to about 3 cm.

One test performed with measuring tape to compare with the calculated stride length gave a difference of 1 cm.

9.3.7 The Kinetic gait model

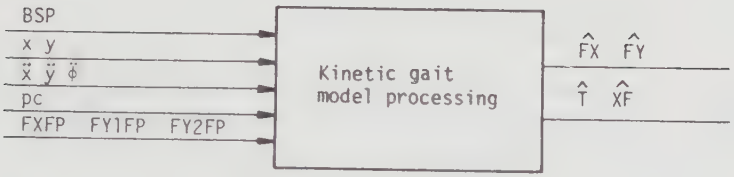

Figure 23. The kinetic gait model.

The purpose with the kinetic gait model is the computation of resulting forces and moments at the ankle, knee and hip joints. Also the point of attack for the ground reaction force XF is computed.

This section is divided into three subsections where I deals with the effects of some simplifications in the kinetic gait model. II analyses the errors in forces and moments in terms of the errors in the input variables, and III presents some experiments concerning the accuracy in the force and moment determinations.

I The kinetic gait model

The kinetic gait model includes several simplifications such as:

a) The model is two dimensional.

b) The body is described with seven rigid segments.

c) The segments are connected in one point.

These are just examples of what can be said about the limitations of the model. Many other effects, like that the BSP varies with the motions etc. which have been handled previously, will not be discussed here.

We discuss the points a) - c) very briefly.

a) We have accepted a two dimensional system. If more information is wanted a third dimension must be implemented.

b) With further diodes we could describe e.g. head and arms separately. Since our interest concerns hip, knee and ankle joints and in an ideal computation the trunk, head and arms will not have any influence.

c) We only regard total resultant joint forces and moments regardless of their origin.

The purpose of the kinetic gait model is computation of resultant joint forces and moments. The model is considered as adequate if the results are good. This is discussed in III.

II Analysis of error sources in the estimation of forces and moments

The kinetic model is a place where several of the variables and parameters are used for the computation of the forces and moments. An analysis of their contribution to the errors of forces and moments therefore will indicate which of the variables and parameters that are accurate enough and which ought to be better.

Figure 24 shows the modelled subject during gait. Notice also the denominations in this figure. As mentioned, we are interested in the forces and moments in the joints. We also assume that we have two force plates so that the external reactions on both legs are known.

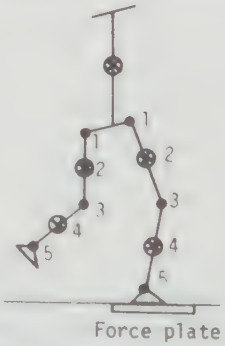

Figure 24. The modelled subject.

Forces

The following relations apply for each leg independent of gait phase.

$$\begin{bmatrix} FX_5 \\ FX_3 \\ FX_1 \end{bmatrix} = \begin{bmatrix} 1 & 0 & 0 \\ 1 & -m_4 & 0 \\ 1 & -m_4 & -m_2 \end{bmatrix} \begin{bmatrix} FXFR \\ \ddot{x}_4 \\ \ddot{x}_2 \end{bmatrix}$$

$$\underline{FX} \qquad \underline{M} \qquad \ddot{\underline{X}}$$

(where FXFR and FYFR are the external force components acting on the foot)

$$\begin{bmatrix} FY_5 \\ FY_3 \\ FY_1 \end{bmatrix} = \begin{bmatrix} 1 & 0 & 0 \\ 1 & -m_4 & 0 \\ 1 & -m_4 & -m_2 \end{bmatrix} \left\{ \begin{bmatrix} FYFR \\ \ddot{y}_4 \\ \ddot{y}_2 \end{bmatrix} + g \begin{bmatrix} 0 \\ 1 \\ 1 \end{bmatrix} \right\}$$

$$\underline{FY} \qquad \underline{M} \qquad \ddot{\underline{Y}} \qquad \underline{G}$$

or shorter:

$$\begin{cases} \underline{FX} = \underline{\underline{M}} \cdot \ddot{\underline{X}} \\ \underline{FY} = \underline{\underline{M}}(\ddot{\underline{Y}} + \underline{G}) \end{cases}$$

If we let $\underline{m} = \begin{bmatrix} m_4 \\ m_2 \end{bmatrix}$ and assume that there is no error in g we can write

$$\underline{\Delta FX} = \frac{\partial \underline{FX}}{\partial \underline{\underline{m}}} \underline{\Delta m} = + \frac{\partial \underline{FX}}{\partial \ddot{\underline{X}}} \ddot{\underline{\Delta X}}$$

$$\underline{\Delta FY} = \frac{\partial \underline{FY}}{\partial \underline{\underline{m}}} \underline{\Delta m} + \frac{\partial \underline{FY}}{\partial \ddot{\underline{Y}}} \ddot{\underline{\Delta Y}}$$

Consequently:

$$\underline{\Delta FX} = \begin{bmatrix} 0 & 0 \\ -\ddot{x}_4 & 0 \\ -\ddot{x}_4 & -\ddot{x}_2 \end{bmatrix} \begin{bmatrix} \Delta m_4 \\ \Delta m_2 \end{bmatrix} + \begin{bmatrix} 1 & 0 & 0 \\ 1 & -m_4 & 0 \\ 1 & -m_4 & -m_2 \end{bmatrix} \begin{bmatrix} \Delta FXFR \\ \Delta \ddot{x}_4 \\ \Delta \ddot{x}_2 \end{bmatrix} =$$

$$= \begin{bmatrix} 0 \\ -\ddot{x}_4\ \Delta m_4 \\ -\ddot{x}_4\ \Delta m_4 - \ddot{x}_2\ \Delta m_2 \end{bmatrix} + \begin{bmatrix} \Delta FXFR \\ \Delta FXFR - m_4\ \Delta \ddot{x}_4 \\ \Delta FXFR - m_4\ \Delta \ddot{x}_4 - m_2\ \Delta \ddot{x}_2 \end{bmatrix}$$

$$\underline{\Delta FY} = \begin{bmatrix} 0 \\ -(\ddot{y}_4+g)\Delta m_4 \\ -(\ddot{y}_4+g)\Delta m_4 - (\ddot{y}_2+g)\Delta m_2 \end{bmatrix} + \begin{bmatrix} \Delta FYFR \\ \Delta FYFR - m_4\ \Delta \ddot{y}_4 \\ \Delta FYFR - m_4\ \Delta \ddot{y}_4 - m_2\ \Delta \ddot{y}_2 \end{bmatrix}$$

Estimation of the errors in FX

The numbers used are taken from measurements and are only approximate.

Variable	|magnitude|	|error|
FXFR	~ 100	8
m_2	6	0.6
m_4	4	0.4
$\ddot{x}_2$	3	0.4
$\ddot{x}_4$	5	0.4

Table 14. Approximate magnitudes and errors of some variables. (SI-units)

If we assume that the errors are uncorrelated, this gives:

$|\Delta FX_5| < 8N$

$|\Delta FX_3| < \sqrt{(5 \cdot 0.4)^2 + (4 \cdot 0.4)^2 + 8^2} \approx 8N$

$|\Delta FX_1| < \sqrt{(5 \cdot 0.4)^2 + (3 \cdot 0.6)^2 + 0.4 \cdot 4)^2 + (0.4 \cdot 6)^2 + 8^2} \approx 9N$

Even though we use maximum estimates, we see that the errors are small. Through separating the evaluation for swing phase (where FXFR=0) and stance phase (where $\ddot{x} \approx 0$) we can reduce the estimated errors.

Estimation of the errors in FY

Variable	|magnitude|	|error|
FYFR	1000	8
m_2	6	0.6
m_4	4	0.4
$\ddot{y}_2$	2	0.4
$\ddot{y}_4$	5	0.4

Table 15. Approximate magnitudes and errors of some variables. (SI-units)

This gives:

$|\Delta FY_5| < 8 + 10 = 18N$ (A systematic error, $m_{foot} \cdot g \approx 10$ N, is included.)

$|\Delta FY_3| < 10N$

$|\Delta FY_1| < 13N$

We see that the errors are not very large. Through separating the evaluation for swing and stance phase, we can reduce these estimated errors.

Moments

The following relation apply for each leg independent of gait phase.

$$\begin{bmatrix} T_5 \\ T_3 \\ T_1 \end{bmatrix} = \begin{bmatrix} 0 & 0 & 0 \\ 0 & -j_4 & 0 \\ 0 & -j_4 & -j_2 \end{bmatrix} \begin{bmatrix} 0 \\ \ddot{\varphi}_4 \\ \ddot{\varphi}_2 \end{bmatrix} +$$

$$\underline{T} \qquad \underline{\underline{J}} \qquad \underline{\ddot{\Phi}}$$

$$+ \begin{bmatrix} XFFR-x_5 & 0 & 0 \\ XFFR-x_4 & x_4-x_3 & 0 \\ XFFR-x_4 & x_4-x_2 & x_2-x_1 \end{bmatrix} \begin{bmatrix} FY_5 \\ FY_3 \\ FY_1 \end{bmatrix} +$$

$$\underline{\underline{X}} \qquad \underline{FY}$$

$$+ \begin{bmatrix} y_5 & 0 & 0 \\ y_4 & -(y_4-y_3) & 0 \\ y_4 & -(y_4-y_2) & -(y_2-y_1) \end{bmatrix} \begin{bmatrix} FX_5 \\ FX_3 \\ FX_1 \end{bmatrix}$$

$$\underline{\underline{Y}} \qquad \underline{FX}$$

or shorter:

$$\underline{T} = \underline{\underline{J}}\ \underline{\ddot{\Phi}} + \underline{\underline{X}}\ \underline{FY} + \underline{\underline{Y}}\ \underline{FX}$$

$\underline{\Delta T}$ is most easily computed by:

$$\begin{bmatrix} T_5 + \Delta T_5 \\ T_3 + \Delta T_3 \\ T_1 + \Delta T_1 \end{bmatrix} = \begin{bmatrix} 0 & 0 & 0 \\ 0 & -j_4-\Delta j_4 & 0 \\ 0 & -j_4-\Delta j_4 & -j_2-\Delta j_2 \end{bmatrix} \begin{bmatrix} 0 \\ \ddot{\varphi}_4+\Delta\ddot{\varphi}_4 \\ \ddot{\varphi}_2+\Delta\ddot{\varphi}_2 \end{bmatrix}$$

$$+\begin{bmatrix}(XFFR-x_5)+\Delta(XFFR-x_5) & 0 & 0\\ (XFFR-x_4)+\Delta(XFFR-x_4) & (x_4-x_3)+\Delta(x_4-x_3) & 0\\ (XFFR-x_4)+\Delta(XFFR-x_4) & (x_4-x_2)+\Delta(x_4-x_2) & (x_2-x_1)+\Delta(x_2-x_1)\end{bmatrix}\begin{bmatrix}FY_5+\Delta FY_5\\ FY_3+\Delta FY_3\\ FY_1+\Delta FY_1\end{bmatrix}+$$

$$+\begin{bmatrix}y_5+\Delta y_5 & 0 & 0\\ y_4+\Delta y_4 & -(y_4-y_3)-\Delta(y_4-y_3) & 0\\ y_4+\Delta y_4 & -(y_4-y_2)-\Delta(y_4-y_2) & -(y_2-y_1)-\Delta(y_2-y_1)\end{bmatrix}\begin{bmatrix}FX_5+\Delta FX_5\\ FX_3+\Delta FX_3\\ FX_1+\Delta FX_1\end{bmatrix}$$

Which, if we neglect second order errors, gives

$$\begin{bmatrix}\Delta T_5\\ \Delta T_3\\ \Delta T_1\end{bmatrix}=\begin{bmatrix}0\\ -j_4\Delta\ddot{\varphi}_4\\ -j_4\Delta\ddot{\varphi}_4-j_2\Delta\ddot{\varphi}_2\end{bmatrix}+\begin{bmatrix}0\\ -\ddot{\varphi}_4\cdot\Delta j_4\\ -\ddot{\varphi}_4\cdot\Delta j_4-\ddot{\varphi}_2\Delta j_2\end{bmatrix}+$$

$$+\begin{bmatrix}(XFFR-x_5)\cdot\Delta FY_5\\ (XFFR-x_4)\cdot\Delta FY_5+(x_4-x_3)\Delta FY_3\\ (XFFR-x_4)\cdot\Delta FY_5+(x_4-x_2)\Delta FY_3+(x_2-x_1)\Delta FY_1\end{bmatrix}+$$

$$+\begin{bmatrix}FY_5\ \Delta(XFFR-x_5)\\ FY_5\ \Delta(XFFR-x_4)+FY_3\ \Delta(x_4-x_3)\\ FY_5\ \Delta(XFFR-x_4)+FY_3\ \Delta(x_4-x_2)+FY_1\Delta(x_2-x_1)\end{bmatrix}+$$

$$+\begin{bmatrix}y_5\cdot\Delta FX_5\\ y_4\cdot\Delta FX_5-(y_4-y_3)\cdot\Delta FX_3\\ y_4\cdot\Delta FX_5-(y_4-y_2)\cdot\Delta FX_3-(y_2-y_1)\cdot\Delta FX_1\end{bmatrix}+$$

$$+\begin{bmatrix} FX_5 \cdot \Delta y_5 \\ FX_5 \cdot \Delta y_4 - FX_3 \cdot \Delta(y_4 - y_3) \\ FX_5 \cdot \Delta y_4 - FX_3 \cdot \Delta(y_4 - y_2) - FX_1 \cdot \Delta(y_2 - y_1) \end{bmatrix}$$

Estimation of the errors in T

The numbers are taken from measurements or are estimated in other ways and are only approximate.

Variable	|magnitude|	|error|
j_2	0.13	0.020
j_4	0.10	0.015
$\ddot{\varphi}_2$	20 (rad/s^2)	1 (rad/s^2)
$\ddot{\varphi}_4$	50 (rad/s^2)	1 (rad/s^2)
x_i or $(x_i - x_j)$	0.25	0.015
y_i or $(y_i - y_j)$	0.40	0.02
FX_1	100	9
FX_3	100	8
FX_5	100	8
FY_1	800	13
FY_3	800	10
FY_5	800	18

Table 16. Approximate magnitudes and errors of some variables. [SI-units]

If we assume that the errors are uncorrelated,this gives an estimate of the magnitude of the total error.

$|\Delta T_5| < 17$ Nm

$|\Delta T_3| < 24$ Nm

$|\Delta T_1| < 29$ Nm

These estimated errors can be compared with the joint moments which reach about 150 Nm.

Notice that the term $\Sigma j \ddot{\varphi}$ is about 8 Nm with an error of about 1 Nm which is completely neglectable.

III Experiments concerning the accuracy of forces, moments and the point of attack

a) Forces

During single limb support the forces can be estimated in two independent ways. One way origins from the force plate and the other from computations of accelerations and masses. If two force plates are included, even a double limb support can be investigated.

In our case, only having one force plate, we have used the fact that during single limb support the external force acting on the swinging foot is zero. With the gait model in our test version we then use the Newtonian equations of the kinetic gait model, passing from ankle to knee to hip on the swinging leg. Then we continue over the trunk to hip to knee and to ankle of the supporting leg. The comparison of the calculated force in the ankle with the force from the force plate measurement gives an estimate of the sum of the errors in the five segments. This error sum we call $\varepsilon_1+\varepsilon_2+\varepsilon_3+\varepsilon_4+\varepsilon_5$ according to figure 25.

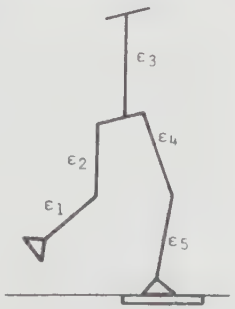

Figure 25. Force errors for the seqments.

In a system with two force plates a joint force is computed from one leg why it at most contains $\varepsilon_1+\varepsilon_2$ or $\varepsilon_4+\varepsilon_5$. This is especially important since we know that ε_3 is the major error, because the trunk, arms and head contain 65-70% of the total mass.

Figure 26 presents two independent measurements for x- respectively y-direction.

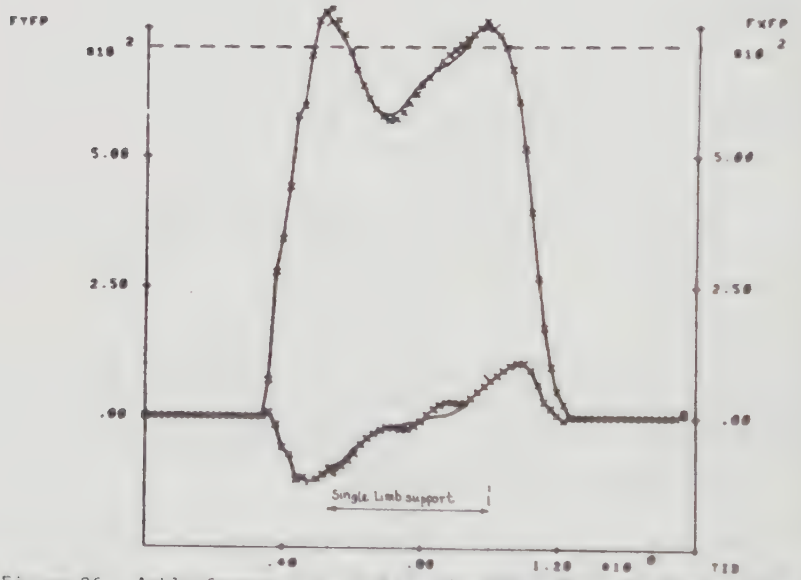

Figure 26. Ankle forces in x- and y- directions from the force plate measurement (solid lines respectively from the kinetic model (crosses).

We see that the total errors $\varepsilon_1+\varepsilon_2+\varepsilon_3+\varepsilon_4+\varepsilon_5$ in both x- and y-directions, are about 20 N. The real errors $\varepsilon_1+\varepsilon_2$ or $\varepsilon_4+\varepsilon_5$ are probably much smaller.

b) Moments

For the moments we can use the same approach as for the forces.

The force plate gives FXFP, FY1FP and FY2FP from which the moment TFP is calculated. As a point of comparison we have again chosen the ankle of the supporting foot. To transfer the moment to this point

requires the lever from the force plate to the ankle joint. It seems reasonable that the lever, which includes errors from the kinematic ankle measurement and from the positioning of the force plate in the camera system, differs about 1 cm from the true value of the lever. This implies an error of $0.01 \cdot g \cdot M$ which is typically about 7 Nm.

From the kinetic model, during single limb support, an independent estimate by computation from the swinging foot and over to the ankle of the supporting foot is obtained. Input quantities to the model are masses, moments of inertia, accelerations, angular accelerations and levers.

The relation for the ankle moment computed in this way is an expression of the form:

$$T_{ankle} = \Sigma j \cdot \ddot{\varphi} - \Sigma r_y \cdot m \cdot \ddot{x} + \Sigma r_x \cdot m \cdot \ddot{y} + \Sigma r_x \cdot m \cdot g$$

where r_x and r_y are levers from the moment axis through the ankle.

An analysis shows that the dominant term is: $m \cdot (x_{cm} - x_{ankle}) \cdot g$ for the trunk complex.
Thereafter follows: $m \cdot (y_{cm} - y_{ankle}) \cdot \ddot{x}_{cm}$ for the trunk complex
and $m \cdot (x_{cm} - x_{ankle}) \cdot \ddot{y}_{cm}$ for the trunk complex.
The term $\Sigma j \ddot{\varphi}$ is neglectable.

Since the trunk complex is outstandingly the most troublesome because of its large mass and long distance to the ankle, it is understandable that the divergence in the experiment is many times greater than it would be in a complete system where the trunk never is involved.

Figure 27 shows the result of the moment experiment.

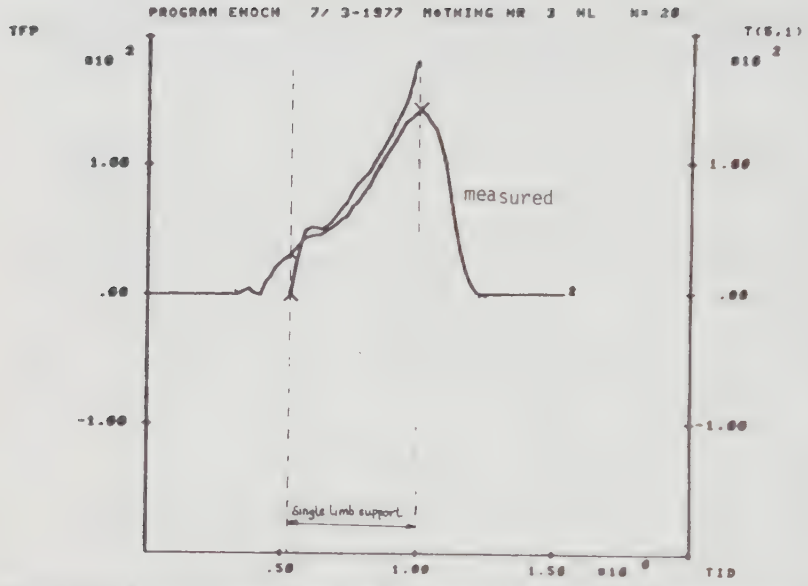

Figure 27. Ankle moment from the force plate measurement respectively the kinetic model.

We see that the maximum error is about 35 Nm.

c) Point of attack of the ground reaction force

The point of attack of the ground reaction force can be calculated from the forces and moments and is consequently only a combination of the variables just investigated. The experiment can be presented from another dimension namely the metric distance XFFP-XF where XFFP is the estimated point of attack obtained from the force plate and XF the estimate obtained from the kinetic model. See figure 28.

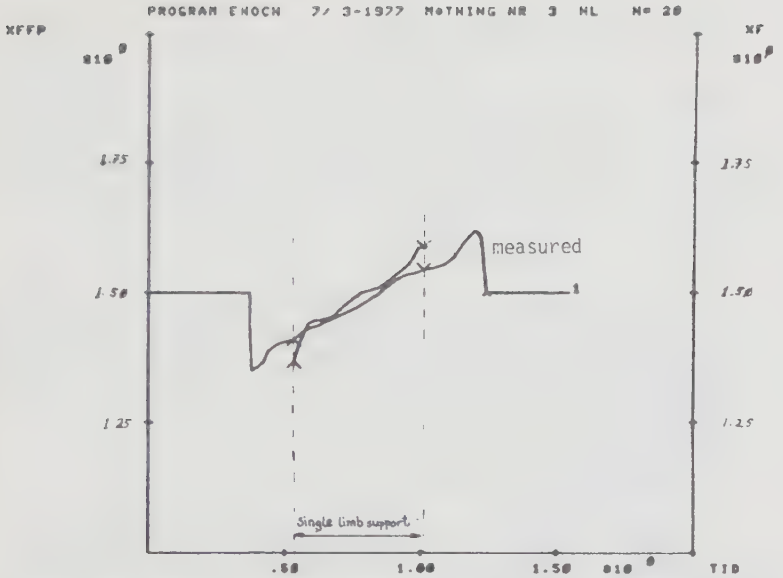

Figure 28. Point of attack from the force plate measurement respectively the kinetic model.

We see that the difference is about ± 4 cm. As for forces and moments the main part of the difference is caused of the trunk complex.

9.3.8 The experimental condition branch

For a correct interpretation of the results obtained from an experiment, it is important that the experimental conditions will be described in an unambigous way. This must be done of the biomechanist, who performs the experiment. An important aspect is the question of stationarity. Here the device for this is evaluated.

If a net impulse is transferred from the ground to the subject during one gait phase, then the gait is not stationary. (It shall also be noted that even if the net impulse transfered is zero, this does not logically imply a stationary gait.)

The impulse measures are:

$P = \int FXFP\ dt$ evaluated between two phases changes of the same type. This gives the net transfered impulse from the ground in x-direction.

$Pr = \frac{\int FXFP\ dt}{\int |FXFP|\ dt}$ evaluated over one gait phase gives the relativ impulse in y-

For this we have $-1 \leq Pr \leq 1$, where negative sign means retardation and positive sign acceleration.

For measurements which are meant to be stationary we usually have $-0.15 < Pr < 0.15$. In figure 29 we give an example of extreme retardation with $P = -88.1$ and $Pr = -0.80$, interpreted in a) display of the gait b) the ground reaction force in x-direction.

Accuracy of P and Pr

We have estimated the error $\Delta FXFP$ of the force plate to approximately ± 8 N. The integral $\int \Delta FXFP\ dt$ integrated over typically 100 samples then gives an error of approximately $\frac{8}{\sqrt{100}} = 0.8$ Ns while $\int |FXFP|\ dt$ is typically about 50-100 Ns.

The error in P and Pr therefore are about 1%.

a)

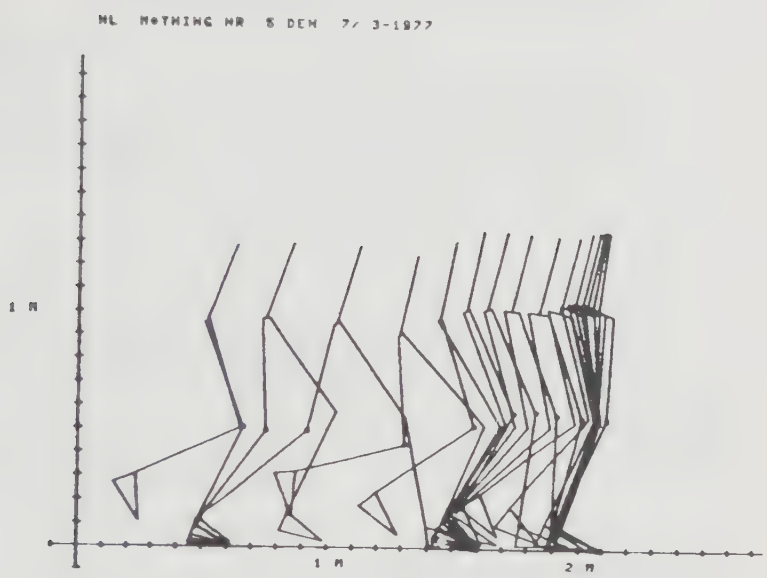

b)

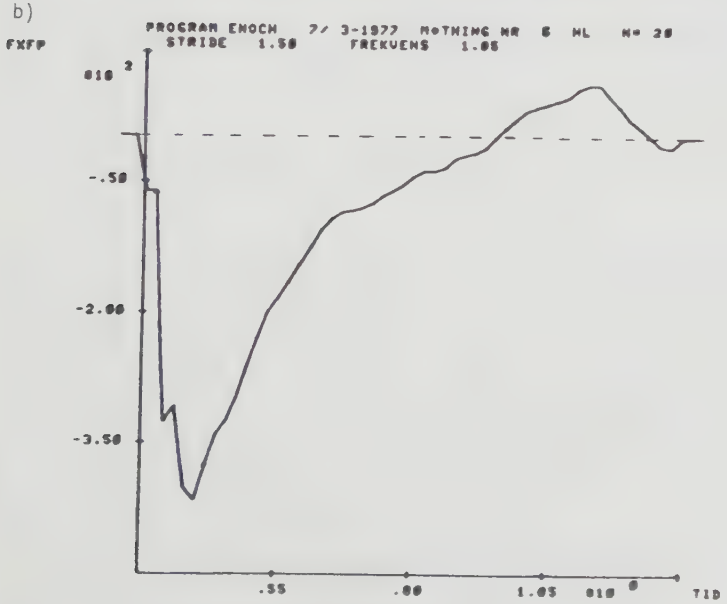

Figure 29 a and b. Extreme retardation.

9.4 The time consumption for investigation of a subject

The time consumption for different parts, and for the whole investigation of a subject, here presented, are based on our use of the system.

When the calibration of the camera positions is performed, a complete investigation includes body data measurements, preparation of the subject, measurements, analysis, and result presentation.

The camera calibration described in section 5.2.4 only has to be performed if a camera has been moved after the last calibration. This calibration takes about 10 minutes, where most of the time is required for careful positioning of six diodes on the calibration board. With six diodes permanently fixed on the board the calibration would take only a few minutes.

Body data measurements take about 5-10 minutes and two minutes to manually feed into the computer.

Preparation of the subject, where the large moment is the attaching of the light emitting diodes, now takes 20-30 minutes. This time would be significantly reduced with a better design of the diode connections.

To perform and store a measurement takes less than a minute.

The time for analysis of the data ranges up to 10 minutes for a complete analysis.

Result presentation time depends of how many diagrams and tables that are wanted. Our limitations are in the speed of the graphic terminal with its hard copy unit and of the line printer.

A complete investigation (calibration is seldom needed) takes less than one hour.

What is said above refers to our experience and time measurements during experimental conditions.

REFERENCES

Allum J H J, A Least Mean Square CUBIC Algorithm for On-Line Differential of Sampled Analog Signals, IEEE trans. Computers, Vol C-24, No 6, pp 585-590, June 1975.

Aoki M, Optimization of Stochastic Systems, Academic Press, New York, N.Y., 1967.

Braune W, Fischer O, Ueber der Schwerpunkt des Menslicher Koerpers....., Abh. d. Koenigl. Sachs. Gesellsch. Math. Phys. CL, 26, 561, 1890.

Bresler B, Frankel J P, The Forces and Moments in the Leg During Level Walking. Trans. Am. Soc. Mech. Eng. 72, 27 (Paper No 48-A-62), 1950.

Broman H, Kvasnička J, Liander B, Varnauskas E, A Computerized System for Optimal Filtering of Left Ventricular Pressure Data, IEEE transaction on Biomedical Engineering, Vol BME-22, No 4, pp 287-292, July 1975.

Bryson A E, Ho Y C, Applied Optimal Control, Ginn and Company, Waltham, Mass., 1969.

Cavanagh P R, Recent Advances in Instrumentation and Methodology of Biomechanical Studies, BIOMECHANICS V-B, University Park Press, pp 399-411, 1975.

Chandler R F, Clauser C E, Mc Conville J T, Reynolds H M, Young J W, Investigation of Inertial Properties of the Human Body, DOT HS-801 430, 1975.

Contini R, Body Segment Parameters (Pathological) Technical Report No 1584.03, School of Engineering and Science, University of N.Y., 10 453, 1970.

Contini R, Body Segment Parameters, Part II, Artificial Limbs, Vol 16, No 1, 1972.

Drillis R, Contini R, Body Segment Parameters. Tech. Rept. 1166.03, School of Engineering and Science, University of N.Y., Sept. 1966.

Elftman H, The Measurement of the External Forces in Walking, Science 88, p 152, 1938.

Fischer O, Der Gang des menschen, Abt. d. Koenigl. Saech. Geselbsch. d. Wissensch., Math. Phys. D., 1895-1904.

Gold B, Rader C M, Digital Processing of Signals, McGraw Hill, New York, 1969.

Golden R M, Kaiser J F, Design of Wideband Sampled-Data Filters. Bell Syst. Tech. J., 43, Pt. 2, pp 1533-1546, July 1964.

Gustafsson L, Lanshammar H, Program Documentation for the ENOCH System, Institute of Technology, Uppsala University, UPTEC 77 21 R, Uppsala 1977.

Hofstetter E, Oppenheim A, Siegel J, A new Technique for the Design of Non-Recursive Digital Filters, Proc. 5th Annu. Princeton Conf. Inform. Sci. Systems, pp 64-72, 1971.

Jahnberg S, Reglertekniskt studium av banprotesfunktion, delrapport 2, FOA 2 rapport C 2515-H5, Januari 1972.

Jarrett M O, Andrews B J, Paul J P, Quantitative Analysis of Locomotion using Television, World Congress, I.S.P.O. Montreux, October 1974.

Jarrett M O, Andrews B J, Paul J P, A Television/Computer System for the Analysis of Human Locomotion, I.E.R.E. Golden Jubilee Conference on the Applications of Electronics in Medicine, April 1976.

Kistler Instrumente AG, Operating instructions, charge amplifier, type 5001, Winterthur, Switzerland, 1972.

Kistler Instrumente AG, Operating instructions multicomponent measuring platform for biomechanics and industry, type 9261A, Winterthur, Switzerlnad, 1974.

Kuo F, Kaiser J, System Analysis by Digital Computer, John Wiley & Sons, New York, 1966.

Lamoreux L W, Kinematic Measurement in the Study of Human Walking, Bulletin of Prosthetics Research, BPR 10-15, Spring 1971.

Lanczos C, Applied Analysis, Prentice Hall, Englewood Cliffs, N.J., 1956.

Lanshammar H, Söderström T, Forthcoming report on numerical differentiation.

McLellan J H, Parks T W, A Unified Approach to the Design of Optimum FIR Linear-Phase Digital Filters, IEEE Trans. Circuit Theory, CT-20(6), pp 697-701, 1973.

McLellan J H, Parks T W, Rabiner L R, A Computer Program for Designing Optimum FIR Linear Phase Digital Filters, IEEE Trans. Audio Electroacoustics, AU-21(6), pp 506-526, 1973.

Monroe A J, Digital Processes for Sampled Data Systems, John Wiley & Sons, New York, 1962.

Murray M P, Drought A B, Kory R C, Walking Patterns of Normal Men, The Journal of Bone and Joint Surgery, Vol 46-A, No 2, pp 335-360, March 1964.

Paul J P, Forces Transmitted by Joints in the Human Body, Proc. Instn Mech. Engrs 1966-1967, Vol 181, PT 3 F, 1967.

Rabiner L R, Graham N Y, Helms H D, Linear Programming Design of IIR Digital Filters with Arbitrary Magnitude Function, IEEE transactions on Acoustics, Speech and Signal Processing, Vol ASSP-22, No 2, pp 117-123, April 1974.

Reed D J, Reynolds P J, A Joint Angle Detector, J. Appl. Physiol., Vol 27, No 5, pp 745-748, 1969.

Scheid F, Numerical Analysis, Schaum's outline series, McGraw-Hill, New York, 1968.

The Selspot System (A), Technical Manual, Selective Electronic Company, Partille, Sweden.

The Selspot System (B), An Optoelectronic Movement Monitoring System (Sales brochure), Selective Electronic Company, Partille, Sweden.

Steiglitz K, Computer-Aided Design of Recursive Digital Filters, IEEE Trans Audio Electroacoustics, AU-18(2), pp 123-129, 1970.

Sutherland D H, Hagy J L, Measurement of Gait Movement from Motion Picture Film, The Journal of Bone and Joint Surgery, Vol 54-A, No 4, pp 787-797, June 1972.

Winter D, Sidwall G, Hobson D, Measurement and Reduction of Noise in Kinematics of Locomotion, J. Biomechanics, Vol 7, pp 157-159, 1974a.

Winter D A et al., Television-Computer Analysis of Kinematics of Human Gait, Computers and Biomedical Research, 5, pp 498-504, 1972.

Winter D A et al., Kinematics of Normal Locomotion - A Statistical Study Based on T.V. Data, J. Biomechanics, 7, pp 479-486, 1974b.

Wirta R W, Taylor D R, Finley F R, Laboratory for Kinesiologic Analysis, Bulletin of Prosthetic Research, pp 165-172, Spring 1970.

Woltring H J, Calibration and Measurement in 3-Dimensional Monitoring of Human Motion by Optoelectronic Means, Biotelemetry 2:169-196, Basel, 1975.

ISBN 91-506-0120-2